The Phase Diagram and Equation of State of Improved Lattice QCD for High Temperatures and small Chemical Potentials

Dissertation

zur Erlangung des Doktorgrades
an der Fakultät für Physik
der Universität Bielefeld

vorgelegt von
Christian Schmidt

Juli 2003

Acknowledgments

It is with the greatest pleasure that I thank my doctoral advisor Prof. Dr. Frithjof Karsch for his guidance and collaboration. His skillful mentorship and availability during the full duration of this work have proven to be invaluable. He also provided me with the possibility of participating in conferences and workshops around the world.

In addition I would like to thank especially Prof. Dr. Edwin Laermann, who was always open for questions and many fruitful discussions. Together with Dr. Olaf Kaczmarek he attended the project during the full three years of my work. They both helped to bring this work to a successful conclusion.

I am particularly indebted to Prof. Dr. Simon J. Hands, Dr. Chris R. Allton and Dr. Shinji Ejiri. I thank you all for hosting me during my visit at the University of Wales in Swansea (including the financial support). Most of the results which are presented here have been obtained in the Bielefeld-Swansea Collaboration. I have benefitted immensely from this collaboration, especially from the work of Dr. Shinji Ejri.

I gratefully acknowledge several interesting discussions with Prof. Dr. Krishna Rajagopal, Prof. Dr. Dirk Rischke and Paul Romatschke.

I like to express all my gratefulness to the members of the Particle Physics Group at the Physics Faculty of Bielefeld for enlightening discussions about physics and many other things. Especially commendable for their friendships, valuable discussions and gracious support are Dr. Hendrik van Hees, Sven Holtmann, Sven Stickan, Thomas Schulze and my roommates Michael Seniuch and Lars Fromme. Moreover I benefited from the work and experience of some former members of the group, Dr. Andreas Peikert, Dr. Peter Schmidt, and Dr. Ines Wetzorke. From the beginning, they provided me with their knowledge and ensured my smooth integration into the group.

Schliesslich gilt mein ganz besonderer Dank meinen Eltern, die mir mit ihrer jahrelangen grosszügigen Unterstützung überhaupt erst das Studium und die daran anschliessende Promotion ermöglichten. Meiner Freundin Wibke Sonntag danke ich für ihre Liebe und jahrelange Geduld und Begleitung.

Christian Schmidt
Bielefeld, July 2003

Contents

Chapter 1

Introduction

Nuclear matter is build from hadronic bound states of quarks, hold together by the strong interaction, mediated via gluon exchange. The study of strongly interacting matter under extreme conditions, i.e. temperatures that have been reached in the early universe or densities like in the core of neutron stars, is one of the most exciting topics in contemporary physics. It deals with fundamental questions like "What happens if you make things hotter and hotter?" or "What happens if you keep squeezing and squeezing?". The understanding of matter under extreme conditions is mandatory for cosmology and astrophysics. Moreover during the last decade, much effort has been devoted to experimentally detecting the quark-gluon plasma (QGP) state in high energy heavy-ion collisions. The QGP is the expected state of matter at high temperatures and densities, after melting away the hadronic structure of matter and liberating the quarks and gluons. Experiments are running at BNL and CERN with the goal to observe experimentally the creation of this new state of matter [1, 2]. On the theoretical site, novel color superconducting and superfluid phases have been conjectured at high baryon densities [3]. For these reasons numerical studies of strongly interacting quarks and gluons, that obey the laws Quantum Chromo Dynamics (QCD), with both temperature $T \neq 0$ and quark chemical potential $\mu_q \neq 0$, are more urgent than ever. Precise information about the QCD phase diagram and the QCD equation of state are indispensable to the understanding of heavy-ion collision experiments.

The nature of the QCD transition from a gas of hadronic resonances to the QGP is one of the most important aspects of the QCD phase diagram. One expects that there exists a large region in the parameter space of quark masses (m_u, m_d, m_s), temperature (T) and chemical potential (μ_q), where the transition is a true thermodynamical phase transition, which is of first order. Moreover at the boundary of this region, the transition is expected to be of second order, which should lead to critical behavior in the vicinity of this surface. At fixed physical quark masses, this is known

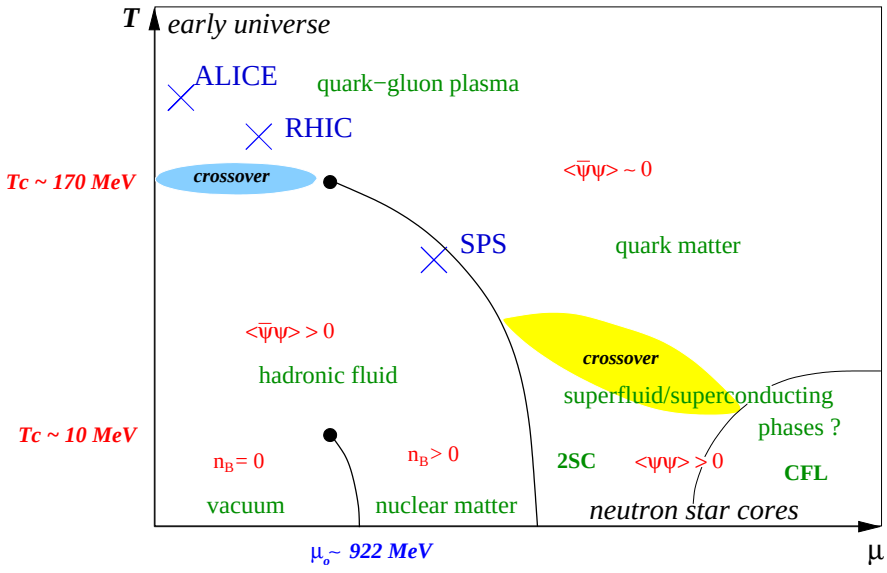

Figure 1.1: Schematic view of the QCD phase diagram [4]. ALICE, RHIC and SPS are names of relativistic heavy-ion accelerators or experiments at BNL and CERN, and 2SC and CFL refer to diquark condensates.

as the second order end point of a line of first order phase transitions, as shown in Figure 1.1. Detailed studies of the QCD phase diagram and critical phenomena are thus of great theoretical interest. Furthermore, it is a fascinating feature, that these studies may influence our thinking about observable effects of the critical point in the BNL Relativistic Heavy-ion Collider (RHIC) or future GSI experiments, for instance in event-by-event fluctuations [5]. An example of a critical point, which one was already able to study in nuclear collisions, is the end point of the nuclear liquid-gas transition (boiling of the nuclear matter liquid to yield a gas of nucleons). It can be observed in low energy multi-fragmentation experiments [6, 7] and occurs at a temperature of 10 MeV, much lower than the one we are studying here. Of course we not only expect observable effects when the evolution trajectory of a system created in a heavy-ion collision passes near or through the QCD critical point, but also expect consequences, when the evolution trajectory of the early universe itself would have done this. In cosmological scenarios the inhomogeneities of the universe we can observe today are sensitive to the nature of the QCD phase transition which occurred in the early universe shortly after the big bang.

In this work we estimate the QCD critical point and determine its universality class. Besides a first approximation of the critical temperature ($T^{crit} \approx 165$ MeV) and the critical chemical potential ($\mu_q^{crit} \approx 152$ MeV) fixing its location in 3-flavor QCD, we also give a numerical "proof" that the QCD critical point belongs to the universality class of the 3d-Ising model [8] and investigate

the dependence of its location on independent variations of two degenerate light quark masses and one heavier strange quark mass. Moreover, we calculate the curvature of the transition line $T_c(\mu_q)$ as a function of the quark chemical potential ($T_c(\mathrm{d}^2T_c/\mathrm{d}\mu_q^2)|_{\mu_q=0} \simeq -0.14(6)$) and obtain results consistent with earlier calculations [9, 10].

Also the equation of state belongs to the most basic category of information needed in phenomenological investigations of heavy-ion collisions. The non-perturbative study of QCD thermodynamics at small but non-zero baryon density are directly applicable to the density regime currently investigated experimentally at RHIC. Here corrections to quantities evaluated at $\mu_q = 0$ are both small and calculable. In a relativistic heavy ion collision of duration $\sim 10^{-22}s$, thermal equilibration is possible only for processes mediated by the strong interaction, rather than the full electroweak equilibrium achievable, say, in the core of a neutron star. This means that each quark flavor is a conserved charge, and conditions at RHIC are thus approximately described by

$$\mu_u = \mu_d = \mu_q \neq 0 \quad ; \qquad \mu_I \equiv 2(\mu_u - \mu_d) = 0 \quad ; \qquad \mu_s = 0 \quad , \tag{1.1}$$

with $\mu_q \approx 15$ MeV [11] when we relate the quark and baryon number chemical potentials via $\mu_B = 3\mu_q$. We will present numerical results for the equation of state, i.e. pressure $p(\mu_q, T)$ and quark density $n_q(\mu_q, T)$, obtained from lattice QCD simulations with two flavors of equal mass quarks, which should give a qualitatively correct description of RHIC physics, and provide a useful starting point for quantitative studies of the physical case of 2+1 flavor with realistic light and strange quark masses.

Trying to quantify non perturbative aspects of the QCD phase diagram requires non perturbative calculations within the framework of lattice regularized QCD, which was shown to be the most powerful approach to QCD thermodynamics at zero chemical potential [12, 13, 14]. The great problem one is confronted with lattice QCD at finite density is the so called "sign problem". Direct simulations using standard Monte Carlo importance sampling is hampered because the QCD path integral measure $\det^{n_f} M$, where $M(\mu_q)$ is the Euclidean space fermion kinetic operator, is complex once $\mu_q \neq 0$. Recently progress has been made to circumvent this problem for small chemical potentials. In the studies which have appeared to date two fundamentally distinct approaches* have emerged. In the reweighting method results from simulations at $\mu_q = 0$ are reweighted on a configuration-by-configuration basis with the correction factor $[\det M(\mu_q)/\det M(0)]^{n_f}$ yielding formally exact estimates for expectation values. Indeed, it is found that if reweighting is performed

*Another interesting method to study lattice QCD at small but finite density is the canonical approach for small but exact baryon number. This has been done up to now in the static limit of QCD [15] only, but should in principle work in full QCD as well.

simultaneously in two or more parameters, convergence of this method on moderately-sized systems is considerably enhanced [16]. This method has been used on lattice sizes up to $12^3 \times 4$ to map out the pseudo critical line and estimate the location of the critical endpoint. In QCD with tow light and a heavier strange quark this led to the estimate $\mu_q^{crit} \simeq 240$ MeV, $T^{crit} \simeq 160$ MeV [9]. In this study unimproved staggered fermions have been used with only semi-realistic quark masses. More recently the equation of state in the entire region to the left of the endpoint has been calculated this way [17]. However, it remains questionable whether the thermodynamic limit can be reached using this technique.

Analytic approaches use data from regions where direct simulations are possible, either by calculating derivatives with respect to μ_q (or more precisely with respect to the dimensionless combination μ_q/T) to construct a Taylor expansion for quantities of interest [18, 19, 20, 21], or more radically by analytically continuing results from simulations with imaginary μ_q (for which the integration measure remains real) to real μ_q. The second technique has been used to determine $T_c(\mu_q)$ for QCD with both $n_{\rm f} = 2$ [10] and $n_{\rm f} = 4$ [22], in the latter case one finds evidence that the line is first order in nature. Fortunately, the pseudo critical line found in [10] is in reasonable agreement with that found by reweighting; moreover the radius of convergence within which analytic continuation from imaginary μ_q is valid corresponds to $\mu_q/T \leq \pi/3$ [23]. The leading non-trivial term of quadratic order in the Taylor expansion appears to provide a good approximation throughout this region. In general though, while such approaches have no problem approaching the thermodynamic limit, it is not yet clear if and how they can be extended into the region around the critical endpoint and to observables that vary strongly with μ_q like e.g. the pressure or energy density.

In our investigation of the phase diagram we use a hybrid of the two techniques, by making a Taylor series estimate of the reweighting factor $[\det M(\mu_q)/\det M(0)]^{n_f}$ to $\mathcal{O}(\mu_q^2)$. Since this is considerably cheaper than a calculation of the full determinant, we are able to explore a larger $16^3 \times 4$ system, and also exploit an improved action in both gauge and fermion [24] sectors, thus dramatically reducing discretization artifacts on what at $T_c(\mu_q = 0) \simeq 170$ MeV is still a coarse lattice. For the evaluation of the equation of state we extend the Taylor series to the next order $\mathcal{O}(\mu_q^4)$ but this time remain entirely within the analytic framework, using derivatives calculated at $\mu_q = 0$ to evaluate non-zero density corrections to the pressure p and quark number susceptibility $\chi_q \equiv \partial n_q/\partial \mu_q$, as well as the quark number density n_q itself. In fact, since the correction Δp can be evaluated at fixed temperature, it turns out to be considerably easier to calculate than the equation of state at $\mu_q = 0$ [12, 14]. Since we now have the first two non-trivial terms in the Taylor expansion, we are also able to estimate its radius of convergence as a function of T, and confirm that close to $T_c(\mu_q = 0)$ the results for the critical line curvature can be trusted out to

$\mathcal{O}(100\,\mathrm{MeV})$, whereas at higher temperatures a considerably larger radius of convergence is likely to be found. Finally we consider mixed derivatives with respect to both μ_q and the other bare parameters β and m, which are required to estimate energy ϵ and entropy s densities. Due to the presence of a critical singularity, these latter quantities appear considerably harder to calculate in the critical region using this approach.

This thesis summarizes and extents previous work [8, 19, 25, 26, 27, 28] on the QCD phase diagram and equation of state at non-zero chemical potential. It is organized as follows: In Chapter 2 we recall the basic concepts of lattice QCD and the improvement of lattice actions. We also introduce the reweighting method and discuss the cutoff dependence of improved and unimproved actions at finite μ_q. In Chapter 3 we study the phase diagram and nature of the QCD phase transition. We investigate the chiral critical point in 3-flavor QCD and estimate its quark mass and chemical potential dependence. After an analysis of the transition temperature T_c as function of $\mu \neq 0$, we conclude with a mean-field calculation of an effective chiral Hamiltonian. In Chapter 4 we study the equation of state . We give $p(T, \mu_q)$, $n_B(T, \mu_q)$ and investigate in how far the results can be understood in terms of the hadronic resonance gas. We summarize and conclude in Chapter 5. The appendices contain further technical details to the discussion of cutoff effects, the linear sigma model, and the Monte Carlo simulations.

Chapter 2

Lattice QCD

In this chapter we will recall the basic steps for thermodynamic investigations of strongly interacting quarks and gluons on the lattice. The key step is the regularization of the path integral by the introduction of appropriate lattice versions of the QCD Lagrangian and the interpretation of the Boltzmann factor as a probability distribution. Furthermore we will argue that improved actions are of great importance for the high temperature and density regime and will present a possible improvement scheme. Finally we will outline the first steps toward a finite chemical potential formulation. It is, however, not the aim of this chapter to give a detailed introduction to lattice gauge theory, here we refer to standard text books like [29, 30, 31].

2.1 Quarks and gluons on the lattice

The starting point for all thermodynamic investigations is the partition function. The grand canonical partition function of QCD can be represented in terms of an Euclidean path integral over the fermion fields (ψ, $\bar{\psi}$) and the gauge field (A),

$$Z(T,V,\mu) = \int \mathcal{D}\psi\, \mathcal{D}\bar{\psi}\, \mathcal{D}A \;\; \exp\{-S_E(T,V,\mu)\} \quad , \tag{2.1}$$

were A and ψ, $\bar{\psi}$ obey periodic and anti-periodic boundary conditions in the Euclidean time, respectively. Here the external control parameters are the temperature (T), the volume (V) and the chemical potential (μ). The Euclidean action (S_E) contains a purely gluonic contribution (S_G) and a fermionic contribution (S_F) which includes the coupling between the fermionic and gluonic sector

$$S_E(T,V,\mu) \;\; \equiv \;\; S_G(T,V) \, + \, S_F(T,V,\mu_f) \quad , \tag{2.2}$$

$$S_G(V,T) = \int_0^{1/T} dx_4 \int_V d^3\mathbf{x}\, \frac{1}{2}\,\mathrm{Tr}\, F_{\mu\nu}F_{\mu\nu} \quad , \tag{2.3}$$

$$S_F(T,V,\mu) = \int_0^{1/T} dx_4 \int_V d^3\mathbf{x} \sum_{f=1}^{n_f} \bar{\psi}_f \left(\gamma_\mu \left[\partial_\mu - igA_\mu\right] + m_f - \mu_f\gamma_4\right)\psi_f \quad . \tag{2.4}$$

For the gluons we have only a dynamical contribution, essentially given by the square of the field strength tensor ($F_{\mu\nu} = \partial_\mu A_\nu - \partial_\nu A_\mu - ig[A_\mu, A_\nu]$) whereas for the fermions we have a sum over all different quark flavors with quark mass m_f concerning a dynamical term ($\bar{\psi}_f\gamma_\mu\partial_\mu\psi_f$), a mass term ($m_f\bar{\psi}_f\psi_f$), an interaction term ($-igA_\mu\bar{\psi}_f\gamma_\mu\psi_f$) with the QCD coupling constant g and a term coupling to the chemical potential ($\mu_f\bar{\psi}_f\gamma_4\psi_f$).

The introduction of a four dimensional space time lattice of size $N_\sigma^3 \times N_\tau$ regularizes the path integral given in Equation (2.1). Volume and temperature of the system are then related to the lattice spacing a by

$$V = (aN_\sigma)^3, \qquad T = (aN_\tau)^{-1} \quad . \tag{2.5}$$

To discretize both, the gluon and the fermion action, we have to deal with link variables $U_\mu(x)$ which are associated with the link between two neighboring sites of the lattice and describe the parallel transport from site x to $x + \hat{\mu}a$,

$$U_\mu(x) = P\,\exp\left\{ ig \int_x^{x+\hat{\mu}a} dx_\mu A_\mu(x) \right\} \quad , \tag{2.6}$$

where P denotes the path ordering. The link variables are elements of the $SU(3)$ color group. As one can easily see, a product of link variables around an elementary plaquette will give a discretized version of the gauge action, we find

$$W_{\mu\nu}^{(1,1)}(x) = 1 - \frac{1}{3}\,\mathrm{Re}\,\square = 1 - \frac{1}{3}\,\mathrm{Re}\;\mathrm{Tr}\, U_\mu(x)U_\nu(x+\hat{\mu}a)U_\mu^\dagger(x+\hat{\nu}a)U_\nu^\dagger(x)$$
$$= \frac{g^2a^4}{2}\,\mathrm{Tr}\, F_{\mu\nu}F_{\mu\nu} + \mathcal{O}\left(a^6\right) \quad . \tag{2.7}$$

Or to be more precise, the discrete gauge action is given by the Wilson action [32, 33], which is the sum over all elementary plaquettes in the space time lattice,

$$S_G = \sum_x \sum_{1\le\mu<\nu\le 4} \beta\, W_{\mu\nu}^{(1,1)}(x) \quad , \tag{2.8}$$

with the gauge coupling $\beta = 6/g^2$. This action reproduces the continuum version up to cutoff errors of order $\mathcal{O}(a^2)$.

For a lattice action of free fermions, one can simply replace the derivative in the fermion Lagrangian by a finite difference scheme, i.e. $\partial_\mu \psi_f(x) = (\psi_f(x+\hat{\mu}a) - \psi_f(x-\hat{\mu}a)/2a$. It is however well known, that this naive discretization scheme does not reproduce the correct particle content in the continuum limit. The massless fermion propagator has poles not only at zero momentum, but also at all other corners of the Brillouin zone. Thus one is left with 16 rather than one fermion species. There are essentially three ways known to circumvent this "fermion doubling problem". One solution is the introduction of a term which is proportional to $a\,\partial_\mu^2 \psi_f(x)$ (Wilson fermions [32, 33]). This term vanishes in the continuum limit ($a \to 0$) and eliminates all fermion doublers for any finite a. Unfortunately this term also breaks the global chiral symmetry $SU(n_f)_L \times SU(n_f)_R$ completely, which is supposed to play an important role for QCD thermodynamics. Another solution is to distribute the Dirac and flavor indices over several lattice sites (staggered fermions [34]). This solution reduces the fermion doublers to four degenerate species, which can be interpreted as four different flavors of quarks. Here a continuous subgroup of the chiral symmetry $(U(1)_L \times U(1)_R)$ is preserved. The interplay between fermion doublers and chiral symmetry can be understood in terms of a No-Go theorem [35]. Within this theorem it has been shown that a lattice regularization with an exact chiral symmetry but without fermion doublers cannot be achieved. Nevertheless, progress has been made with chiral fermions, for instance one can circumvent the No-Go theorem by introducing an extra fifth dimension (domain wall fermions [36], overlap fermions [37]). At present, however, very little has been done to study QCD thermodynamics on the lattice with chiral fermions [38, 39, 40].

Here we concentrate on the staggered fermion formulation introduced by Kogut and Susskind [34]. Also the numerical results we present in Chapter 3 and Chapter 4 are results from calculations performed with dynamical staggered fermions. The fermion action can be written as

$$S_F^{KS} = \sum_{x,y} \bar{\chi}(x)\, M^{KS}(x,y)\, \chi(y) \quad , \tag{2.9}$$

were the staggered fermion matrix M^{KS} is given by

$$M(m_q) = \frac{1}{2} \sum_\mu \eta_\mu(x) \left[\delta(x+\hat{\mu}a, y) U_\mu(x) - \delta(x, y+\hat{\mu}a) U_\mu^\dagger(x) \right] + \delta(x,y) m_q \quad . \tag{2.10}$$

Through the distribution of Dirac and flavor components over the lattice, we are left with a Grassman valued fermion field (χ, $\bar{\chi}$), which carries color indices only. The only remnant of the gamma structure of the fermion action is the staggered phase ($\eta_\mu(x)$), which takes the values ± 1 and thus naturally divides the lattice in even and odd sites,

$$\eta_\mu(x) = (-1)^{\left(\frac{x_1}{a} + \cdots + \frac{x_{\mu-1}}{a}\right)} \quad . \tag{2.11}$$

Another possibility to write down the fermion matrix is to absorb the bare quark mass (m_q) in the lattice fermion fields:

$$M(K) = K \sum_{\mu} \eta_{\mu}(x) \left[\delta(x + \hat{\mu}a, y) U_{\mu}(x) - \delta(x, y + \hat{\mu}a) U_{\mu}^{\dagger}(x) \right] + \delta(x, y) \quad . \tag{2.12}$$

Now the bare quark mass is given by $m_q = 1/(2K)$ with the hopping parameter K. To reproduce the conventional continuum normalization we need to rescale the fermion fields, $\chi_{\text{lattice}} = \sqrt{1/2K}\chi_{\text{continuum}}$.

Since the action is quadratic in the fermion fields, they can be integrated out and we end up with the following lattice partition function,

$$Z(N_\sigma, N_\tau, \beta, m_q) = \int \prod_{x,\mu} dU_{\mu}(x) \, \left(\det M^{KS}(m_q) \right)^{n_f/4} \, e^{S_G(\beta)} \quad . \tag{2.13}$$

Here the important parameters are the lattice size (N_σ, N_τ), the quark mass (m_q) and the lattice gauge coupling (β). The introduction of the chemical potential on the lattice will be discussed in Section 2.3. The fourth root of the fermion determinant was taken to embrace the fact that the staggered fermion matrix as written in Equation (2.10) corresponds to $n_f = 4$ in Equation (2.13). We use $n_f = 2$ and $n_f = 3$ for simulations of two and three flavors of degenerate quarks and split the power of the determinant to allow for simulations, with different quark masses for two light (u,d) and a heavier strange quark (s),

$$Z(N_\sigma, N_\tau, \beta, m_{q,2}, m_{q,1}) = \int \prod_{x,\mu} dU_{\mu}(x) \, \left(\det M^{KS}(m_{q,2}) \right)^{2/4} \, \left(M^{KS}(m_{q,1}) \right)^{1/4} \, e^{S_G(\beta)} \, . \tag{2.14}$$

The quark mass of the two degenerate quark flavors is $m_{q,2}$, while $m_{q,1}$ is the quark mass of the additional quark flavor. This procedure is, of course, correct in the continuum limit, where the quark flavors fully decouple, whereas at finite lattice spacing a the staggered fermion action (2.9) breaks the flavor symmetry. However, it has been shown [41] that these flavor symmetry breaking terms enter at order $\mathcal{O}(a^2)$ only.

An important point to mention is that on the lattice all observables are dimensionless quantities and are thus calculated in appropriate units of the lattice spacing a. This has two major consequences. First of all the continuum limit at fixed temperature, i.e. the limit ($a \to 0, N_\tau \to \infty$) for fixed $T = 1/aN_\tau$, is for bulk thermodynamic quantities quite cumbersome. Since observables like pressure and energy density have dimension $[T^4]$, a measurement of e.g. the pressure p will provide pa^4 and thus yields a result which decreases as N_τ^{-4} in magnitude. Lattice data are however always expectation values based on a finite set of gauge field configurations and thus include a statistical error. It therefore rapidly becomes difficult to calculate bulk thermodynamic quantities

on lattices with large temporal extent N_τ. This is the reason why it is of particular importance to use improved actions with small discretization errors for finite temperature calculations as described in the next section. The second consequence is that we have on the lattice no other scale than the lattice spacing a. The conversion of lattice units to physical units thus is non-trivial. Additional zero temperature calculations with the same value of the cutoff (bare couplings) are required to determine an observable which is known in physical units. Of course, we have experimental results only for physical quark masses, i.e. two light quark flavors (up and down quark) and one heavier strange quark. Nonetheless certain observables are quite insensitive to changes in the quark masses, e.g. quenched hadron masses* ($\tilde{m}_H$) or the string tension ($\tilde{\sigma}$) are believed to be suitable observables to set a physical scale. We thus may use calculations of these quantities to define a temperature scale,

$$T/\sqrt{\sigma} = 1/\sqrt{\tilde{\sigma}}N_\tau \qquad \text{or} \qquad T/m_H = 1/\tilde{m}_H N_\tau \quad . \tag{2.15}$$

In the limit of infinite quark masses (pure $SU(3)$ gauge theory) as well as in the massless limit (chiral limit) we have only one bare coupling (β) in the Euclidean action which controls the lattice spacing a. Asymptotically a and β are then related through the leading order renormalization group equation,

$$a\Lambda_L \sim (6b_0/\beta)^{-b_1/2b_0^2}\, e^{-\beta/12b_0} \quad , \tag{2.16}$$

where the two universal coefficients are given by,

$$b_0 = \frac{1}{16\pi^2}\left[11 - \frac{2}{3}n_f\right] \quad , \qquad b_1 = \left(\frac{1}{16\pi^2}\right)^2\left[102 - \left(10 + \frac{8}{3}\right)n_f\right] \quad , \tag{2.17}$$

and Λ_L is a scale parameter which unambiguously can be related to the scale parameter in other regularization schemes, e.g. to $\Lambda_{\overline{MS}}$. The continuum limit thus is reached with increasing β.

2.2 From standard to improved actions

As mentioned above the lattice actions suffer from errors due to the finite lattice spacing (cutoff effects). Therefore observables which are sensitive to the ultraviolet cutoff show a strong a dependence and one is forced to perform simulations at quite small lattice spacing to be able to extract continuum results or to extrapolate to the continuum limit reliably. Unfortunately this increases

*We denote here dimensionless lattice observables by $\tilde{O}$, the corresponding physical observable by O. Quite often, however, we will also adopt the customary lattice notation, which explicitly specifies the cutoff dependence in the continuum limit, e.g. $\tilde{m}_H \equiv m_H a$ or $\tilde{\sigma} \equiv \sigma a^2$.

the computational effort dramatically. Various procedures to reduce those systematic errors have been suggested in the past, including the early Symanzik improvement program [42, 43], renormalization group improved actions [44, 45] as well as classically perfect actions [46, 47, 48]. Here we will introduce the improvement scheme we also use for our numerical calculations presented in Chapter 3 and Chapter 4. A quantitative analysis of the cutoff effects at least for the fermionic sector is given in Section 2.4. The corresponding analysis for the gauge part of the action can be found in [49].

2.2.1 Improved gauge actions

In order to eliminate the $\mathcal{O}(a^2)$ and higher order corrections to the lattice version of the Euclidean gauge action one can add appropriately chosen large loops to the basic 4-link plaquette term appearing in the standard Wilson action (2.8). As the only condition is to reproduce the correct continuum limes, this is a great deal of freedom. A simple class of improved actions is, for instance, obtained by adding larger planar loops, i.e. we will consider the generalized Wilson actions,

$$S^I = \sum_{x,\nu>\mu} \sum_{l=1}^{\infty} \sum_{k=1}^{l} a_{k,l} W_{\mu,\nu}^{(k,l)} \equiv \sum_{x,\nu>\mu} S_{\mu,\nu}^I(x) \quad , \tag{2.18}$$

where $W_{\mu,\nu}^{(k,l)}$ denotes a symmetrized combination of $k \times l$ Wilson loops in the $(\hat{\mu}, \hat{\nu})$-plane of the lattice,

$$W_{\mu,\nu}^{(k,l)}(x) = 1 - \frac{1}{6} \text{ Re } \text{ Tr } \left(L_\mu^{(k)}(x)\, L_\nu^{(l)}(x + k\hat{\mu}a)\, L_\mu^{(k)\dagger}(x + l\hat{\nu}a)\, L_\nu^{(l)\dagger}(x) + (k \leftrightarrow l) \right) \quad . \tag{2.19}$$

Here we have introduced the short hand notation for straight links of length l in the direction $\hat{\mu}$,

$$L_\mu^{(l)}(x) = \prod_{i=0}^{l-1} U_\mu(x + i\hat{\mu}a) \quad . \tag{2.20}$$

With a suitable choice of the coefficients $a_{k,l}$ it can be achieved that the generalized Wilson actions reproduce the continuum action up to some order $\mathcal{O}(a^{2n})$ [42, 43]. To get an action with corrections starting at $\mathcal{O}(a^{2n})$ one has to add loops up to length n in at least one direction. After expanding the link variables $U_\mu(x)$ in powers of a one finds for the non-vanishing coefficients of some simple improved actions,

		cutoff effects start at:
$I \equiv (1,1):$	$a_{1,1} = 1,$	$\mathcal{O}(a^2)$
$I \equiv (1,2):$	$a_{1,1} = \frac{5}{3}, \quad a_{1,2} = -\frac{1}{6},$	$\mathcal{O}(a^4)$
$I \equiv (2,2):$	$a_{1,1} = \frac{4}{3}, \quad a_{2,2} = -\frac{1}{48},$	$\mathcal{O}(a^4)$
$I \equiv (3,3):$	$a_{1,1} = \frac{3}{2}, \quad a_{2,2} = -\frac{3}{80}, \quad a_{3,3} = \frac{1}{810}.$	$\mathcal{O}(a^6)$

(2.21)

Within this nomenclature the action $S^{(1,1)}$ denotes the standard one-plaquette action. The actions $S^{(1,2)}$, originally proposed by Symanzik[†] [42, 43], includes planar 2×1 loops in addition to the standard plaquette term. In $S^{(2,2)}$ we added the 2×2 loops only and $S^{(3,3)}$ includes planar 2×2 and 3×3 loops.

Throughout this thesis we will use the Symanzik improved 2×1 action $S^{(1,2)}$, which is the simplest extension of the Wilson action. It has been shown in [49] that a remarkable reduction of the cutoff effects is achieved with this action already on $N_\tau = 4$ lattices. To quantify this statement, in the ideal gas limit the gluonic energy density achieves already 98.7% of the Stefan-Boltzmann value on $N_\tau = 4$ lattices.

One should note, that the improvement discussed so far is tree-level improvement on the classical level $\mathcal{O}(g^0)$. The generalized Wilson actions may be further improved perturbatively by eliminating the leading cutoff effects also at $\mathcal{O}(g^2)$, i.e. $a_{k,l} \to a^{(0)}_{k,l} + g^2 a^{(1)}_{k,l}$, or by introducing non-perturbative modifications. In most cases the structure of the improved actions is the same as that of the generalized Wilson actions (2.18), only the determination of the coefficients changes. Nevertheless the general case of course also can involve non-planar Wilson loops.

2.2.2 Improved staggered fermions

Improving fermion actions is at least a twofold problem. On the one hand one faces cutoff effects (short distance properties of the observables). Here the effects are even larger than in the gluonic sector, which can for instance be observed when comparing results for $N_\tau = 4$ [52] and $N_\tau = 6$ [53] lattices. On the other hand also the global symmetries of the continuum Lagrangian are explicitly broken at finite lattice spacing a. This influences the long distance properties of the observables, e.g. the light particle sector of the lattice regularized theory is modified (Goldstone modes). Both effects alter the thermodynamics of lattice QCD. The use of improved actions thus is mandatory in the fermionic sector.

Again one has a lot of freedom in choosing the operators which can be added to the standard staggered fermion action in order to take into account higher orders in the discretization of the derivative. However, for full QCD simulations one also has to keep the computational effort on a relatively low level, thus one is restricted to use simple bilinear operators only. We consider here a generalized form of the staggered fermion action consisting of terms which respect the hypercube structure of the staggered fermion action. In addition to the standard 1-link terms this action also includes all possible 3-link terms resulting either from the introduction of a higher order

[†]The action $S^{(1,2)}$ was invented by Symanzik for ϕ^4-theory and generalized to $SU(3)$ lattice gauge theory by Weisz and Wohlert [50, 51]

difference scheme for the discretization of the fermion action or from the smearing of the 1-link term (fat-links):

$$\begin{aligned}
S_F &= \sum_x \bar{\chi}(x) \sum_\mu \eta_\mu(x) \\
&\times \Big\{ c_{1,0} \Big[U_\mu^{\rm fat}(x)\chi(x+\hat{\mu}a) - U_\mu^{\rm fat\dagger}(x-\hat{\mu}a)\chi(x-\hat{\mu}a) \Big] \\
&\quad + c_{3,0} \Big[U_\mu^{(3,0)}(x)\chi(x+3\hat{\mu}a) - U_\mu^{(3,0)\dagger}(x-3\hat{\mu}a)\chi(x-3\hat{\mu}a) \Big] \\
&\quad + c_{1,2} \sum_{\nu\neq\mu} \Big[U_{\mu,\nu}^{(1,2)}(x)\chi(x+\hat{\mu}a+2\hat{\nu}a) - U_{\mu,\nu}^{(1,2)\dagger}(x-\hat{\mu}a-2\hat{\nu}a)\chi(x-\hat{\mu}a-2\hat{\nu}a) \\
&\quad + U_{\mu\nu}^{(1,-2)}(x)\chi(x+\hat{\mu}a-2\hat{\nu}a) - U_{\mu,\nu}^{(1,-2)\dagger}(x-\hat{\mu}a+2\hat{\nu}a) \Big] \Big\} \\
&\quad + m \sum_x \bar{\chi}(x)\chi(x) \quad , \qquad (2.22)
\end{aligned}$$

were we denote the long links as

$$\begin{aligned}
U_\mu^{(3,0)}(x) &= U_\mu(x)U_\mu(x+\hat{\mu}a)U_\mu(x+2\hat{\mu}a), \\
U_{\mu,\nu}^{(1,2)}(x) &= \frac{1}{2}\Big[U_\mu(x)U_\nu(x+\hat{\mu}a)U_\nu(x+\hat{\mu}a+\hat{\nu}a) + U_\nu(x)U_\nu(x+\hat{\nu}a)U_\mu(x+2\hat{\nu}a) \Big] \\
U_{\mu,\nu}^{(1,-2)}(x) &= \frac{1}{2}\Big[U_\mu(x)U_\nu^\dagger(x+\hat{\mu}a-\hat{\nu}a)U_\nu^\dagger(x+\hat{\mu}a-2\hat{\nu}a) \\
&\qquad + U_\nu^\dagger(x-\hat{\nu}a)U_\nu^\dagger(x-2\hat{\nu}a)U_\mu(x-2\hat{\nu}a) \Big] \\
U_\mu^{\rm fat}(x) &= \frac{1}{1+6\omega}\Big\{ U_\mu(x) + \omega \sum_{\nu\neq\mu} \Big[U_\nu(x)U_\mu(x+\hat{\nu}a)U_\nu^\dagger(x+\hat{\mu}a) \\
&\qquad + U_\nu^\dagger(x-\hat{\nu}a)U_\mu(x-\hat{\nu}a)U_\nu^\dagger(x+\hat{\mu}a-\hat{\mu}a) \Big] \Big\} \quad . \qquad (2.23)
\end{aligned}$$

When replacing the spin-diagonalized quark fields $\chi(x)$, $\bar{\chi}(x)$ by a four-component Dirac spinor $\psi(x)$, $\bar{\psi}(x)$ and the staggered phases $\eta_\mu(x)$ by the Dirac matrices γ_μ, one recovers an action with 16 fermion doublers in the continuum limit. We will refer to this as the naive form of the action. The concept of a fat link, i.e. replacing a link by a weighted sum of the link itself and the surrounding staples, was first introduced in [54] and analyzed in more detail way in [55]. It has been shown, that fat links significantly improve the flavor symmetry. Together with the fat-link-weight (we use $\omega = 0.2$) there are thus 4 parameters in the action. In order to reproduce the correct naive continuum limit the coefficients have to satisfy the normalization condition

$$c_{1,0} + 3\,c_{3,0} + 6\,c_{1,2} = \frac{1}{2} \quad . \qquad (2.24)$$

More constraints on the coefficients can be derived by improving, for instance, the rotationally symmetry of the fermion propagator. This has been discussed in [24]. To insure that the free propagator is rotational invariant up to order $\mathcal{O}(p^4)$ one finds the constraint

$$c_{1,0} + 27\,c_{3,0} + 6\,c_{1,2} = 24\,c_{1,2} \quad . \qquad (2.25)$$

Two simple choices which eliminate the bended or straight 3-link terms in the action (2.22) respectively, are to set either $c_{1,2} \equiv 0$ which yields the familiar Naik action [56]

$$c_{1,0} = \frac{9}{16}, \qquad c_{3,0} = -\frac{1}{48} \quad , \tag{2.26}$$

or to set $c_{3,0} \equiv 0$ which leads to

$$c_{1,0} = \frac{3}{8}, \qquad c_{1,2} = \frac{1}{48} \quad , \tag{2.27}$$

which we will call the p4 action. Since for the Naik action the $\mathcal{O}(p^4)$ terms are completely eliminated one even gets an $\mathcal{O}(a^2)$ improvement, which seems quite accidental in this approach. We, however, decided to use the p4 action, which becomes clear from the high temperature limit discussed in Section 2.4.

Of course this strategy of improvement can be systematically extended to order $\mathcal{O}(g^2)$. Such an action would involve a large number of new terms, including 4-fermion operators, thus it is impractical for numerical calculation. Fat links, however, modify cutoff dependent terms in thermodynamic observables at $\mathcal{O}(g^2a^2)$ and can reduce the flavor symmetry breaking in the staggered formulation.

2.3 Lattice QCD at non-zero density

2.3.1 Introducing the chemical potential on the lattice

The commonly used way to introduce a finite chemical potential on the lattice [57, 58] is to modify the temporal links appearing in the Euclidean lattice action as follows[‡]:

$$\begin{aligned} U_4(x) &\rightarrow \exp\{a\mu\}\, U_4(x) \qquad \text{(forward temporal link)} \quad , \\ U_4^\dagger(x) &\rightarrow \exp\{-a\mu\}\, U_4^\dagger(x) \qquad \text{(backward temporal link)} \quad . \end{aligned} \tag{2.28}$$

[‡]The naive way to introduce a chemical potential is to proceed in analogy with the continuum expression. Thus one may think a similar term as in Equation (2.4), a modification of every forward temporal link with a factor $a\mu$ and every backward temporal link with a factor $-a\mu$, will do the job. However it has been shown by Karsch and Hasenfratz [57] that the naive generalization of the continuum prescription leads to quadratic divergences even for free fermions: in the continuum limit ($a \rightarrow 0$) the energy density ϵ is proportional to $(\mu/a)^2$ instead of the correct finite result $\epsilon \sim \mu^4$ (for massless fermions). The above discussed modification (2.28) yields the correct Stefan-Boltzmann value. Moreover the definition of the chemical potential on the lattice is not unique, it appears that Equation (2.28) is a special case of a whole class of actions introduced by Gavai [59].

This can be easily seen to be correct by writing the quark propagator[§] as a sum over world lines

$$\Delta^{ab}_{\alpha\beta}(x,y) = \sum_{\text{path}\,\Gamma} K^{|\Gamma|} \left\{ \prod_{\Gamma} \gamma_\mu \right\}_{\alpha\beta} \left\{ \prod_{\Gamma} U_\mu \right\}_{ab} \quad , \tag{2.29}$$

where K is the hopping parameter and Γ denotes all possible paths on the lattice, connecting the space-time points x and y. The modification (2.28) now automatically encourages time-like forward propagation and inhibits time-like backward propagation. In closed fermion loops one obtains factors of $\exp\{\pm N_\tau a\mu\} = \exp\{\pm\mu/T\}$. Notice that only those fermion loops which actually wind around the toroidal lattice pick up factors of $\exp\{\pm\mu/T\}$. All others which double back have factors that cancel, i.e. as long as the gluonic action is made of Wilson loops, it remains constant under the transformation (2.28). With these loops we can form the grand canonical partition function

$$\begin{aligned} Z(T,V,\mu) &= \int \mathcal{D}\psi\, \mathcal{D}\bar{\psi}\, \mathcal{D}U \exp\{S_F(T,V,\mu) + S_G(T,V)\} \\ &= \text{Tr } (\exp\{\mu N/T - H/T\}) \quad . \end{aligned} \tag{2.30}$$

Here N are the eigenvalues of the charge operator (Q), which correspond to the number of baryons in the system and H is the QCD Hamiltonian. (In the low energy hadronic phase non-zero net quark number density appears as non-zero net baryon number density, which is a third of the quark number density.) To achieve this result, the anti-periodic boundary conditions of the fermion fields are mandatory. Differentiating the action with respect to μ reveals the operator form of the charge [58]:

$$\begin{aligned} Q(x_4) &= \sum_{x_1,x_2,x_3} J_4(x) \\ J_4(x) &= K\left[\bar{\psi}(x)\gamma_4 e^{a\mu} U_4(x)\psi(x+\hat{4}a) - \bar{\psi}(x+\hat{4}a)\gamma_4 e^{-a\mu} U_4^\dagger(x)\psi(x)\right] \quad . \end{aligned} \tag{2.31}$$

The J_4 operator looks like the kinetic term (in the limit $a \to 0$), but counts a factor $-K$ instead of K for a downward path whenever it is used. In this way one sees that $\langle J_4(x)\rangle$ is the expectation value of the number of paths through x in the $+\hat{4}$ direction. The rest of the vector,

$$J_i = K\left[\bar{\psi}(x)\gamma_i U_i(x)\psi(x+\hat{\imath}a) - \bar{\psi}(x+\hat{\imath}a)\gamma_i U_i^\dagger(x)\psi(x)\right] \quad , \tag{2.32}$$

together with J_4 forms a conserved vector current which again counts the flux of world lines through x. The generalization to improved staggered fermion actions is straightforward. The quark matrix

[§]We use here naive fermions for reasons of simplicity. Staggered fermion as discussed above are expressed in a spin-diagonal basis. In order to connect the staggered fields to the physical quark fields one has to introduce a transformation matrix, which acts on hypercubic blocks and makes the expression a bit more complicated

we finally use (p4 action) writes

$$
\begin{aligned}
M(x,y) \;=\; & \sum_i \eta_i(x)\Big\{\frac{3}{8}\Big[U_i^{\rm fat}(x)\,\delta(x+\hat{\imath}a,\,y) - U_i^{\rm fat\dagger}(x-\hat{\imath}a)\,\delta(x-\hat{\imath}a,\,y)\Big] \\
& +\frac{1}{48}\sum_{j\neq i}\Big[U_{i,j}^{(1,2)}(x)\,\delta(x+\hat{\imath}a+2\hat{\jmath}a,\,y) - U_{i,j}^{(1,2)\dagger}(x-\hat{\imath}a-2\hat{\jmath}a)\,\delta(x-\hat{\imath}a-2\hat{\jmath}a,\,y) \\
& +U_{i,j}^{(1,-2)}(x)\,\delta(x+\hat{\imath}a-2\hat{\jmath}a,\,y) - U_{i,j}^{(1,-2)\dagger}(x-\hat{\imath}a+2\hat{\jmath}a)\,\delta(x-\hat{\imath}a+2\hat{\jmath}a,\,y)\Big] \\
& +e^{2a\mu}U_{i,4}^{(1,2)}(x)\,\delta(x+\hat{\imath}a+2\hat{4}a,\,y) - e^{-2a\mu}U_{i,4}^{(1,2)\dagger}(x-\hat{\imath}a-2\hat{4}a)\,\delta(x-\hat{\imath}a-2\hat{4}a,\,y) \\
& +e^{2a\mu}U_{i,4}^{(1,-2)}(x)\,\delta(x+\hat{\imath}a-2\hat{4}a,\,y) - e^{-2a\mu}U_{i,4}^{(1,-2)\dagger}(x-\hat{\imath}a+2\hat{4}a)\,\delta(x-\hat{\imath}a+2\hat{4}a,\,y)\Big]\Big\} \\
& +\eta_4(x)\Big\{\frac{3}{8}\Big[e^{a\mu}U_4^{\rm fat}(x)\,\delta(x+\hat{4}a,\,y) - e^{-a\mu}U_4^{\rm fat\dagger}(x-\hat{4}a)\,\delta(x-\hat{4}a,\,y)\Big] \\
& +\frac{1}{48}\sum_i\Big[e^{a\mu}U_{4,i}^{(1,2)}(x)\,\delta(x+\hat{4}a+2\hat{\imath}a,\,y) - e^{-a\mu}U_{4,i}^{(1,2)\dagger}(x-\hat{4}a-2\hat{\imath}a)\,\delta(x-\hat{4}a-2\hat{\imath}a,\,y) \\
& +e^{a\mu}U_{4,i}^{(1,-2)}(x)\,\delta(x+\hat{4}a-2\hat{\imath}a,\,y) - e^{-a\mu}U_{4,i}^{(1,-2)\dagger}(x-\hat{4}a+2\hat{\imath}a)\,\delta(x-\hat{4}a+2\hat{\imath}a,\,y)\Big]\Big\} \\
& +m\,\delta(x,\,y) \quad , \qquad (2.33)
\end{aligned}
$$

where the link matrices are as defined in Equation (2.23). Note that for any improved action involving terms in which $\bar{\psi}(x)$ and $\psi(y)$ are separated by more than a single link, there is no longer a local conserved baryon number current bilinear $J_\nu(x)$ such that $\sum_\nu \langle J_\nu(x) - J_\nu(x-\hat{\nu})\rangle = 0$ for non-zero lattice spacing.

2.3.2 The complex action problem

Having now a satisfactory definition of the chemical potential on the lattice, there are still great problems that remain when one wants to simulate QCD at non zero chemical potential ($\mu \neq 0$). Standard Monte Carlo techniques make use of the positivity of the integrand in Equation (2.13) by interpreting the Boltzmann factor

$$
\begin{aligned}
\exp\{S(m,\,\mu,\,\beta)\} &= \det\left(M^{KS}(m,\,\mu)\right)^{n_f/4}\exp\{S_G(\beta)\} \\
&= \exp\Big\{\frac{n_f}{4}\;\mathrm{Tr}\;\ln M^{KS}(m,\,\mu) + S_G(\beta)\Big\} \qquad (2.34)
\end{aligned}
$$

as probability distribution. At $\mu = 0$ the positivity of the Boltzmann factor is guaranteed by the γ_5-hermiticy of the quark matrix¶:

$$
M^\dagger(m,\,0) = \gamma_5 M(m,\,0)\gamma_5 \quad . \qquad (2.35)
$$

¶Actually for staggered fermions we have $M^\dagger_{x,y}(m,\,0) = \epsilon(x)\,M_{x,y}(m,\,0)\,\epsilon(y)$, with the phase $\epsilon(x) = (-1)^{(x_1+x_2+x_3+x_4)/a}$.

This property of the quark matrix implies $\det M(m,\,0) = (\det M(m,\,0))^*$, i.e. a real determinant. Positivity of the determinant follows from the fact, that the eigenvalues of the matrix occur in complex conjugated pairs. Monte Carlo simulations can then, for instance, be performed by using the positive definite matrix $M^\dagger M$ within the pseudo fermion method [60]. For $\mu > 0$ the Equation (2.35) does not hold any longer, instead we have the property

$$M^\dagger(m,\,\mu) = \gamma_5 M(m,\,-\mu)\gamma_5 \quad . \tag{2.36}$$

For a purely imaginary chemical potential $i\mu_I$, with $\mu_I \in \mathbb{R}$, the determinant persists to be positive and real. In the general case it is quite illuminative to analyze the spectrum of eigenvalues of the quark matrix. For free naive fermions we find in momentum space

$$\lambda_p = m \pm i\sqrt{\sum_{k=1}^{3}\sin^2(p_k) + \sin^2(p_4 + ia\mu)} \quad . \tag{2.37}$$

The mass shifted spectrum $(\lambda_p - m)$ now deviates from the imaginary axis ($\mu = 0$) by a maximum of $\max|\,\mathrm{Re}\;\lambda_p - m| = \sinh(a\mu)$. In the interacting case the same general picture holds except that eigenvalues only occur in pairs, λ and $-\lambda$ they do no longer occur in complex conjugate pairs. This means that the fermion determinant develops a complex phase and in turn also the trace of the fermion matrix. Also many physical observables, for instance quantities such as $\langle\bar\psi\psi\rangle$ or $\langle J_4\rangle$ are no longer real gauge configuration by gauge configuration — although their averages are.

In general the determinant can be factorized into a modulus ρ and a phase θ. The phase can then be added to the observable O in a Monte Carlo simulation which only uses ρ to generate statistically distributed configurations with a Boltzmann factor ρe^{S_G}. Expectation values are then defined via

$$\langle O\rangle \equiv \left\langle Oe^{i\theta}\right\rangle_\rho \Big/ \left\langle e^{i\theta}\right\rangle_\rho \quad . \tag{2.38}$$

Here we denote by $\langle\;\;\rangle_\rho$ an expectation value with the measure $|\det M|e^{S_G}$. Unfortunately we have $\left\langle e^{i\theta}\right\rangle_\rho \propto e^{-\mathrm{const.}\cdot V}$, where V is the system volume. Acquiring sufficient statistics therefore becomes exponentially difficult as the thermodynamic limit is approached. This is known as the "Sign Problem" and has plagued the study of $\mu \neq 0$ since its inception. There are essentially two approaches that promise to circumvent the problem to a large extent. For a recent overview see [61]. The approach we will follow here is to perform QCD simulations at $\mu = 0$ and attempt to continue the results to $\mu \neq 0$. This can be done either by calculating terms in the Taylor expansion about $\mu = 0$ or by directly reweighting configurations.

2.3.3 The reweighting method

The reweighting method developed by Ferrenberg and Swendsen [62, 63] is a very useful technique to investigate critical phenomena. In lattice QCD, one can in principle calculate any observable $O(w)$ from a data set obtained in simulations at w_0. Here w is to be understood as the set of all lattice parameters $w = \{m,\, \mu,\, \beta\}$. The reweighting is possible by introducing a reweighting factor $R(w, w_0)$ in the expectation value,

$$\langle O \rangle_w = \langle OR(w, w_0) \rangle_{w_0} \,/\, \langle R(w, w_0) \rangle_{w_0} \quad . \tag{2.39}$$

Here $\langle \quad \rangle_w$ denotes in contrast to Equation (2.38) the expectation value at the point w in parameter space. The reweighting factor splits into a fermionic and a gauge part and is given by

$$R(w, w_0) = [\det M(w) / \det M(w_0)] \exp\{S_G(w) - S_G(w_0)\} \quad . \tag{2.40}$$

First attempts to obtain results for $\mu \neq 0$ on the basis of this formula are due to Barbour and collaborators, which became famous as the "Glasgow method" [64]. However, since all configurations were collected at $T = 0$, the necessary overlap between the true ensemble at $T = 0$ and the interesting transition region[‖] could not be achieved and only unphysical results were produced. Multi-parameter reweighting was first applied to the problem of finite density QCD by [16]. This is mandatory to follow the critical line in the $(T,\, \mu)$ plane and ensures the overlap between both the quark-gluon and the hadronic phase on each side of the transition line. Note that the reweighting method suffers form the same general problem that leads to the sign problem, i.e. since both nominator and denominator in Equation (2.39) become exponentially small in the thermodynamic limit, the maximal reweighting distance rapidly shrinks with increasing volume. Nevertheless one is able to achieve interesting results on small volumes and a narrow region around $\mu = 0$ which is accessible by reweighting. This also allows to compute terms in the Taylor series for suitable observables. Of course derivatives with respect to μ can also be calculated at $\mu = 0$ without reweighting, this only complicates the expectation value which has to be evaluated. However the advantage is that the region of applicability of a Taylor series in μ is not influenced by the sign problem. It may nonetheless be limited by a finite radius of convergence, dictated by the presence of the critical point in the $(T,\, \mu)$ plane or an unphysical critical point in the complex μ plane.

The reweighting factor of the gauge part is easy to compute. Since the generalized Wilson actions are linear in the lattice coupling β we have

$$S_G^{(1,2)}(\beta) - S_G^{(1,2)}(\beta_0) = (\beta - \beta_0) \sum_{x,\mu>\nu} \left(\frac{5}{3} W_{\mu\nu}^{(1,1)}(x) - \frac{1}{6} W_{\mu\nu}^{(1,2)}(x) \right) \quad . \tag{2.41}$$

[‖] At $T = 0$ every observable should be independent of μ until the onset of nuclear matter at $\bar{\mu}_q \approx m_B/3$.

To compute the fermion part, in principle a calculation of the fermion determinant is required for each point (m, μ) one wants to study. Such a calculation is quite expensive. Fodor and Katz have performed such calculations, and have succeeded in tracing out the critical line and locating the critical end point on small lattices [9]. As far as one is interested in the first derivatives of thermodynamic observables with respect to μ, the fermionic part of the reweighting factor can also be expanded [19]. In fact, one expands in the lattice chemical potential $\mu = a\mu_q$ while the physically relevant parameter which ultimately governs the convergence of the series is $\mu_q/T \equiv N_\tau \mu$ or the fugacity $\exp\{\mu_q/T\}$. The Taylor expansion for the fermionic part of the reweighting factor around $\mu = 0$ is

$$\begin{aligned} \frac{n_f}{4} \ln\left(\frac{\det M(\mu)}{\det M(0)}\right) &= \frac{n_f}{4} \sum_{n=1}^{\infty} \frac{\mu^n}{n!} \frac{\partial^n \ln\det M(\mu)}{\partial \mu^n} \\ &\equiv \sum_{n=1}^{\infty} \mathcal{R}_n \mu^n \quad . \end{aligned} \tag{2.42}$$

We similarly expand fermionic observables such as the chiral condensate, which is given by the trace of the inverse of the fermion matrix:

$$\left\langle \bar{\psi}\psi \right\rangle = \frac{n_f}{4} \left\langle \text{ Tr } M^{-1} \right\rangle \quad . \tag{2.43}$$

Using the following identity for the derivative of the inverse of a matrix

$$\frac{\partial M^{-1}}{\partial x} = -M^{-1} \frac{\partial M}{\partial x} M^{-1} \quad , \tag{2.44}$$

expressions for $\partial^n(\ln\det M)/\partial\mu^n$ and $\partial^n(\text{ Tr } M^{-1})/\partial\mu^n$ in terms of traces over products of local operators and inverse matrices can be developed:

$$\frac{\partial(\ln\det M)}{\partial\mu} = \text{Tr}\left(M^{-1}\frac{\partial M}{\partial\mu}\right) \quad , \tag{2.45}$$

$$\frac{\partial^2(\ln\det M)}{\partial\mu^2} = \text{Tr}\left(M^{-1}\frac{\partial^2 M}{\partial\mu^2}\right) - \text{Tr}\left(M^{-1}\frac{\partial M}{\partial\mu}M^{-1}\frac{\partial M}{\partial\mu}\right) \quad , \tag{2.46}$$

$$\frac{\partial \text{ Tr } M^{-1}}{\partial\mu} = -\text{Tr}\left(M^{-1}\frac{\partial M}{\partial\mu}M^{-1}\right) \quad , \tag{2.47}$$

$$\frac{\partial^2 \text{ Tr } M^{-1}}{\partial\mu^2} = -\text{Tr}\left(M^{-1}\frac{\partial^2 M}{\partial\mu^2}M^{-1}\right) + 2\,\text{Tr}\left(M^{-1}\frac{\partial M}{\partial\mu}M^{-1}\frac{\partial M}{\partial\mu}M^{-1}\right) \quad . \tag{2.48}$$

Further derivatives of $\ln\det M$ up to $\partial^4/\partial\mu^4$ are given in the Chapter 4. This notation is quite useful because it now is possible to apply the random noise method, which enables us to compute on rather large volumes in comparison with other studies of QCD with $\mu \neq 0$ [9, 17]. Using N random noise vectors η_{ki}, where the index k labels the noise vector and the index i is the

internal index of the vector running over the lattice points, we rewrite the traces appearing in the Equations (2.45)-(2.48) as

$$\mathrm{Tr}\left(\frac{\partial^{n_1} M}{\partial\mu^{n_1}} M^{-1} \frac{\partial^{n_2} M}{\partial\mu^{n_2}} \cdots M^{-1}\right) = \lim_{N\to\infty} \frac{1}{N} \sum_{k=1}^{N} \eta_k^\dagger \frac{\partial^{n_1} M}{\partial\mu^{n_1}} M^{-1} \frac{\partial^{n_2} M}{\partial\mu^{n_2}} \cdots M^{-1} \eta_k \quad . \tag{2.49}$$

Here the random vectors have to satisfy the condition $\lim_{N\to\infty}(1/N)\sum_{k=1}^{N} \eta_{ki}^* \eta_{kj} = \delta_{ij}$. The expressions $M^{-1}\eta_k \equiv x$ and $M^{-1}(\partial M/\partial\mu)\cdots\eta_k \equiv x$ are then obtained by solving $Mx = \eta_k$ and $Mx = (\partial M/\partial\mu)\cdots\eta_k$. The right-hand site (RHS) of Equation (2.49) can be approximated by using a finite number of noise vectors N. The error is expected to decrease as $(N \times N_{\mathrm{conf}})^{-1/2}$, where N_{conf} is the number of configurations.

By using the derivatives of both the reweighting factor and fermionic observable up to n-th order in μ we obtain the observable as a continuous function for small μ, which is correct up to the n-th order. To be more specific, let us define the Taylor expansion of an operator O by $O(\mu) \equiv \sum_{n=0}^{\infty} O_n \mu^n$. Then to $\mathcal{O}(\mu^2)$ the expression 2.39 for $\langle O\rangle_{(\beta,\,\mu)}$ can be written as

$$\langle O\rangle_{\beta,\,\mu} = \frac{\left\langle (O_0 + O_1\mu + O_2\mu^2)\exp\{\mathcal{R}_1\mu + \mathcal{R}_2\mu^2 - \Delta S_G\}\right\rangle}{\langle \exp\{\mathcal{R}_1\mu + \mathcal{R}_2\mu^2 - \Delta S_G\}\rangle} \quad , \tag{2.50}$$

where expectation values on the RHS are measured with respect to an ensemble generated at $(\beta_0,\, 0)$ and ΔS_G is the gauge action difference corresponding to Equation (2.41). The extension to multi-histogram reweighting, i.e. using several ensembles generated on different points $(\beta_i,\, 0)$ is straightforward [63]. For pure gluonic operators such as the Polyakov loop, we do not need the expansion of the operator itself, since it does not depend on the chemical potential. Furthermore, we should note that at $\mu = 0$ the odd order derivatives of both $\ln\det M$ and $\mathrm{Tr}\, M^{-1}$ are purely imaginary and the even order derivatives are real, we find

$$\begin{aligned} \left(\frac{\partial^n \ln\det M}{\partial\mu^n}\right)^* &= (-1)^n \frac{\partial^n \ln\det M}{\partial\mu^n} \quad , \\ \left(\frac{\partial^n\, \mathrm{Tr}\, M^{-1}}{\partial\mu^n}\right)^* &= (-1)^n \frac{\partial^n\, \mathrm{Tr}\, M^{-1}}{\partial\mu^n} \quad . \end{aligned} \tag{2.51}$$

Using this property and the fact that Z is a real function of β, m, and μ we can explicitly confirm that all odd order derivatives of expectation values of physical observables are zero at $\mu = 0$. This is what we expect from the invariance of physics under changing μ to $-\mu$, i.e. by interchanging particles and anti-particles.

In order to discuss the region of applicability of the reweighting approach we have to analyze the complex phase of the determinant. It can be expressed in terms of odd order derivatives:

$$\theta = \frac{n_f}{4}\mathrm{Im}\left[\mu\frac{\partial \ln\det M}{\partial\mu} + \frac{\mu^3}{3!}\frac{\partial^3 \ln\det M}{\partial\mu^3} + \cdots\right] \quad . \tag{2.52}$$

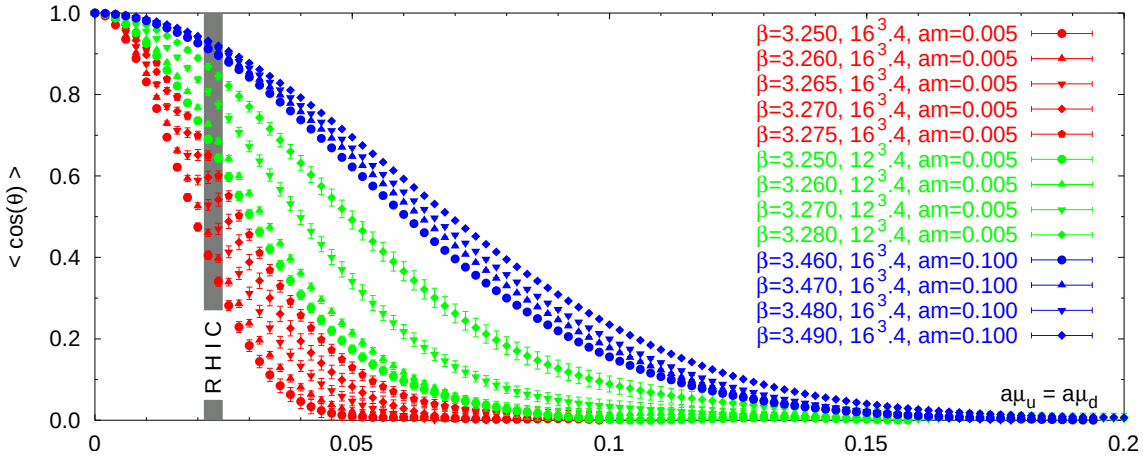

Figure 2.1: The suppression factor $\langle cos(\theta)\rangle$ from the complex phase θ of the determinant of the quark matrix for three degenerate flavors and several lattice sizes and simulation points (β, m), as a function of the up and down quark chemical potential $(a\mu_{u,d})$.

The reweighting factor is suppressed with Re $(e^{i\theta})$. We thus consider first the expectation value $\langle\cos(\theta)\rangle$ in Figure 2.1, which gives an impression of the maximal reweighting distance. A small value for the expectation value $\langle\cos(\theta)\rangle$ indicates that frequent changes of the sign of the reweighting factor occur. The phase was approximated by cutting the series (2.52) after the first term. Although all the data we show in Figure 2.1 are form simulations with three degenerate flavors of quarks, the lattice chemical potential on the x axis is only the up and down quark chemical potential, the strange quark chemical potential was taken to be zero during the reweighting. We find, however, no difference in the magnitude of the suppression factor $\langle\cos(\theta)\rangle$ when simulating either $n_f = 2$ or $n_f = 3$ quark flavors with the large quark mass $am = 0.1$, but reweighting a two flavor chemical potential in both cases. This can be seen in Table 2.1, where we analyze the fluctuations of the phase in detail. Although the average of the phase remains zero, its fluctuations increase with the chemical potential and force the suppression factor $\langle\cos(\theta)\rangle$ to decrease (sign In). problem Table 2.1 we give the standard deviation (STD) of $(N_\sigma^3 N_\tau)^{-1}$ Im Tr $[(\partial M/\partial\mu)M^{-1}]$. From this value we can estimate when the sign problem becomes serious. This is when the fluctuations of the leading term in Equation (2.52) become of order $\mathcal{O}(1)$. We define a maximal chemical potential by $a\mu_2^{\max}$ which is reached when the fluctuations become $\pi/2$. The index 2 denotes that the flavor factor in Equation (2.52) was set to two, independent of the number of dynamical flavors used for the simulation. We find values from $0.08 - 0.09$ for $am = 0.1$ on a $16^3 \times 4$ lattice. For decreasing masses and increasing volume these numbers become smaller. Nevertheless in all cases the reweighting range is broad enough to extract physical results in the RHIC regime. Moreover

$12^3 \times 4, \qquad n_f = 3$

m	β	$\left\langle \text{ Im Tr } [(\partial M/\partial\mu)M^{-1}] \right\rangle$	$\langle\epsilon\rangle$	STD	STD(impr.)	$a\mu_2^{\max}$
0.005	3.250	$2.00 \cdot 10^{-4}$	$1.11 \cdot 10^{-2}$	$1.14 \cdot 10^{-2}$	$8.46 \cdot 10^{-4}$	0.040
	3.260	$-2.28 \cdot 10^{-4}$	$1.01 \cdot 10^{-2}$	$1.06 \cdot 10^{-2}$	$2.42 \cdot 10^{-3}$	0.043
	3.270	$1.22 \cdot 10^{-4}$	$8.19 \cdot 10^{-3}$	$8.67 \cdot 10^{-3}$	$1.92 \cdot 10^{-3}$	0.052
	3.280	$1.90 \cdot 10^{-4}$	$6.67 \cdot 10^{-3}$	$7.02 \cdot 10^{-3}$	$1.36 \cdot 10^{-3}$	0.065

$16^3 \times 4, \qquad n_f = 3$

m	β	$\left\langle \text{ Im Tr } [(\partial M/\partial\mu)M^{-1}] \right\rangle$	$\langle\epsilon\rangle$	STD	STD(impr.)	$a\mu_2^{\max}$
0.005	3.250	$-9.48 \cdot 10^{-8}$	$7.09 \cdot 10^{-3}$	$7.43 \cdot 10^{-3}$	$1.72 \cdot 10^{-3}$	0.026
	3.260	$-1.24 \cdot 10^{-4}$	$6.49 \cdot 10^{-3}$	$6.94 \cdot 10^{-3}$	$2.07 \cdot 10^{-3}$	0.028
	3.265	$-6.89 \cdot 10^{-5}$	$6.00 \cdot 10^{-3}$	$6.32 \cdot 10^{-3}$	$1.54 \cdot 10^{-3}$	0.030
	3.270	$8.52 \cdot 10^{-5}$	$5.39 \cdot 10^{-3}$	$5.69 \cdot 10^{-3}$	$1.43 \cdot 10^{-3}$	0.034
	3.275	$1.68 \cdot 10^{-5}$	$4.90 \cdot 10^{-3}$	$5.22 \cdot 10^{-3}$	$1.47 \cdot 10^{-3}$	0.037
0.100	3.460	$-1.39 \cdot 10^{-5}$	$2.09 \cdot 10^{-3}$	$2.38 \cdot 10^{-3}$	$1.03 \cdot 10^{-3}$	0.081
	3.470	$-2.00 \cdot 10^{-5}$	$2.04 \cdot 10^{-3}$	$2.28 \cdot 10^{-3}$	$0.89 \cdot 10^{-3}$	0.084
	3.480	$-1.39 \cdot 10^{-5}$	$1.98 \cdot 10^{-3}$	$2.19 \cdot 10^{-3}$	$0.79 \cdot 10^{-3}$	0.088
	3.490	$3.12 \cdot 10^{-5}$	$1.93 \cdot 10^{-3}$	$2.08 \cdot 10^{-3}$	$0.64 \cdot 10^{-3}$	0.092

$16^3 \times 4, \qquad n_f = 2$

m	β	$\left\langle \text{ Im Tr } [(\partial M/\partial\mu)M^{-1}] \right\rangle$	$\langle\epsilon\rangle$	STD	STD(impr.)	$a\mu_2^{\max}$
0.100	3.640	$-1.15 \cdot 10^{-4}$	$1.99 \cdot 10^{-3}$	$2.33 \cdot 10^{-3}$	$1.10 \cdot 10^{-3}$	0.082
	3.650	$1.02 \cdot 10^{-5}$	$1.94 \cdot 10^{-3}$	$2.23 \cdot 10^{-3}$	$0.99 \cdot 10^{-3}$	0.086
	3.660	$-3.06 \cdot 10^{-5}$	$1.89 \cdot 10^{-3}$	$2.12 \cdot 10^{-3}$	$0.77 \cdot 10^{-3}$	0.090
	3.670	$-1.40 \cdot 10^{-5}$	$1.85 \cdot 10^{-3}$	$2.06 \cdot 10^{-3}$	$0.85 \cdot 10^{-3}$	0.093

Table 2.1: The average of $\left\langle \text{ Im Tr } [(\partial M/\partial\mu)M^{-1}] \right\rangle$, its error for each configuration $\langle\epsilon\rangle$, its standard deviation (STD) and improved standard deviation (STD(impr.)) and the maximal chemical potential for two flavor reweighting ($a\mu_2^{\max}$).

we note once again, that the analytic continuation of physical quantities is not restricted by the reweighting range. This is also true in the case when the analytic coefficients of the Taylor series are obtained from reweighted data.

We should also mention that the value of Im Tr $[(\partial M/\partial\mu)M^{-1}]$ calculated on each configuration also contains an error due to the finite number N of noise vectors. For $N = 10 - 15$ this error is not small compared to the STD, as seen in Table 2.1. The phase fluctuation discussed above includes the error due to finite N, and we suspect that the true fluctuations become smaller as N increases. To confirm this, we reanalyzed the standard deviation STD= $\sqrt{\langle\{ \text{Im Tr } [(\partial M/\partial\mu)M^{-1}]\}^2\rangle - \langle \text{Im Tr } [(\partial M/\partial\mu)M^{-1}]\rangle^2}$ by treating the calculation of $\langle\{ \text{Im Tr } [(\partial M/\partial\mu)M^{-1}]\}^2\rangle$ more carefully. Since the noise sets must be independent, we subtract the contributions from using the same noise vector for each factor. Details are given in the Appendix C.2. The results are quoted as STD(impr.) in Table 2.1. They are expected to be closer to the $N = \infty$ limit and indeed suggest that the STD becomes considerably smaller for larger N and the region of applicability becomes wider as N increases.

The above outlined method for reweighting in the chemical potential can also be used for quark mass reweighting. In that case the corresponding Taylor series in the quark mass m around the simulation point (β_0, m_0, 0) have to be used in Equation (2.50).

2.4 Analyzing the cutoff dependence

In this Section we discuss the influence of a non-zero chemical potential μ_q on the cutoff effects present in calculations of bulk thermodynamic observables on a lattice with finite temporal extent N_τ. For $\mu_q = 0$ this issue has been discussed extensively for both gluonic and fermionic sectors of QCD. In particular, it has been shown that the use of improved actions is mandatory if one wants to ensure that discretization errors in the calculation of quantities like the pressure p or energy density ϵ are below the 10% level already on moderately sized lattices $N_\tau \lesssim (8 - 10)$ [24]. We now want to extend these considerations to the case $\mu_q \neq 0$, which affects the quark sector only. Following [24] we will concentrate on an evaluation of the pressure. As we will be evaluating thermodynamic quantities using a Taylor expansion in μ_q/T we want to understand the cutoff dependence of $p(\mu_q)$ and its expansion coefficients in terms of μ_q/T.

In the limit of high temperature or density, due to asymptotic freedom thermodynamic observables like p or ϵ are expected to approach their free gas, ie. Stefan-Boltzmann (SB) values. In this limit cutoff effects become most significant as the relevant momenta of partons contributing to the thermodynamics are $\mathcal{O}(T)$ and thus of similar magnitude as the UV cutoff a^{-1}. Short

distance properties thus dominate the ideal gas behavior and cutoff effects, which are controlled by the lattice spacing expressed in units of the temperature, $Ta \equiv 1/N_\tau$, are expected to become important. In the continuum the pressure of an ideal gas of quarks and anti-quarks is given by

$$\frac{p}{T^4}\Big|_\infty = \frac{3n_f}{\pi^2 T^3}\int_0^\infty dk\, k^2 \ln\left[(1+z\exp\{-\varepsilon(k)/T\})(1+z^{-1}\exp\{-\varepsilon(k)/T\})\right] \quad , \tag{2.53}$$

with the fugacity $z \equiv \exp\{\mu_q/T\}$ and the relativistic single particle energies $\varepsilon(k) = \sqrt{k^2+m^2}$. For massless quarks one finds from an evaluation of the integral the pressure as a finite polynomial in μ_q/T:

$$\frac{p}{T^4}\Big|_\infty = \frac{7n_f\pi^2}{60} + \frac{n_f}{2}\left(\frac{\mu_q}{T}\right)^2 + \frac{n_f}{4\pi^2}\left(\frac{\mu_q}{T}\right)^4 \quad . \tag{2.54}$$

For m non-zero the pressure is a series in the fugacity:

$$\frac{p}{T^4} = \left(\frac{m}{T}\right)^2 \frac{n_f}{2\pi^2}\sum_{\ell=1}^{\infty}(-1)^{\ell+1}\,\ell^{-2}\,K_2(\ell m/T)\,(z^\ell + z^{-\ell}) \quad , \tag{2.55}$$

where K_2 is a Bessel function. Of course, Equation (2.55) can also be reorganized as a power series in μ_q/T. It is well known that the straightforward lattice representation of the QCD partition function in terms of the standard Wilson gauge and staggered fermion actions leads to a systematic $\mathcal{O}(a^2)$ cutoff dependence of physical observables. In the infinite temperature limit this gives rise to $\mathcal{O}((aT)^2 \equiv 1/N_\tau^2)$ deviations of the pressure from the SB value (2.54);

$$\frac{p}{T^4}\Big|_{N_\tau} = \frac{p}{T^4}\Big|_\infty + \frac{d}{N_\tau^2} + O(N_\tau^{-4}) \quad . \tag{2.56}$$

Using improved discretization schemes it is possible to ensure that cutoff effects only start to contribute at $\mathcal{O}(N_\tau^{-4})$ [56], or to considerably reduce the magnitude of the coefficient d relative to the standard discretization scheme for staggered fermions [24].

For $\mu_q = 0$ the pressure of free staggered fermions on lattices with infinite spatial volume ($N_\sigma = \infty$) but finite temporal extent N_τ is given by

$$\begin{aligned}\frac{p}{T^4}\Big|_{N_\tau} &= \frac{3}{8}n_f N_\tau^4 \frac{1}{(2\pi)^3}\int_0^{2\pi} d^3\vec{p}\Bigg[N_\tau^{-1}\sum_{p_4}\ln\left(\omega^2(p)+4f_4^2(p)\right) \\ &\quad -\frac{1}{2\pi}\int_0^{2\pi} dp_4 \ln\left(\omega^2(p)+4f_4^2(p)\right)\Bigg] \quad .\end{aligned} \tag{2.57}$$

In the first term the sum $\sum_{p_4}$ runs over all discrete Matsubara modes, i.e. $p_4 \in \{(2n+1)\pi/N_\tau | n = 0,\ldots,N_\tau-1\}$, whereas in the second term we have an integral over p_4 which gives the vacuum contribution. For quarks of mass m the function $\omega^2(p)$ is given by $\omega^2(p) \equiv 4\sum_{\mu=1}^3 f_\mu^2(p) +$

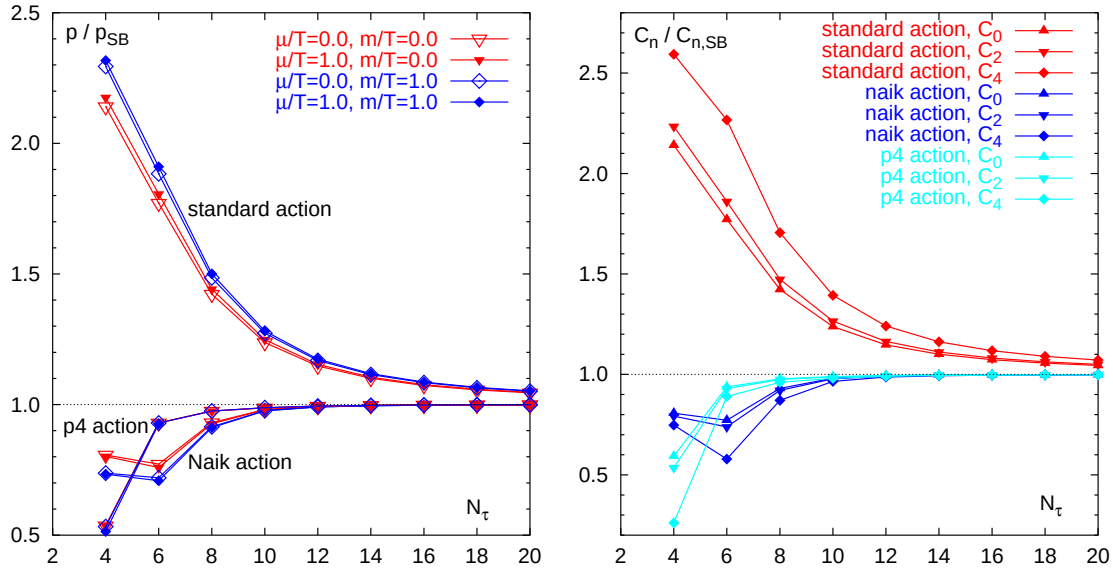

Figure 2.2: The pressure calculated on lattices with temporal extent N_τ in units of the continuum ideal Fermi gas value. (a) shows results for the standard, Naik and p4 actions at $(\mu_q/T,\, m/T) = (0,\, 0),\, (0,\, 1), (1,\, 0)$ and $(1,\, 1)$; (b) the coefficients $\mathcal{C}_0$, $\mathcal{C}_2$, $\mathcal{C}_4$ of the μ_q/T expansion of $p(m/T = 0)$ divided by the corresponding SB constant as a function of N_τ.

$N_\tau^{-2}(m/T)^2$. Here we have introduced functions $f_\mu(p)$ to describe the momentum dependence of the propagator for the standard, Naik [56] and p4 staggered fermion actions [24]:

$$f_\mu(p) = \frac{1}{2}\sin p_\mu \qquad \text{(standard staggered action)} \quad , \tag{2.58}$$

$$f_\mu(p) = \frac{9}{16}\sin p_\mu - \frac{1}{48}\sin 3p_\mu \qquad \text{(Naik action)} \quad , \tag{2.59}$$

$$f_\mu(p) = \frac{3}{8}\sin p_\mu + \frac{2}{48}\sin p_\mu \sum_{\nu\neq\mu}\cos 2p_\nu \qquad \text{(p4 action)} \quad . \tag{2.60}$$

The introduction of a non-zero chemical potential is easily achieved by substituting every temporal momentum p_4 by $p_4 - i\mu \equiv p_4 - iN_\tau^{-1}(\mu_q/T)$. The integrals in Equation (2.57) have been evaluated numerically for different N_τ. Results for different values of μ_q/T and m/T are shown for the different fermion actions in Figure 2.2. For the standard action cutoff effects remain $\geq 10\%$ out to $N_\tau \approx 16$, whereas both improved actions are hard to distinguish from the continuum result at $N_\tau = 10$. We note that lines for different μ_q/T values but the same quark mass fall almost on top of each other. Cutoff effects are thus almost independent of μ_q. The effect of $\mu_q \neq 0$ on the cutoff dependence of the pressure is even smaller than the effect of quark mass $m \neq 0$.

As can be seen from Equation (2.54) for moderate values of μ_q/T the μ-dependence of the continuum ideal gas pressure is dominated by the leading $\mathcal{O}((\mu_q/T)^2)$ contribution. In order to

control the cutoff dependence of the various expansion terms we have expanded the integrand of Equation (2.57) up to order $\mathcal{O}((\mu_q/T)^6)$. For the standard action the series starts with

$$\begin{aligned}
\ln\left(\omega^2(p) + \sin^2\left(p_4 - \frac{i}{N_\tau}\frac{\mu_q}{T}\right)\right) \;=\; & \ln D \\
- \quad & \frac{2i\cos p_4 \sin p_4}{D\,N_\tau}\left(\frac{\mu_q}{T}\right) \\
- \quad & \frac{-1 + 4\,D\,\cos 2p_4 + \cos 4p_4}{4\,D^2\,N_\tau^2}\left(\frac{\mu_q}{T}\right)^2 \\
- \quad & \frac{i\,\left(-1 + 4\,D^2 + 6\,D\,\cos 2p_4 + \cos 4p_4\right)\,\sin 2p_4}{6\,D^3\,N_\tau^3}\left(\frac{\mu_q}{T}\right)^3 \\
+ \quad & O\left(\left(\frac{\mu_q}{T}\right)^4\right) \quad .
\end{aligned} \tag{2.61}$$

Here we use the shorthand notation $D = 4\sum_{\mu=1}^{4} f_\mu^2(p)$. The remaining orders as well as the series for Naik and p4 actions are given in Appendix A. A common feature of these expansions is that the odd terms are pure imaginary and the integral and sum over p_4 of those terms vanish due to a factor $\sin(np_4)$ which always appears. To be more precise, this factor always forms the pattern $\sin(np_4)\cos(mp_4)$ which can be shown to vanish, either after summation over the discrete set of p_4 values, or integration from 0 to 2π, for n, $m \in \mathbb{N}$. Performing the momentum integration and the summation over Matsubara modes we obtain the coefficients of the μ_q/T expansion of the pressure;

$$\left.\frac{p}{T^4}\right|_{N_\tau} = n_f \sum_{i=0}^{\infty} \left.\mathcal{C}_i\right|_{N_\tau} \left(\frac{\mu_q}{T}\right)^i \quad . \tag{2.62}$$

We checked numerically that with increasing N_τ the coefficients $\mathcal{C}_0$, $\mathcal{C}_2$ and $\mathcal{C}_4$ do indeed converge to their corresponding SB values,

$$\lim_{N_\tau\to\infty} \mathcal{C}_0 = \frac{7\pi^2}{60} \quad ; \qquad \lim_{N_\tau\to\infty} \mathcal{C}_2 = \frac{1}{2} \quad ; \qquad \lim_{N_\tau\to\infty} \mathcal{C}_4 = \frac{1}{4\pi^2} \quad . \tag{2.63}$$

Figure 2.2(b) shows $\mathcal{C}_0$, $\mathcal{C}_2$ and $\mathcal{C}_4$ for the standard, Naik and p4 actions with massless quarks, normalized to the corresponding SB value. We see here again that the cutoff dependence of the pressure at $\mu \neq 0$ is qualitatively the same as at $\mu = 0$.

For massless quarks the coefficient $\mathcal{C}_6$ should vanish with increasing N_τ, as checked in Figure 2.3(a). It is expected that this term will approach zero like N_τ^{-2} in the large N_τ limit. In order to define the numerical factor, we plot $\mathcal{C}_6 N_\tau^2$ over N_τ^{-2}. A fit yields $\mathcal{C}_6 \approx -0.015\,N_\tau^{-2}$ for the standard action. This is at least an order of magnitude larger than for the p4 improved action, for which the dominant cutoff dependence seems to be $\mathcal{O}(N_\tau^{-4})$ as for the Naik action.

In the case of massive quarks the expansion (2.62) no longer terminates at $\mathcal{O}(\mu_q^4)$. After expanding (2.53) in terms of μ_q/T and performing a numerical integration we find for the expansion

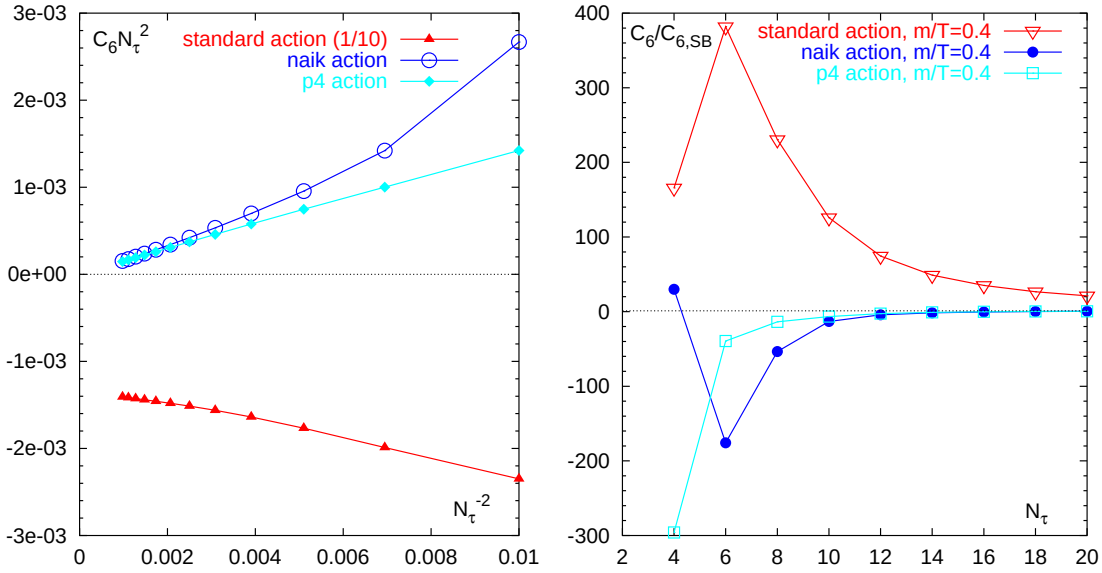

(a) (b)

Figure 2.3: (a) The coefficients $\mathcal{C}_6$ in the massless case, multiplied with N_τ^2 as a function of N_τ^{-2} (results for standard staggered fermions are divided by 10) and (b) the ratio $\mathcal{C}_6(N_\tau)/\mathcal{C}_6(\infty)$ at $m/T = 0.4$ for the standard, Naik and p4 actions.

coefficients $\mathcal{C}_i(m/T)$ up to $i = 6$ the values given in Table 2.2. The mass value $m/T = 0.4$ is the value we use in our numerical calculations, corresponding to $N_\tau = 4$ and $am = 0.1$. We note that the coefficient $\mathcal{C}_6$ no longer vanishes. As shown in Figure 2.3(b), for N_τ finite there are large deviations from the continuum value. Even at $N_\tau = 4$, however, the absolute value of this coefficient is still a factor of about 10^{-4} smaller than the leading term $\mathcal{C}_0$. The deviations thus do not show up in the calculation of the complete expression for the pressure shown in Figure 2.2(a). These terms, however, become more important in higher derivatives of the pressure such as the quark number susceptibility χ_q. In summary, for a gas of free quarks we find that the μ_q/T expansion up to $O((\mu_q/T)^4)$ is sufficient for $\mu_q/T < 1$ and $m/T < 1$. In the continuum the deviation from the full expression over this range is smaller than 0.01%. On the lattice, however, cutoff effects lead to deviations of approximately 10% on coarse ($N_\tau = 4$) lattices.

	$m/T = 0.4$		$m/T = 1.0$	
i	$\mathcal{C}_i(m/T)$	$\mathcal{C}_i(m/T)/\mathcal{C}_i(0)$	$\mathcal{C}_i(m/T)$	$\mathcal{C}_i(m/T)/\mathcal{C}_i(0)$
0	1.113632	0.967	$9.528163 \cdot 10^{-1}$	0.827
2	$4.880455 \cdot 10^{-1}$	0.976	$4.313914 \cdot 10^{-1}$	0.863
4	$2.531101 \cdot 10^{-2}$	0.999	$2.471397 \cdot 10^{-2}$	0.976
6	$1.877659 \cdot 10^{-6}$	—	$5.036816 \cdot 10^{-5}$	—

Table 2.2: Continuum values for the coefficients $\mathcal{C}_i$ of the μ_q/T expansion of the pressure of a massive gas of quarks for the mass values $m/T = 0.4$ and $m/T = 1.0$.

Chapter 3

The phase diagram

The properties of the QCD phase transition depend on the number of flavors and their masses. We do expect that the nature of the transition, e.g. its order and details of the critical behavior, are controlled by global symmetries of the QCD Lagrangian. Exact global symmetries only exist in the limits of either infinite or vanishing quark masses. For any non-zero, finite value of quark masses the global symmetries are explicitly broken. In fact, in the case of QCD the explicit global symmetry breaking induced by the finite quark mass is very much similar to that induced by an external ferromagnetic field in spin models. We thus expect that a continuous phase transition, which may exist in the zero or infinite quark mass limit, will turn into a non-singular crossover behavior for any finite value of quark mass. On the other hand a possible first order transition may persist for some time before it ends in a continuous transition. The question is whether or not the QCD physical point, which is QCD with the physically realized spectrum of quark masses, is near a true phase transition. Note that also in the most likely case of a smooth crossover the fluctuations in an appropriate order parameter, induced by a nearby critical point, could be large enough to provide measurable effects in heavy ion collisions in terms of event-by-event fluctuations [5]. This question is however a quantitative question, which we have to answer through direct numerical calculations.

3.1 The deconfinement and chiral phase transition

The most important observables we should analyze in order to map out the QCD phase diagram are the order parameters of the deconfinement and chiral phase transitions occurring in the infinite mass and zero mass limit, respectively. As already mentioned, we have exact global symmetries only

in these two limiting cases. In the limit of infinitely heavy quarks, the pure gauge limit, the QCD Lagrangian is invariant under generalized gauge transformations. These are gauge transformations, which are periodic in time direction up to an element of the center of the gauge symmetry group. This is the so called $Z(3)$-center symmetry of the pure gauge theory. Sensitive to this symmetry is the Polyakov loop, which winds around the lattice in time direction,

$$L(\vec{x}) = \mathrm{Tr} \prod_{k=0}^{N_\tau} U_4(\vec{x}, ka) \quad . \tag{3.1}$$

The Polyakov loop has a physical interpretation also. It describes the world line of a static quark source at the point $\vec{x}$. The large distance behavior of the heavy quark free energy, $F_{\bar{q}q}$, provides a unique distinction between confinement below T_c and deconfinement for $T > T_c$. The heavy quark free energy* can be calculated from the expectation value of the Polyakov loop correlation function

$$\exp\left\{-\frac{F_{\bar{q}q}(r,T)}{T}\right\} = \left\langle \mathrm{Tr}\, L(\vec{x})\, \mathrm{Tr}\, L^\dagger(\vec{y})\right\rangle \quad . \tag{3.2}$$

For large separations ($r = |\vec{x} - \vec{y}| \to \infty$) the correlation function approaches $|\langle L\rangle|^2$, where $\langle L\rangle = \langle \sum_{\vec{x}} \mathrm{Tr}\, L(\vec{x})\rangle$ denotes the Polyakov loop expectation value which therefore characterizes the behavior of the heavy quark free energy at large distances and is an order parameter for deconfinement in the $SU(3)$ gauge theory,

$$\langle L\rangle \begin{cases} = 0 & \Leftrightarrow \quad \text{confined phase}, \quad T < T_c \\ > 0 & \Leftrightarrow \quad \text{deconfined phase}, \quad T > T_c \end{cases} \quad . \tag{3.3}$$

In the limit of vanishing quark masses the classical QCD Lagrangian is invariant under chiral symmetry transformations; for n_f massless quark flavors the symmetry is $U_V(1) \times U_A(1) \times SU_L(n_f) \times SU_R(n_f)$. Only the $SU(n_f)$ flavor part of this symmetry is spontaneously broken in the vacuum, which gives rise to $(n_f^2 - 1)$ Goldstone particles, the pions. The axial $U_A(1)$ symmetry is realized in the classical Lagrangian, but not a property of the QCD partition function. There it is explicitly broken due to quantum corrections, the axial anomaly, and is replaced by a discrete $Z(n_f)$ symmetry. The basic observable which reflects the chiral properties of QCD is the chiral condensate,

$$\left\langle \bar{\psi}\psi\right\rangle = \frac{\partial}{\partial m_q} \ln Z = \frac{n_f}{4} \left\langle \mathrm{Tr}\, M^{-1}\right\rangle \quad . \tag{3.4}$$

*In the $T \to 0$ limit this is just the heavy quark potential; at non-zero temperature $F_{\bar{q}q}$ does, however, also include a contribution from the overall change of entropy that arises from the presence of external quark and anti-quark sources.

It is thus an obvious order parameter in the chiral limit,

$$\langle\bar{\chi}\chi\rangle \begin{cases} > 0 & \Leftrightarrow \quad \text{symmetry broken phase,} \quad T < T_c \\ = 0 & \Leftrightarrow \quad \text{symmetric phase,} \qquad\quad T > T_c \end{cases} \quad . \tag{3.5}$$

Closely related to the two order parameters $\langle L\rangle$ and $\langle\bar{\psi}\psi\rangle$ are the corresponding susceptibilities, the Polyakov loop susceptibility (χ_L) and the chiral susceptibility ($\chi_{\bar{\psi}\psi}$)[†],

$$\chi_L = N_\sigma^{-3}\left(\langle L^2\rangle - \langle L\rangle^2\right) = N_\sigma^{-3}\left\langle(\delta L)^2\right\rangle \quad , \tag{3.6}$$

$$\chi_{\bar{\psi}\psi} = N_\sigma^{-3}N_\tau^{-1}\left(\left\langle(\bar{\psi}\psi)^2\right\rangle - \left\langle\bar{\psi}\psi\right\rangle^2\right) = N_\sigma^{-3}N_\tau^{-1}\left\langle(\delta\bar{\psi}\psi)^2\right\rangle \quad . \tag{3.7}$$

Here we introduce the normalized operator, $\delta X = X - \langle X\rangle$, for any operator X. Note that $\langle L\rangle$ and $\langle\bar{\psi}\psi\rangle$ are defined to be extensive quantities. The susceptibilities measure the fluctuations of the related operator and in case of χ_L and $\chi_{\bar{\psi}\psi}$ peaks in the susceptibilities thus signal a sudden change in the order parameters $\langle L\rangle$ and $\langle\bar{\psi}\psi\rangle$. χ_L and $\chi_{\bar{\psi}\psi}$ are expected to diverge at a true phase transition point. Away from the thermodynamic limit, i.e. in a finite volume, or at a quark mass which corresponds to the crossover regime, those divergencies weaken to a well pronounced peak. This is shown in Figure 3.1 for the case of 3-flavor QCD with light quarks. The simulations have been performed with the p4 improved action on a $16^3 \times 4$ lattice and a quark mass of $m = 0.005$. This is an almost realistic quark mass value, which corresponds to a pion mass of $m_\pi \approx 170$ MeV. We calculate the observables for 7 different values of the gauge coupling in the interval $\beta \in [3.25, 3.285]$. We then made use of the reweighting formula (2.39) to obtain results for different quark masses. The logarithm of the reweighting factor was Taylor expanded in the quark mass up to order $\mathcal{O}(\Delta m^2)$, which gives in analogy to Equation (2.42)

$$\begin{aligned} \frac{n_f}{4}\ln\left(\frac{\det M(m)}{\det M(m_0)}\right) &= \frac{n_f}{4}\Big(\ \mathrm{Tr}\ \left(M^{-1}\right)(m-m_0) - \ \mathrm{Tr}\ \left(M^{-1}M^{-1}\right)(m-m_0)^2/2 \\ &+ \ \mathcal{O}\left((m-m_0)^3\right)\Big) \quad . \end{aligned} \tag{3.8}$$

The Polyakov loop itself is independent of the quark mass, while the chiral condensate was expanded up to order $\mathcal{O}(\Delta m)$,

$$\bar{\psi}\psi = \frac{n_f}{4}\Big(\ \mathrm{Tr}\ \left(M^{-1}\right) - \ \mathrm{Tr}\ \left(M^{-1}M^{-1}\right)(m-m_0) + \mathcal{O}\left((m-m_0)^2\right)\Big) \quad . \tag{3.9}$$

Hence the error in $\langle L\rangle$ and χ_L is of order $\mathcal{O}(\Delta m^3)$ and that of $\langle\bar{\psi}\psi\rangle$ and $\chi_{\bar{\psi}\psi}$ is of order $\mathcal{O}(\Delta m^2)$. Due to this truncation error and additional finite size effects the susceptibilities shown in Figure 3.1 remain finite in the plotted quark mass regime.

An interesting feature is, that the location of the maxima in both susceptibilities, χ_L and $\chi_{\bar{\psi}\psi}$ occur at the same temperature (gauge coupling β) within statistical accuracy, although the height of these susceptibilities is strongly quark mass dependent. This has also been confirmed in lattice simulations for a much wider range of quark masses [13].

[†]Throughout this work we consider only the disconnected part of the chiral susceptibility.

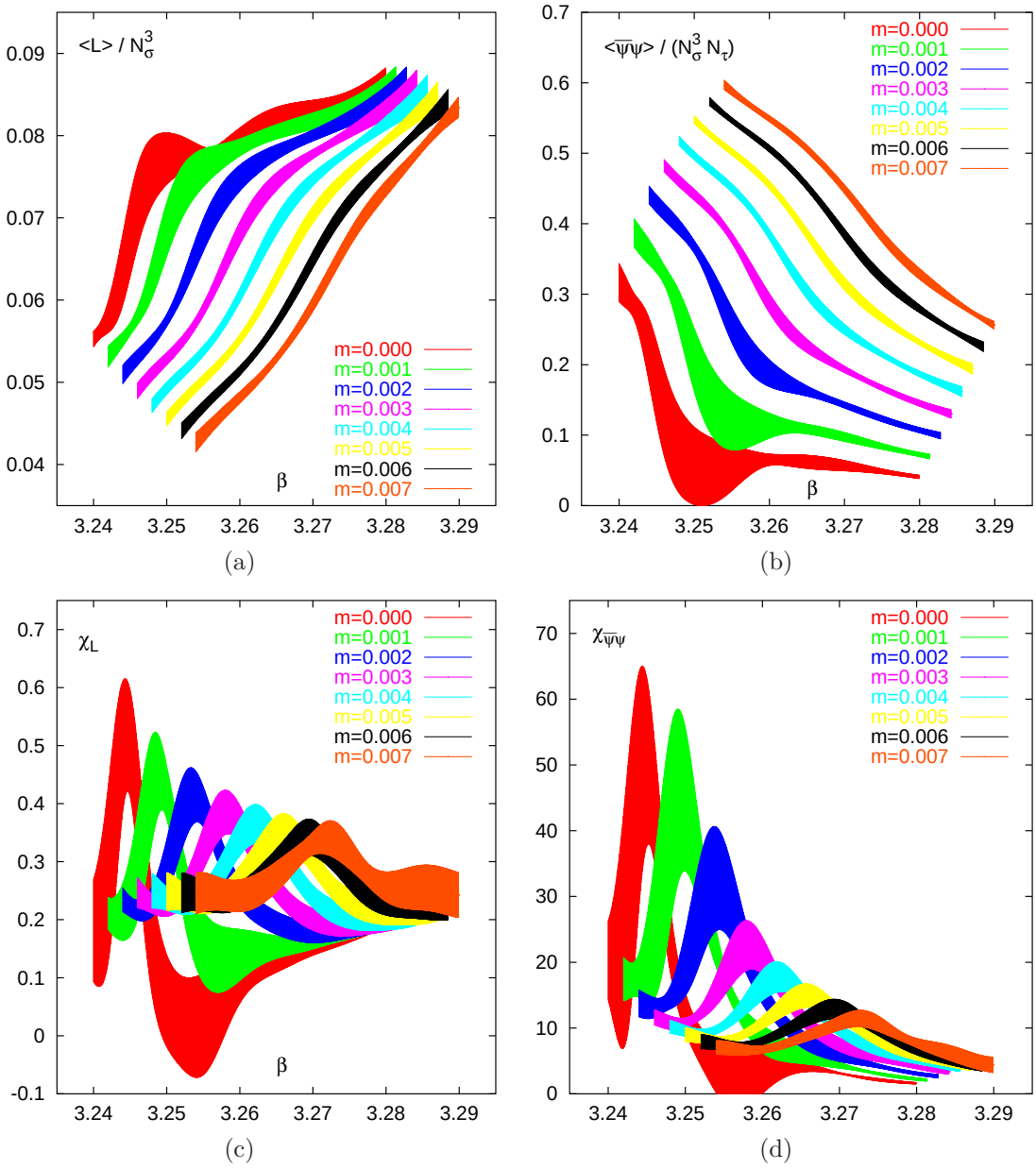

Figure 3.1: Deconfinement and chiral symmetry restoration in 3-flavor QCD: (a) the Polyakov loop $\langle L \rangle$, which is the order parameter for deconfinement in the pure gauge limit, and (b) the chiral condensate $\langle \bar{\psi}\psi \rangle$, which is the order parameter in the chiral limit, for different quark masses. Also shown are the corresponding susceptibilities χ_L (c) and $\chi_{\bar{\psi}\psi}$ (d) as a function of the gauge coupling β. The lattice simulations were performed with a quark mass of m=0.005, while results with other quark masses are obtained from mass reweighting. The lattice size is $16^3 \times 4$.

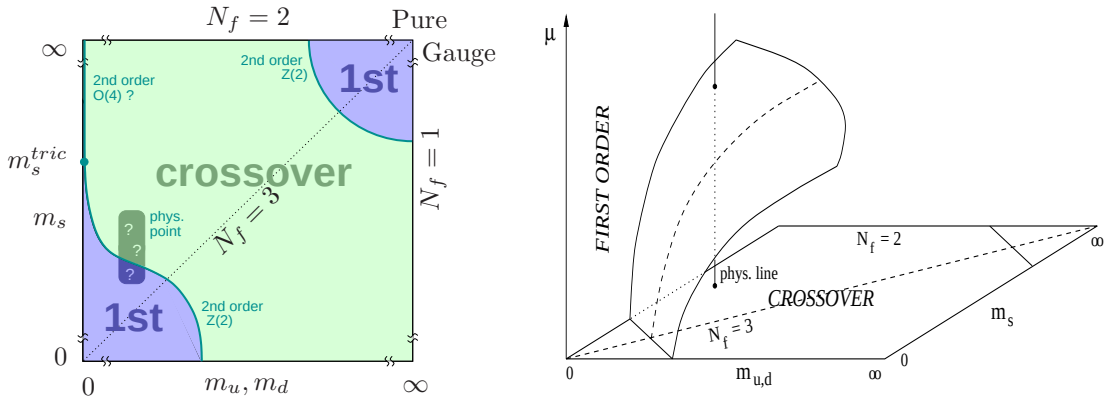

Figure 3.2: (a) Anticipated first order regime and line of second order phase transitions in the quark mass plane of degenerate (u,d)-quark masses and a strange quark mass m_s for vanishing chemical potential. (b) A sketch of the first order regime and critical surface at non-zero μ_q.

3.2 The critical surface

Our current understanding of qualitative aspects of the QCD phase diagram is based on universality arguments for the symmetry breaking patterns in the heavy [65] as well as the light quark mass regime [66, 67]. For the light quarks the global chiral symmetry is expected to control the critical behavior of the QCD phase transition. In particular the order of the transition is expected to depend on the number of light or massless flavors. With the help of a renormalization group analysis of the chiral Lagrangian (3.23) Pisarski and Wilczek derived the basic aspects of the n_f-dependence of the phase diagram. At vanishing baryon number density (or zero chemical potential) the transition is first order for $n_f \geq 3$ and second order for $n_f = 2$. This basic pattern has indeed been observed in lattice calculations [8, 68, 69]. The anticipated phase diagram of 3-flavor QCD at vanishing baryon number density is shown in Figure 3.2(a). An interesting aspect of the phase diagram is the occurrence of a second order phase transition line in the light quark mass regime, the boundary of the region of first order transitions. On this line the transition is controlled by an effective 3-dimensional theory with global $Z(2)$ symmetry [8, 67], which is not a symmetry of the QCD Lagrangian. Thus it is obvious that here neither the Polyakov loop nor the chiral condensate will serve as an order parameter on this line. As this boundary lies in the light quark mass regime it may well be that this second order transition is equally important for the critical or crossover behavior of QCD with a realistic quark mass spectrum as the critical point in the chiral limit of 2-flavor QCD. In particular, we note that the critical exponent α, which characterizes the singular behavior of the specific heat, is positive for the 3-d, $Z(2)$ model, whereas it is negative for the $O(4)$ model. A nearby $Z(2)$ symmetric critical point in the QCD phase diagram will thus induce larger

energy density fluctuations than would be expected in the vicinity of the chiral critical point. It therefore will be important to determine in detail the location of the physical point in the QCD phase diagram.

For non vanishing chemical potential the second order phase transition line in the light quark mass regime is expected to become a critical surface, which bends over the quark mass plane, still separating the first order phase transition form the crossover regime. This is shown in Figure 3.2(b). It suggests that a system of strongly interacting quarks and gluons, which only has a smooth crossover transition at $\mu_q = 0$, will nonetheless undergo a thermal phase transition at $\mu_q > 0$, which is of first order above a certain critical chemical potential.

3.2.1 Scaling fields and the chiral critical point

It is part of the problem of analyzing the universal behavior on the critical surface, that one has to identify the relevant operators and the corresponding scaling fields (couplings) of the effective theory. The construction of appropriate scaling fields has been discussed in detail in the case of the liquid-gas phase transition [70, 71]. The concepts developed in this context have recently also been used to locate and explore the properties of the electro-weak phase transition [72, 73] as well as the critical point in the ferromagnetic, 3-d, 3-state Potts model [74]. In the case of three degenerate quark masses and zero chemical potential, the lattice formulation of QCD depends on two bare couplings, the bare quark mass m and the gauge coupling β. The generic phase diagram in the plane of these two bare couplings is shown in Figure 3.3 for the small quark mass region. In the vicinity of the second order endpoint, $(\beta_c(\bar{m}), \bar{m})$, the dynamics and the universal critical behavior is controlled by an effective Hamiltonian, which can be expressed in terms of two operators $\mathcal{E}$, $\mathcal{M}$, i.e. the energy-like and ordering-field like operators that couple to the two relevant scaling fields τ and ξ,

$$\mathcal{H}_{eff}(\tau, \xi) = \tau\mathcal{E} + \xi\mathcal{M} \quad . \tag{3.10}$$

Under renormalization group transformations the multiplicative rescaling of the couplings ξ and τ is controlled by the two relevant eigenvalues that characterize the universal critical behavior in the vicinity of the second order critical point. The singular part of the free energy density thus scales like

$$f_s(\tau, \xi) = b^{-3} f_s(b^{y_t}\tau, b^{y_h}\xi) \quad , \tag{3.11}$$

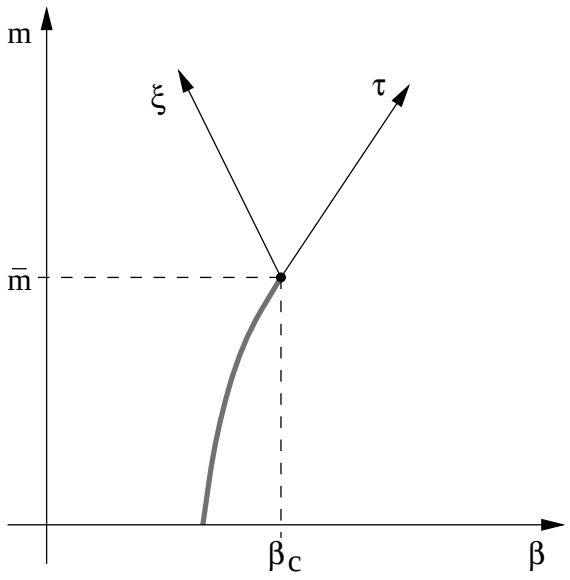

Figure 3.3: Generic phase diagram in the low mass regime of 3-flavor QCD.

where the dimensionless scale factor $b \equiv LT = N_\sigma/N_\tau$ gives the spatial extent of the lattices in units of the inverse temperature. Susceptibilities constructed from $\mathcal{E}$ and $\mathcal{M}$ will show the standard finite size scaling behavior

$$\chi_{\mathcal{E}} \equiv N_\sigma^{-3}\langle(\delta\mathcal{E})^2\rangle \sim a_{\mathcal{E}} b^{\alpha/\nu} \quad , \qquad \chi_{\mathcal{M}} \equiv N_\sigma^{-3}\langle(\delta\mathcal{M})^2\rangle \sim a_{\mathcal{M}} b^{\gamma/\nu} \quad . \tag{3.12}$$

As the symmetry of $\mathcal{H}_{eff}$ that characterizes the critical behavior at the chiral critical point is not shared in any obvious way by the QCD Lagrangian we also may expect that in the vicinity of the chiral critical point the operators appearing in the QCD Lagrangian are mixtures of the energy-like ($\mathcal{E}$) and ordering-field like ($\mathcal{M}$) operators. Similarly the couplings appearing in the QCD Lagrangian are linear combinations of the scaling fields as we have indicated in Figure 3.3. In the vicinity of the critical point one may use a linear ansatz for the couplings

$$\tau = \beta - \beta_c + A\,(m - \bar{m}) \quad , \qquad \xi = m - \bar{m} + B\,(\beta - \beta_c) \quad , \tag{3.13}$$

as well as for $\mathcal{E}$ and $\mathcal{M}$ which are constructed in terms of operators appearing in the original QCD Lagrangian,

$$\mathcal{E} = S_G + r\,\bar{\psi}\psi \quad , \qquad \mathcal{M} = \bar{\psi}\psi + s\,S_G \quad . \tag{3.14}$$

Here S_G and $\bar{\psi}\psi$ denote the gauge action and the chiral condensate on a given gauge field configuration.

As the operators of the QCD Lagrangian, e.g. S_G and $\bar{\psi}\psi$ or related observables like the Polyakov loop expectation value, are mixtures of $\mathcal{E}$ and $\mathcal{M}$, the corresponding susceptibilities will all receive contributions from fluctuations of $\mathcal{E}$ as well as $\mathcal{M}$. Asymptotically therefore all of them will show identical finite size scaling behavior which will be dominated by the larger of the two exponents α/ν and γ/ν, respectively. For the symmetry groups of interest in the QCD context, e.g. the symmetry of three dimensional $Z(2)$ or $O(N)$ spin models, this will be γ/ν. A finite size scaling analysis of susceptibilities constructed from the basic operators of the QCD Lagrangian thus will give access only to the ratio γ/ν, which unfortunately is quite similar for all the above mentioned symmetry groups and thus is not a good indicator for the universality class controlling the critical behavior in the vicinity of the chiral critical point.

The situation is different for cumulants constructed from linear combinations of $\bar{\psi}\psi$ and S_G,

$$B_4(x) \;=\; \frac{\langle \big(\delta M(x)\big)^4 \rangle}{\langle \big(\delta M(x)\big)^2 \rangle^2} \quad , \quad M(x) = \bar{\psi}\psi + x\, S_G \quad . \tag{3.15}$$

From Equation (3.11) it follows that for arbitrary values of x the cumulants are renormalization group invariants which in the infinite volume limit take on a universal value at the critical point $(\tau, \xi) \equiv (0, 0)$. For all values of x different from $1/r$ the cumulants behave asymptotically like the Binder cumulant for the order parameter; cumulants calculated on different size lattices for different quark masses will intersect at some value of the quark mass. In the infinite volume limit these intersection points will converge to a universal value which is characteristic for the universality class of the underlying effective Hamiltonian and, in fact, is quite different for the classes of three dimensional $Z(2)$ and $O(N)$ symmetric spin models; e.g. $B_4 = 1.604$ for $Z(2)$ [75], 1.242(2) for $O(2)$ [76] and 1.092(3) for $O(4)$ [77]. The cumulants $B_4(x)$ thus seem to be appropriate observables to locate the chiral critical point as well as to determine its universality class without knowing in detail the correct scaling fields. We are going to use this observable for our further analysis of the critical surface. As argued above the optimal choice of the parameter x, which is $x = s$, can be used to minimize the finite size effects. In the following we will set however $x = 0$ and present only the analysis of $B_4(0)$, which is the Binder cumulant of the chiral condensate. In a detailed analysis of the quantity $B_4(x)$ for the standard action [8] we have shown that the influence of the parameter x on the determination of the critical point is rather small.

3.2.2 Locating the line of second order phase transitions

As outlined above the Binder cumulant of the chiral condensate $B_4(0)$ is the appropriate quantity to localize the critical point. The method proceeds in two steps. First we determine for fixed

values of quark masses $m_{u,d},\ m_s$ pseudo-critical couplings $\beta_{\rm pc}(m_{u,d}, m_s)$. These are defined as the position of the maxima in the susceptibilities of $\bar{\psi}\psi$, the gauge action S_G and the Polyakov loop, which we find, however, to coincide within statistical accuracy. We then make use of the finite size scaling properties of $B_4(x)$ evaluated at $\beta_{\rm pc}(m_{u,d}, m_s)$. When analyzed as function of the bare quark masses, the Binder cumulants calculated on different lattice sizes $N_{\sigma 1}$ and $N_{\sigma 2}$ will intersect at that points $(m_{u,d}, m_s)_{N_{\sigma 1}, N_{\sigma 2}}$, which will converge to points on the critical line for $(N_{\sigma 1}, N_{\sigma 2}) \to (\infty, \infty)$.

Analyzing $B_4(0)$ for standard staggered fermions first, i.e. using the standard gauge and the standard staggered fermion action, has many advantages, although it provides no reliable value of a critical quark mass due to large cutoff effects. Since the standard action is much simpler than the p4 improved action, high precision Monte Carlo simulations are possible. The evaluation of the quantity $B_4(0)$ requires much more statistics than the chiral condensate, because it measures the fourth moment of the distribution of the chiral condensate. The universal properties of the chiral critical line are independent of the details of the action, thus the universality class can be determined. Furthermore, the critical quark mass in 3-flavor QCD appears to be not too small[‡], therefore numerical simulations are possible directly at the chiral critical point in 3-flavor QCD with a hybrid molecular dynamics algorithm [78]. To do so we performed simulations with unimproved fermions on $N_\sigma^3 \times 4$ lattices, with $N_\sigma = 8,\ 12$ and 16 for $n_f = 3$ and $N_\sigma = 12$ for $n_f = 2+1$. From previous studies [69] one knows that the 3-flavor critical point is located close to $m = 0.035$, thus we performed the 3-flavor calculations for four different values of the quark mass in the interval $m \in [0.03, 0.04]$. The additional $2+1$ flavor calculations are for the fixed value of up and down quark mass $m_u = m_d = 0.03$ and a strange quark mass of $m_s = 0.045,\ 0.06$. The results for the peak heights of the susceptibilities, pseudo-critical couplings, and Binder cumulants are summarized in Table 3.1. The pseudo-critical couplings $\beta_{\rm pc}$ given in Table 3.1 are extracted from the location of the peak in $\left\langle (\delta\bar{\psi}\psi)^2 \right\rangle$. We checked that the Binder cumulants calculated at $\beta_{\rm pc}$ indeed attain their minimum for each value of quark mass and volume.

As expected, the peak heights of the susceptibilities are not useful for the determination of the universality class. In 3-flavor QCD all three susceptibilities show identical finite size scaling close to the critical point. At $m = 0.035$, the ratio of the susceptibilities calculated on lattices of size $N_\sigma^3 \times 4$ with $N_\sigma = 12$ and 16 takes on the value 1.69(23), 1.66(22) and 1.66(24) for chiral, Polyakov loop and action susceptibilities, respectively. This corresponds to a ratio of critical exponents $\gamma/\nu = 1.8(5)$, which is consistent with the 3-dimensional Ising as well as $O(2)$ and $O(4)$ values

[‡]In the chiral limit, i.e. for vanishing quark masses, the fermion matrix becomes singular. Since the inversion of the fermion matrix is necessary for the hybrid-R-algorithm [78], the numerical effort increases with decreasing quark masses.

$n_f = 3$

m	N_σ	$V^{-1}\langle(\delta\bar{\psi}\psi)^2\rangle$	$V^{-1}\langle(\delta L)^2\rangle$	$V^{-1}\langle(\delta S_G)^2\rangle$	$\beta_{\rm pc}$	$B_4(0)$
0.0300	8	13.4(2)	1.32(3)	3.21(10)	5.1403(5)	1.637(37)
	12	32.5(1.4)	3.08(12)	7.34(31)	5.1411(4)	1.524(53)
	16	65.0(4.7)	6.27(44)	14.8(1.0)	5.1396(1)	1.454(87)
0.0325	8	12.9(4)	1.32(4)	3.21(12)	5.1456(6)	1.623(51)
	16	50.5(3.0)	5.00(29)	11.72(70)	5.1458(2)	1.535(69)
0.0350	8	11.9(5)	1.34(5)	3.05(14)	5.1524(5)	1.640(45)
	12	23.5(1.5)	2.52(16)	5.73(40)	5.1508(5)	1.664(55)
	16	39.8(2.8)	4.19(28)	9.52(64)	5.1499(1)	1.72(10)
0.0400	12	16.8(8)	2.05(11)	4.45(24)	5.1598(4)	1.896(63)
	16	23.4(2.1)	2.84(23)	6.03(54)	5.1593(5)	2.02(12)

$n_f = 2 + 1$

$m_{u,d}$	m_s	N_σ	$V^{-1}\langle(\delta\bar{\psi}\psi)^2\rangle$	$V^{-1}\langle(\delta L)^2\rangle$	$V^{-1}\langle(\delta S_G)^2\rangle$	$\beta_{\rm pc}$	$B_4(0)$
0.03	0.045	12	22.6(1.5)	2.46(16)	5.43(35)	5.1500(5)	1.624(79)
0.03	0.060	12	14.5(1.4)	1.74(16)	3.78(34)	5.1565(7)	1.93(14)

Table 3.1: Mass and volume dependence of the susceptibilities, critical couplings and the fourth order cumulants. The chiral condensate, which was used to calculate the chiral susceptibilities and fourth order cumulants in the case of $n_f = 2 + 1$, is the flavor averaged chiral condensate $\bar{\psi}\psi = 2\bar{\psi}\psi_{u,d} + \bar{\psi}\psi_s$.

flavor	$m_{u,d}$	m_s	$\beta_{\rm pc}$
3	0.0334(34)	0.0334(34)	5.1475(68)
2+1	0.0300	0.0378(83)	5.1459(64)

Table 3.2: Critical points in the quark mass plane; calculated under the assumption of the 3d-Ising universality class form the $B_4(0)$ data of the $12^3 \times 4$ lattice.

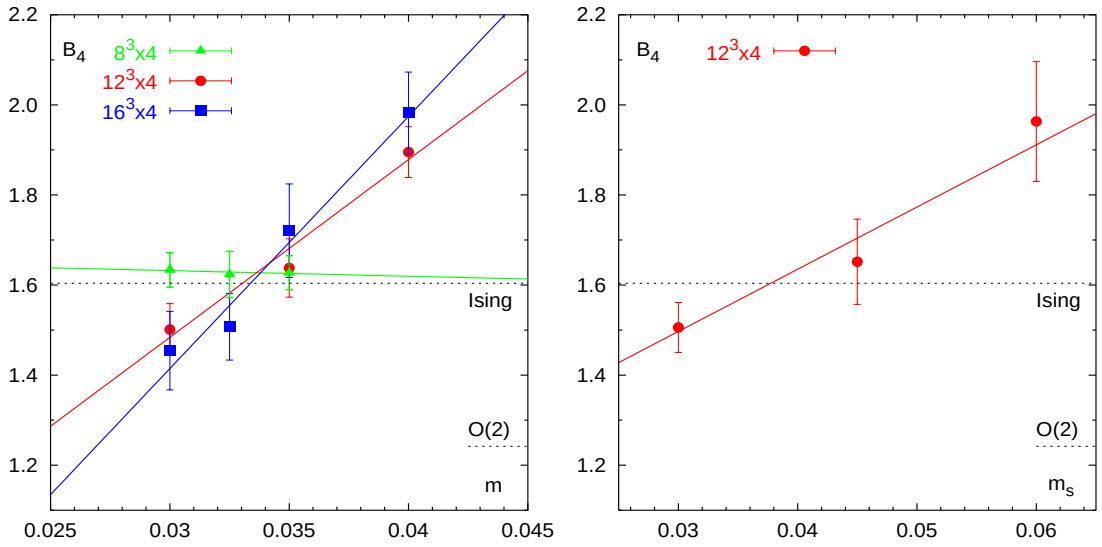

Figure 3.4: The Binder cumulant of the chiral condensate $B_4(0)$ for standard staggered fermions, (a) with 3 degenerate quark flavors and (b) with two light flavors ($m_u = m_d = 0.03$) and one heavier strange quark mass m_s. The solid lines are straight line fits to the data. Also indicated are the universal values of the Binder cumulant for the 3d-Ising and the 3d-$O(2)$ model.

($\gamma/\nu \simeq 1.96$).

The cumulant of the chiral condensate $B_4(0)$ is shown in Figure 3.4(a) along the 3-flavor line in the quark mass plane. We note that the cumulants calculated on different lattice sizes intersect at a quark mass close to $m = 0.035$. After fitting the data with the linear function $B_4(0) = a_0 + a_1 m$, a jackknife analysis yields the critical quark mass of $\bar{m} = 0.0331(12)$ from the intersection point of the $8^3 \times 4$ and the $16^3 \times 4$ lattice. The value of $B_4(0)$ at the intersection point is compatible with the universal value of the Binder cumulant for the 3-dimensional Ising model. In addition, the universal value for the Binder cumulant within the 3-dimensional $O(2)$ symmetric spin model is shown, which is however significantly smaller than the intersection point. This strongly suggests, that the 3-flavor critical point indeed belongs to the universality class of the 3-dimensional Ising model.

We can now use the information about the universality class and follow the line of constant $B_4(0) = 1.604$ in the $(m_{u,d}, m_s)$ quark mass plane. Rather than performing finite size scaling analyses for non-degenerate quark masses we may perform a simulation with non-degenerate quarks and determine the critical line as that of quark mass values at which $B_4(0) = 1.604$. For that purpose, we plot in Figure 3.4(b) the Binder cumulant of the chiral condensate for the $12^3 \times 4$ lattice along the line of constant up and down quark mass $m_{u,d} = 0.03$. At a critical strange quark

mass of $m_s \sim 0.038$ we hit the universal value of $B_4(0) = 1.604$. From straight line fits, of the $B_4(0)$ data along the 3-flavor line and the line of constant $m_{u,d} = 0.03$, calculated on the $12^3 \times 4$ lattice we thus can extract the two critical points given in Table 3.2. The pseudo critical couplings $\beta_{\rm pc}$ given in Table 3.2 are linearly interpolated from the $N_\sigma = 12$ results given in Table 3.1.

Furthermore, one can also apply the method of approximate mass reweighting, via Taylor expansion of reweighting factor and observable (Equations (3.8)-(3.9)). In our standard action calculations we measured no further operators than the chiral condensate, the Polyakov loop and the gluonic action. Mass reweighting can thus only be done up to order $\mathcal{O}(\Delta m)$ in the reweighting factor and the mass dependence of the chiral condensate had to be dropped at all. We, however, generalized our reweighting formula (3.8) to 2-dimensional mass reweighting and use the reweighting factor

$$\begin{aligned} \ln(\mathcal{R}) &= \frac{2}{4}\,\mathrm{Tr}\,\left(M^{-1}\right)(m_{u,d} - m_{u,d\,0}) + \frac{1}{4}\,\mathrm{Tr}\,\left(M^{-1}\right)(m_s - m_{s\,0}) \\ &+ \mathcal{O}\left(\Delta m_{u,d}, \Delta m_s\right) \quad . \end{aligned} \tag{3.16}$$

Using this reweighting technique, we can calculate the line of constant $B_4(0) = 1.604$ in the quark mass plane over a wide range of quark mass values. The result from the data set calculated at $n_f = 3$ and $m = 0.03$ is plotted in Figure 3.5. This line is an approximation of the line of second order phase transition points in the quark mass plane in the vicinity of the 3-flavor critical point. Its validity range is not known, nevertheless it is in agreement with the results of [68, 69]. The slope of the line is -2 within errors, which is the expected value for the slope at the 3-flavor critical point. Also indicated in Figure 3.5 are the two critical points from Table 3.2 and the linear sigma model results from Section 3.4. Due to the unknown mass renormalization factor of the bare lattice quark mass, we rescaled the line of second order phase transitions from the linear sigma model, to bring the 3-flavor critical point from the model on top of the 3-flavor critical point from the lattice calculations. The model calculations suggest a straight line of slope -2 for a wide range of quark mass values. Deviations are visible only for up and down quark mass smaller than $m_{u,d} \lesssim 0.01$.

3.2.3 The physical scale at the chiral critical line

The lattice parameters $m_{u,d}$ and m_s are bare quark masses, thus we rather should discuss the scale at the chiral critical line in terms of hadron masses. To do so we performed additional zero temperature calculations on a 16^4 lattice at $(\beta_{\rm pc}, \bar{m}) = (5.1452, 0.0325)$. For the pseudo-scalar and vector meson mass we find $m_{\rm ps} = 0.463(1)$ and $m_V = 1.387(38)$, respectively. Expressing the pseudo-scalar mass in units of the critical temperature, and using estimates of the critical

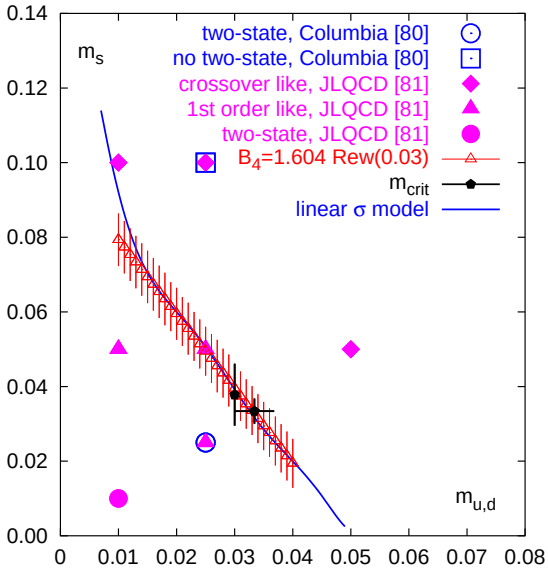

Figure 3.5: Line of constant $B_4(0) = 1.604$ in the quark mass plane, calculated from mass reweighting of the $n_f = 3$ results obtained with standard staggered fermions at quark mass $m = 0.03$. Also shown are the lattice results form other groups [68, 69] and the rescaled line of second order phase transitions from a mean field analysis of the linear sigma model.

temperature in 2 and 3-flavor QCD [13] we estimate for the pseudo-scalar meson mass at the chiral critical point $m_{\rm ps} \simeq 290$ MeV.

The entire analysis of the chiral critical line discussed so far has been performed with unimproved gauge and fermion actions on rather coarse lattices. Improved actions are not expected to modify the results on the universal properties of the chiral critical point, which have been presented above. They may, however, well influence the quantitative determination of the chiral critical point. It has been found in studies of the first order deconfinement transition occurring in the pure gauge sector that the gap in physical observables like the latent heat or surface tension is cutoff dependent. Improved actions generally lead to smaller gaps and a reduced cutoff dependence of these observables [79]. One thus may expect that also in the region of first order chiral transitions the gap in the chiral condensate gets reduced when calculated with improved actions. This will shift the critical point to smaller values of the pseudo-scalar meson mass. We therefore should redo the whole analysis with improved gauge and staggered fermion actions (p4-action). Here we are limited by the huge numerical effort, which is needed to perform calculations with small quark masses. In previous studies no evidence for a first order transition has been found down to bare quark masses $m = 0.01$ [13]. We thus performed Monte Carlo simulations of p4 improved fermions at $m = 0.005$, on lattice sizes $12^3 \times 4$ and $16^3 \times 4$. At quark mass $m = 0.005$ we do, however, still

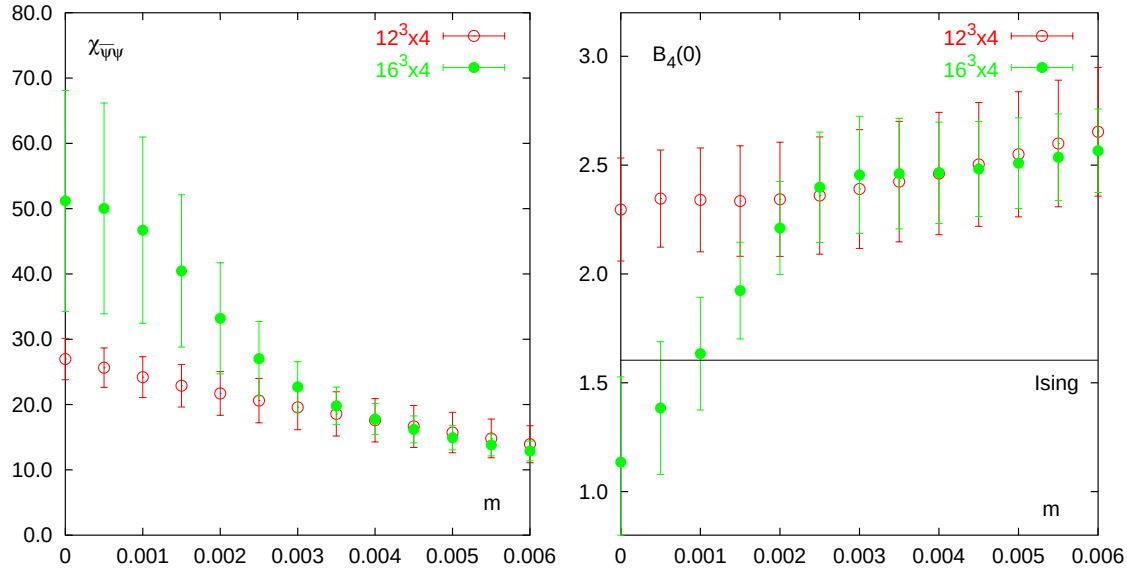

(a) (b)

Figure 3.6: Finite size scaling of the peak height of chiral susceptibility (a) and the Binder cumulant of the chiral condensate $B_4(0)$ (b). Shown are the $12^3 \times 4$ and the $16^3 \times 4$ lattice as function of the quark mass. The results are achieved by mass reweighting from the $m = 0.005$ data set.

find no evidence for a first order phase transition. The chiral susceptibilities, evaluated on lattices with spatial extent $N_\sigma = 12$ and 16 agree within errors. Using the mass reweighting formulas (3.8)-(3.9) we plot the finite size scaling behavior of the chiral condensate and its Binder cumulant $B_4(0)$ in Figure 3.6. A sizeable volume dependence of the chiral condensate can only be observed for quark masses smaller than $m \lesssim 0.003$. At the same quark mass of $m \approx 0.003$ the Binder cumulant on the $16^3 \times 4$ lattice begins to decrease linearly and crosses the universal value of the Ising model at $m \approx 0.001$. This is where we also find a factor of roughly 2 between the peak heights of the two chiral susceptibilities ($\gamma/\nu \approx 1.96$). On the other hand the Binder cumulant evaluated on the $12^3 \times 4$ lattice stays in the whole quark mass range rather flat and well above the universal value of 1.604. This could be due to the small statistics. Whereas for the standard action we were able to collect $(3-4) \cdot 10^4$ trajectories with a trajectory length of $\tau = 0.675$ for each combination of m, β, we have here only $(2-3) \cdot 10^3$ trajectories with $\tau = 0.4$. Another source of error is the finite number of random vectors used for the calculation of $\mathrm{Tr}\ M^{-1}$ (Equation (2.49)). For the standard action 25 random vectors were used, here we have generated only 15 random vectors for each configuration. Also not known is the validity range of the mass reweighting around the simulation point at $m = 0.005$. We checked, however, that direct measurements of $\bar{\psi}\psi$, $\chi_{\bar{\psi}\psi}$ and β_{pc} at $m = 0.01$ are well reproduced by the reweighted data from $m = 0.005$.

Ignoring the results of the $12^3 \times 4$ lattice we can estimate the chiral critical point of 3-flavor

QCD by the intersection point of the Binder cumulant $B_4(0)$, evaluated on the $16^3 \times 4$ lattice, with the universal value of the Ising model 1.604. A jackknife analysis yields $\bar{m} = 0.00071(38)$. Using the hadron spectroscopy presented in [13], i.e. assuming that the pion mass in units of the string tension $\sqrt{\sigma}$ is well described by the parameterization $m_\pi/\sqrt{\sigma} = 5.71(9) \cdot \sqrt{m}$ for quark masses below $m \lesssim 0.01$, this gives a critical pion mass of $m_\pi = 67(17)$ MeV, with $\sqrt{\sigma} = 425$ MeV. This is only about 24% of the value found in the calculations with unimproved staggered fermions but is close to the mean field results from the linear sigma model, which we will present in Section 3.4, and which are shown in Figure 3.8(a). There we plot the phase diagram in the plane of the pion mass, m_π, and kaon mass, m_K. Also indicated is the physical point, which appears to be well separated from the critical line in the crossover region.

3.2.4 The curvature in μ direction

The same finite size scaling pattern of the chiral condensate and its Binder cumulant is expected when extrapolating from the simulation point at $\mu = 0, m = 0.005$ not towards the chiral limit ($m \to 0$), but forwards increasing chemical potential at constant $m = 0.005$. We plot the peak heights of $\chi_{\bar{\psi}\psi}$ and the value of $B_4(0)$ evaluated at $\beta_{\rm pc}$ as a function of the up and down chemical potential $\mu_{u,d}$ in Figure 3.7. The results are obtained by using the reweighting formulas (2.42) and (2.48), i.e. using the Taylor expansion of reweighting factor and observable up to $\mathcal{O}(\mu^2)$. Unfortunately, in the chemical potential direction we are not only limited by the validity of our approximated (Taylor expanded) reweighting method, but also by the sign problem. In Section 2.3.3 we estimated the maximal chemical potential above which the sign problem becomes serious. Thus the results form the $16^3 \times 4$ lattice are plotted only up to $\mu_{u,d} \approx 0.03$. In this region the peak height of $\chi_{\bar{\psi}\psi}$ and the Binder cumulant $B_4(0)$ stay constant. The $16^3 \times 4$ lattice is thus too large for the determination of the 3-flavor critical point within our approximations. The maximal reweighting distance for the $12^3 \times 4$ lattice is much larger. We show here the results up to $\mu_{u,d} \approx 0.06$. At $\mu_{u,d} \approx 0.05$ the peak heights of the susceptibility begins to increase, while the Binder cumulant decreases linearly. When fitting the Binder cumulant in the interval $\mu_{u,d} \in [0.05, 0.06]$ with a straight line, we can estimate the intersection point of $B_4(0)$ with the universal value of the Ising model 1.604. A jackknife analysis yields $\bar{\mu}_{u,d} = 0.074(13)$, which corresponds to $\bar{\mu}_{u,d}/T_c = 0.296(52)$. Using the estimate of the critical temperature $T_c/\sqrt{\sigma} = 0.40(1) + 0.039(4)(m_\pi/\sqrt{\sigma})$ [13], we obtain $\bar{\mu}_{u,d} = 52(10)$ MeV, since the simulation point at $m = 0.005$ corresponds to a pion mass of $m_\pi = 172(3)$ MeV.

Having now estimated two critical points in 3-flavor QCD, both lying on the critical surface, we are able to approximate the critical surface by an appropriate extrapolation ansatz. Since

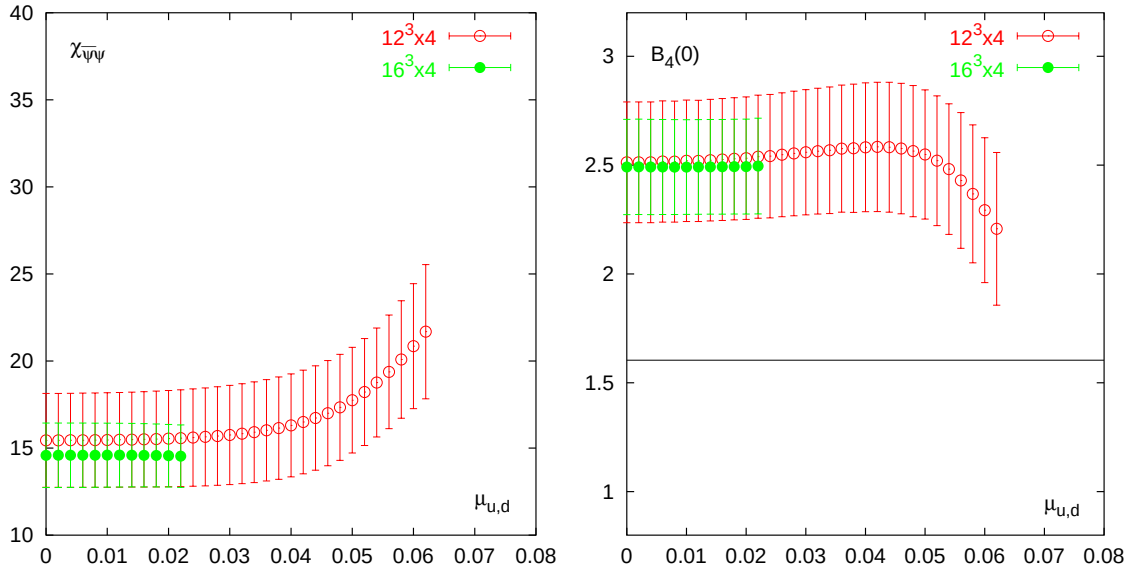

(a) (b)

Figure 3.7: Finite size scaling of the peak height of chiral susceptibility (a) and the Binder cumulant of the chiral condensate $B_4(0)$ (b). Shown are the $12^3 \times 4$ and the $16^3 \times 4$ lattice as function of the up and down quark chemical potential. The results are achieved by reweighting in the chemical potential from the $\mu = 0, m = 0.005$ data set.

all physical observables have to be functions of μ_q^2 and the up and down quark mass $m_{u,d}$ is proportional to m_π^2, we use the quadratic interpolation ansatz

$$\bar{m}_\pi^2(\mu_q) = \bar{m}_\pi^2(0) + A\mu_{u,d}^2 \quad . \tag{3.17}$$

For the parameter A we obtain $A = 0.109(36)$. The physical pion mass value fixes the location of the chiral critical point in 3-flavor QCD, we obtain $\bar{\mu}_{u,d} = 40(9)$ MeV. At $\mu = 0$ the critical strange quark mass in the vicinity of the 3-flavor point $m_s = \bar{m}_{u,d}$ is given by $\bar{m}_s = 3\bar{m}_{u,d} - 2m_{u,d}$. Using the lowest order chiral perturbation theory relation [80] $m_K^2/m_\pi^2 = (m_{u,d} + m_s)/2m_{u,d}$ this translates to

$$m_K^2 = \frac{3}{2}\left(\bar{m}_\pi\right)^2 - \frac{1}{2}m_\pi^2 \quad . \tag{3.18}$$

The Equations (3.17) and (3.18) define a plane in the $(m_\pi^2, m_K^2, \mu_q^2)$ space, which can be parameterized by

$$\bar{\mu}_{u,d}^2 = \left(m_\pi^2 + 2m_K^2 - 3\bar{m}_\pi^2(0)\right)\frac{A}{3} \quad . \tag{3.19}$$

The chiral critical point at the physical values of light and strange quark masses is to be found on this surface. For its location we estimate $\bar{\mu}_{u,d} = 135(21)$ MeV, or in terms of the baryon chemical potential $\bar{\mu}_B = 404(62)$ MeV.

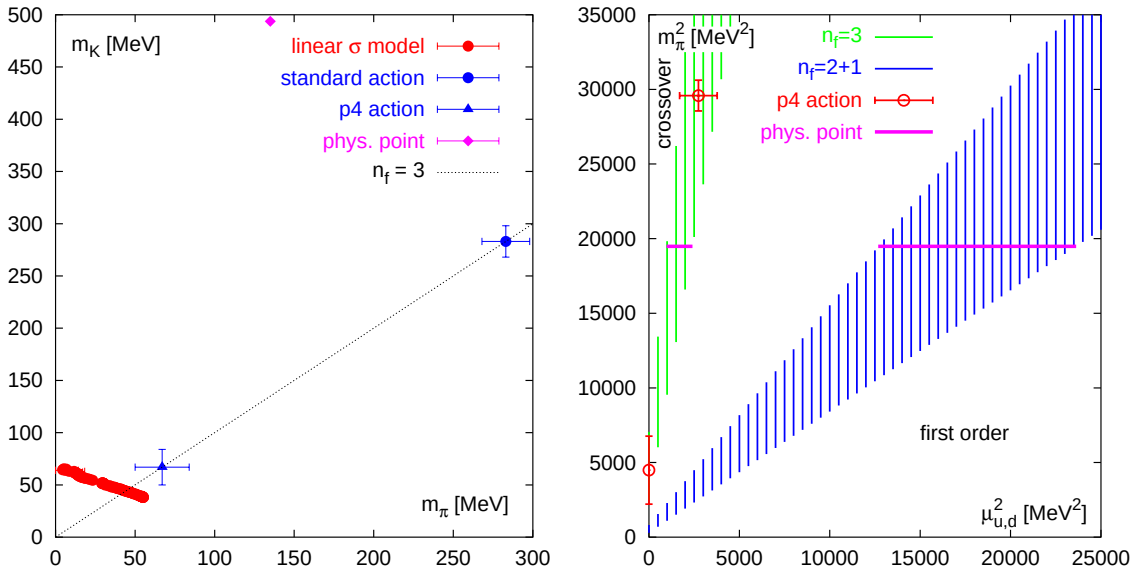

(a) (b)

Figure 3.8: (a) The phase diagram in the plane of pion mass (m_π) and kaon mass (m_K). Indicated is the line of second order phase transitions from the linear sigma model, the 3-flavor critical points from improved and unimproved lattice simulations and the physical point. (b) Curvature of the critical surface in the $\mu_{u,d}$ direction for 3-flavor and 2+1 flavor QCD. Also shown are the critical points from improved lattice calculations and the physical point.

In Figure 3.8(b) we show the curvature of the critical surface as a function of $\mu_{u,d}^2$. The 3-flavor line corresponds to the line of degenerate pion and kaon mass, whereas the line indicated as $2+1$ flavor corresponds to the physical ratio of pion and kaon mass. A critical quark chemical potential of $\bar{\mu}_{u,d} = 135(21)$ MeV appears to be a bit small in comparison with the results of Fodor and Katz [9]. In [9] a critical quark chemical potential of $\bar{\mu}_q \simeq 240$ MeV was obtained from simulations with unimproved staggered fermions at the mass point ($m_\pi \approx 300\,\mathrm{MeV}, m_K \approx 500\,\mathrm{MeV}$). At this point we estimate $\bar{\mu}_q = 144(22)$ MeV, thus the difference cannot be understood by the larger pion mass alone. Cutoff effects due to the unimproved action, which was used in [9], certainly play a role. However, also our approach involves approximations and assumptions on the extrapolation ansatz, which can lead to systematic errors which are difficult to estimate. In any case, both approaches certainly will be refined in future calculations.

3.3 The critical temperature

Finally we turn our attention to the dependence of the critical temperature on the chemical potential, which can be obtained from the pseudo critical couplings. As outlined above we calculate

observables consistently up to $\mathcal{O}(\mu^2)$ and thus expect the results to obtain errors at $\mathcal{O}(\mu^4)$. In our pervious study of $\beta_{\rm pc}(\mu)$, in the case of $n_f = 2$ and quark masses $m = 0.1$ and $m = 0.2$ [19]. At those large quark masses, no significant mass dependence has been observed. One expects, however, that the transition line becomes steeper with decreasing quark masses, we thus concentrate here on our 3-flavor simulations with small quark masses.

Because the first derivative of $\beta_{\rm pc}(\mu)$ is expected to vanish due to symmetry reasons (2.51) we fitted the $\beta_{\rm pc}$ data by a straight line in μ^2. The ranges in μ^2 are chosen small enough to avoid a phase problem. This means that the range for the $16^3 \times 4$ lattice at $m = 0.005$ has to be much smaller than for the other measurements. The results are summarized in Table 3.3. As expected we find no volume dependence for the derivative $\mathrm{d}\beta_{\rm pc}/\mathrm{d}\mu^2$ at the small quark mass $m = 0.005$. A bit more distinct are the differences between $\mathrm{d}\beta_{\rm pc}/\mathrm{d}\mu^2$ estimated from the peak position of either the Polyakov loop or the chiral condensate, here $|\mathrm{d}\beta_{\rm pc}/\mathrm{d}\mu^2|$ generally tends to be larger when estimated form the chiral condensate. The two values, however, always agree within statistical accuracy in our fit range. As expected we find for the large quark mass $m = 0.1$ much smaller values for $|\mathrm{d}\beta_{\rm pc}/\mathrm{d}\mu^2|$, since this derivative should vanish in the static limit ($m \to \infty$). The statistics for $m = 0.005$ is much smaller than for $m = 0.1$, thus we have errors of about 50% at $m = 0.005$, while they are $\approx 25\%$ at $m = 0.1$.

Besides the usual up and down quark chemical potential $\mu_{u,d}$ we also investigate systems with a non-zero 3-flavor chemical potential $\mu_{u,d,s}$ and a non-zero isovector chemical potential μ_I. For the 3-flavor chemical potentials we find generally larger values of $|\mathrm{d}\beta_{\rm pc}/\mathrm{d}\mu^2|$, which is reasonable, since in the case of three degenerate quarks, the 3-flavor chemical potential is only a shift in the up and down chemical potential scale towards more dense systems. Not so obvious are, however, the results for the isovector chemical potentials μ_I. Apparently the slope of $\beta_{\rm pc}(\mu)$ is only half as large as in the isoscalar case. A non-zero isovector chemical potential is achieved by choosing opposite signs for up and down quark chemical potentials, i.e. $\mu_u = -\mu_d$. The quark determinant is then real and positive, and thus allows also to perform simulations using standard Monte Carlo methods [81, 82, 83]. This motivates a comparison between systems with the usual isoscalar chemical potential and the isovector chemical potential. In the framework of a Taylor expansion, terms even in μ are identical for both up and down quarks, but odd terms cancel for the case of $\mu_I \neq 0$. This means for $\mu_I \neq 0$ we set terms proportional to $\mathcal{O}_1, \mathcal{R}_1$ in equation (2.50) to zero. This leads to smaller values of $|\mathrm{d}\beta_{\rm pc}/\mathrm{d}\mu^2|$, which is unexpected since the onset of matter at $T = 0$ is predicted to appear at $\mu_{I0} \simeq m_{PS}/2$ [84] in form of a pion condensate. At our small quark mass this should be clearly separated and in particular smaller than the onset of baryonic matter for isoscalar chemical potentials at $\mu_0 = m_N/3$. One thus could have expected that the transition line is more strongly curved for $\mu_I \neq 0$ than for $\mu_{u,d} \neq 0$.

$\mu \equiv \mu_u = \mu_d$, $\mu_s = 0$						
		from peak in χ_L		from peak in $\chi_{\bar{\psi}\psi}$		fit-range
m	N_σ	$\mathrm{d}\beta_{\mathrm{pc}}/\mathrm{d}\mu^2$	$\beta_{\mathrm{pc}}(0)$	$\mathrm{d}\beta_{\mathrm{pc}}/\mathrm{d}\mu^2$	$\beta_{\mathrm{pc}}(0)$	$[\mu^2_{min}, \mu^2_{max}]$
0.005	16	-0.907(648)	3.2661(12)	-1.037(620)	3.2658(11)	[0,0.0006]
	12	-1.039(517)	3.2654(11)	-1.363(504)	3.2649(8)	[0,0.0006]
		-1.003(538)	3.2653(11)	-1.362(689)	3.2649(8)	[0,0.002]
		-0.967(639)	3.2652(11)	-1.437(705)	3.2650(8)	[0,0.003]
0.1	16	-0.257(64)	3.4792(26)	-0.281(55)	3.4795(23)	[0,0.0006]
		-0.273(64)	3.4792(25)	-0.295(60)	3.4796(23)	[0,0.002]
		-0.302(65)	3.4793(25)	-0.315(68)	3.4796(23)	[0,0.003]
$\mu \equiv \mu_u = \mu_d = \mu_s$						
		from peak in χ_L		from peak in $\chi_{\bar{\psi}\psi}$		fit-range
m	N_σ	$\mathrm{d}\beta_{\mathrm{pc}}/\mathrm{d}\mu^2$	$\beta_{\mathrm{pc}}(0)$	$\mathrm{d}\beta_{\mathrm{pc}}/\mathrm{d}\mu^2$	$\beta_{\mathrm{pc}}(0)$	$[\mu^2_{min}, \mu^2_{max}]$
0.005	16	-1.823(1.520)	3.2662(12)	-2.048(1.451)	3.2658(11)	[0,0.0003]
	12	-2.030(1.169)	3.2653(11)	-2.667(1.360)	3.2649(8)	[0,0.0006]
		-1.944(1.419)	3.2653(11)	-2.861(1.631)	3.2649(8)	[0,0.0012]
0.1	16	-0.329(101)	3.4792(26)	-0.380(129)	3.4795(23)	[0,0.0006]
		-0.488(117)	3.4792(25)	-0.512(167)	3.4796(23)	[0,0.002]
		-0.617(164)	3.4793(25)	-0.644(231)	3.4797(23)	[0,0.003]
$\mu \equiv \mu_I$						
		from peak in χ_L		from peak in $\chi_{\bar{\psi}\psi}$		fit-range
m	N_σ	$\mathrm{d}\beta_{\mathrm{pc}}/\mathrm{d}\mu^2$	$\beta_{\mathrm{pc}}(0)$	$\mathrm{d}\beta_{\mathrm{pc}}/\mathrm{d}\mu^2$	$\beta_{\mathrm{pc}}(0)$	$[\mu^2_{min}, \mu^2_{max}]$
0.005	16	-0.406(68)	3.2661(12)	-0.381(60)	3.2658(11)	[0,0.0006]
	12	-0.435(103)	3.2653(11)	-0.423(74)	3.2650(8)	[0,0.0006]
		-0.399(99)	3.2653(11)	-0.397(70)	3.2649(8)	[0,0.002]
		-0.393(96)	3.2653(11)	-0.392(70)	3.2650(8)	[0,0.003]
0.1	16	-0.265(93)	3.4791(26)	-0.319(55)	3.4796(24)	[0,0.0006]
		-0.301(91)	3.4791(26)	-0.306(53)	3.4796(23)	[0,0.002]
		-0.305(88)	3.4792(25)	-0.307(53)	3.4796(23)	[0,0.003]

Table 3.3: The pseudo critical coupling and its derivative with respect to the chemical potentials $\mu_{u,d}$, $\mu_{u,d,s}$ and μ_I. We fit the data with $\beta_{\mathrm{pc}}(0) + c\mu^2$, where $c = \mathrm{d}\beta/\mathrm{d}(\mu^2) = \frac{1}{2}\mathrm{d}^2\beta/\mathrm{d}\mu^2$. In some cases we show results for different fit ranges which are given in the last column.

Of course, it is desirable to translate the observations from the pseudo critical couplings into physical units to discuss the dependence of the critical temperature T_c on μ. The derivative of T_c with respect to μ^2 can be estimated by

$$\frac{\mathrm{d}^2 T_c}{\mathrm{d}\mu^2} = -\frac{1}{N_\tau^2 T_c}\frac{\mathrm{d}^2\beta_c}{\mathrm{d}\mu^2}\Big/\left(a\frac{\mathrm{d}\beta_c}{\mathrm{d}a}\right) \quad , \tag{3.20}$$

where a is the lattice spacing. Unfortunately this requires the knowledge of the β-function (the dependence of the lattice spacing a on the gauge coupling β). This information may be obtained from the string tension data in Reference [12] at bare quark mass $m = 0.1$ for $n_f = 2, 3$. The string tension data was fitted with an ansatz [85]

$$\sqrt{\sigma a^2}(\beta) = \frac{R(\beta)}{c_0}\left[1 + c_2\frac{R(\beta)}{R(\bar{\beta})} + c_4\frac{R(\beta)}{R(\bar{\beta})}\right] \quad , \tag{3.21}$$

where $R(\beta)$ is the usual two-loop scaling function (2.16) and $\bar{\beta} = 3.7$ for $n_f = 2$ and $\bar{\beta} = 3.5$ for $n_f = 3$. c_0, c_2 and c_4 are fit parameters with $c_0 = 0.0570(35)$, $c_2 = 0.669(208)$ and $c_4 = -0.0822(1088)$ for $n_f = 2$ and $c_0 = 0.0448(15)$, $c_2 = 0.507(115)$ and $c_4 = -0.0071(677)$ for $n_f = 3$. Differentiating the interpolation functions yields $a^{-1}(\mathrm{d}a/\mathrm{d}\beta) = -2.08(43), -2.26(26)$ for $n_f = 2, 3$ respectively. Using $\mathrm{d}\beta_{\mathrm{pc}}/\mathrm{d}\mu_{u,d}^2$ calculated form the chiral condensate as given in Table 3.3 with fit-range $[0 : 0.003]$, we then find $T_c(\mathrm{d}T_c/\mathrm{d}\mu_{u,d}^2) = -0.070(35), 0.045(10)$[§] for $n_f = 2, 3$ at $m = 0.1$. At the small quark mass $m = 0.005$ we do not have the β-function. This would require additional and very costly zero temperature calculations. We thus estimate the β-function perturbatively by the two-loop scaling function (2.16). Here we get $a^{-1}(\mathrm{d}a/\mathrm{d}\beta) = -1.4$ for $n_f = 3$ and $m = 0.005$. Although this perturbative estimate tends to be too small, we still find a larger curvature for $T_c(\mu)$ at the small quark mass with $T_c(\mathrm{d}T_c/\mathrm{d}\mu^2) = -0.11(5)$, this time using the fit-range $[0 : 0.002]$. The quark mass dependence of T_c becomes significant if we compare for our two quark mass values based on perturbative β-functions only. We then find

$$\frac{T_c(\mu_{u,d})}{T_c(0)} = \begin{cases} 1 - 0.025(6)\left(\frac{\mu_q}{T_c(0)}\right)^2, & m = 0.1 \\ 1 - 0.114(46)\left(\frac{\mu_q}{T_c(0)}\right)^2, & m = 0.005 \quad . \end{cases} \tag{3.22}$$

Note that also $T_c(0)$ depends on the quark mass [13]. In Figure 3.9(a) we compare these results for the transition temperature in units of the transition temperature at $\mu = 0$ ($T_0 \equiv T_c(\mu = 0)$). Also shown in Figure 3.9(a) are the results of [10], which have been obtained from simulations with two flavors of unimproved quark masses, for rather large quark masses at imaginary chemical potential. Both methods agree remarkably well. Of course, when $\mu/T = \mathcal{O}(1)$, higher-order terms in the expansion become relevant. However, in [10] it has been shown, that the μ^4 term is statistically insignificant for $\mu/T_0 \lesssim 1$.

[§]The value for $n_f = 2$ is from Reference [19]

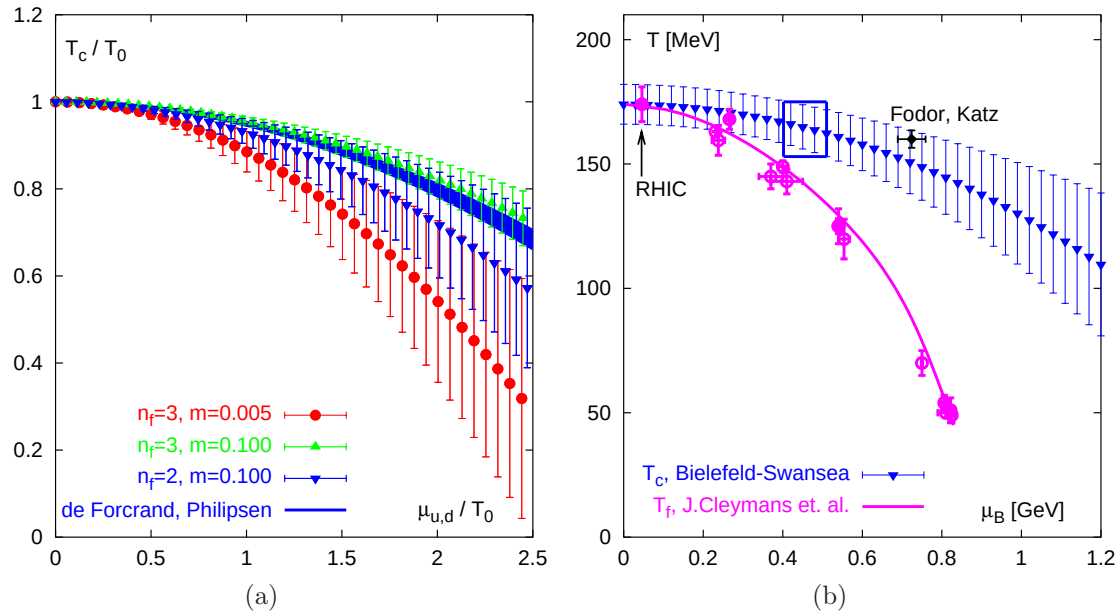

(a) (b)

Figure 3.9: Dependence of the transition temperature T_c on the up and down quark chemical potential ($\mu_{u,d}$) in units of (a) the transition temperature at $\mu = 0$ (T_0) and (b) in physical units. In (a) we show results for different bare quark masses and number of flavors, also shown are the result of de Forcrand and Philipsen [10]. In (b) we compare the transition line with the phenomenological freeze-out line from statistical models [86], also indicated are estimates of the critical point from our calculations (blue box) and Fodor and Katz [9].

In Figure 3.9(b) we compare the transition line for $n_f = 2$ and $m = 0.1$ in the T, μ plane with the phenomenological freeze-out curve form statistical models (4.36) [86]. This suggests that at sufficiently large μ_B there is the chance to observe experimentally a strongly interacting hadron gas phase, whereas for small μ_B hadrons seem to freeze out right after the phase transition from QGP to the hadronic phase. However, assuming that the transition line is parabolic all the way down to $T = 0$, clearly cannot be correct. The curvature is to small to be consistent with the phenomenological expectation that at $T = 0$ a transition from hadronic to quark matter occurs for $\bar{\mu}_B$ some 0.1-0.6 GeV larger than the onset of nuclear matter at $\mu_{B0} \simeq m_N \simeq 0.94$ GeV. The situation is similar for the results of Fodor and Katz [9], and hints at contributions from higher-order derivatives, or even nonanalytic behavior, at larger values of μ.

3.4 The $SU(3)_L \times SU(3)_R$ linear sigma model

In this Section we investigate in how far the basic pattern of the QCD phase transition, i.e., its nature and n_f-dependence can be understood by the global chiral symmetry of the QCD

Lagrangian. For that reason, we present a mean-field calculation of an effective chiral Hamiltonian, the so called linear sigma model, that incorporates the correct symmetries of the QCD Lagrangian and thus has the chance to predict the universal properties, e.g. the order of the transition in the chiral limit.

During the last years the linear sigma model was studied by many groups. For a recent and detailed study see, e.g., [87]. For simplicity, however, we decided to use the method of [88]. In the $SU_L(2) \times SU_R(2)$ case of the linear sigma model a finite chemical potential has already been considered by [89]. The chiral Lagrangian, we use, is given by (in Euclidean notation)

$$\begin{aligned}\mathcal{L}(\Psi,\Phi) &= \bar{\Psi}\left(\gamma_\nu\partial_\nu + \frac{c}{2}\left[(\Phi+\Phi^\dagger)+(\Phi-\Phi^\dagger)\gamma_5\right]\right)\Psi - \mu\bar{\Psi}\gamma_4\Psi \\ &+ \frac{1}{2}\mathrm{Tr}\left(\partial_\nu\Phi^\dagger\partial_\nu\Phi - m_0^2\,\Phi^\dagger\Phi\right) + f_1\left[\mathrm{Tr}\left(\Phi^\dagger\Phi\right)\right]^2 + f_2\,\mathrm{Tr}\left(\Phi^\dagger\Phi\right)^2 \\ &+ g\left[\mathrm{Det}\left(\Phi\right)+\mathrm{Det}\left(\Phi^\dagger\right)\right] - \mathrm{Tr}\left[\frac{H}{2}(\Phi+\Phi^\dagger)\right] \quad . \end{aligned} \tag{3.23}$$

Here, the $\Psi(x)$ field is a three-component fermion field. It can either be identified with nucleons, as it was done in the original sigma model [90], or with constituent quarks [89]. We will, however, restrict our discussion here to a pure mesonic system, which corresponds to the limit $c \to \infty$. Thus we drop the first line of equation 3.23, i.e. the fermionic sector of the Lagrangian. The (3×3)-matrix field $\Phi(x)$ represents the mesons and is written as

$$\Phi(x) = \frac{1}{\sqrt{2}}\sum_{a=0}^{8}\left[\sigma_a(x) + i\pi_a(x)\right]\lambda_a \quad . \tag{3.24}$$

In this parameterization the σ_a and π_a denote the nonets of scalar and pseudoscalar mesons, and the λ_a are the Gell-Mann matrices, with $\lambda_0 = \sqrt{2/3}\,[\mathrm{diag}(1,1,1)]$. One can easily verify that $(\Phi \pm \Phi^\dagger)/2$ indicate the scalar, pseudoscalar part of Φ, respectively. All terms in Equation (3.23) are invariant under chiral transformations except the terms in the last line. The determinant is introduced to represent the axial anomaly in QCD and the symmetry breaking (mass) term which is linear in Φ and is coupled to an external matrix field H which is parameterized by

$$H = \frac{1}{\sqrt{2}}\sum_{a=0}^{8} h_a\lambda_a \quad . \tag{3.25}$$

Two simple symmetry breaking patterns, that can be compared with lattice simulations, are the cases $h_0 \neq 0$, $h_1, \ldots, h_8 = 0$ and $h_0 \neq 0$, $h_8 \neq 0$, $h_7, \ldots, h_8 = 0$, which will be referred to as the $n_f = 3$ and $n_f = 2+1$ cases. If one assumes $h_1, \ldots, h_7 = 0$, the symmetry breaking term can be written as $-h_0\sigma_0 - h_8\sigma_8$. Thus the temperature dependent order parameters are $\langle\sigma_0\rangle(T)$ and $\langle\sigma_8\rangle(T)$. For $n_f = 3$ one has a degenerate (pseudo)scalar meson octet, whereas for $n_f = 2+1$ one can adjust the fields to reproduce a realistic mass splitting inside the octet.

The unknown constants of the model have to be fitted to the experimentally measured meson masses. For m_0^2, f_1, f_2, g we use the values that are given in Table II of [88]. With these values the physical point appears at $(h_0, h_8) \approx (0.0265\text{GeV}^3, -0.0345\text{GeV}^3)$ at which the experimental masses are reproduced quite well. All coupling constants are treated as be temperature independent.

Through an identification of the symmetry breaking term in the sigma model on the meson $(-h_0\sigma_0 - h_8\sigma_8)$ and in QCD on the quark level $(m_u\bar{u}u + m_d\bar{d}d + m_s\bar{s}s)$, a mapping of the pairs of couplings (h_0, h_8) and the condensates $(\langle\sigma_0\rangle, \langle\sigma_8\rangle)$ to the quark level is possible. Using a linear ansatz

$$\begin{array}{rclcrcl} -h_0 &=& \alpha(2m_{u,d} + m_s) & & \alpha\sigma_0 &=& 2\bar{q}q + \bar{s}s \\ -h_8 &=& \beta(m_{u,d} - m_s) & \text{and} & \beta\sigma_8 &=& \bar{q}q - \bar{s}s \end{array} \quad , \tag{3.26}$$

one deduces the following linear mappings

$$\begin{pmatrix} h_0 \\ h_8 \end{pmatrix} \longmapsto \begin{pmatrix} m_{u,d} \\ m_s \end{pmatrix} = \begin{pmatrix} -\frac{1}{3\alpha} & -\frac{1}{3\beta} \\ -\frac{1}{3\alpha} & \frac{2}{3\beta} \end{pmatrix} \begin{pmatrix} h_0 \\ h_8 \end{pmatrix} \quad , \tag{3.27}$$

and

$$\begin{pmatrix} \langle\sigma_0\rangle \\ \langle\sigma_8\rangle \end{pmatrix} \longmapsto \begin{pmatrix} \langle\bar{q}q\rangle \\ \langle\bar{s}s\rangle \end{pmatrix} = \begin{pmatrix} \alpha & \frac{1}{2}\beta \\ \alpha & -\beta \end{pmatrix} \begin{pmatrix} \langle\sigma_0\rangle \\ \langle\sigma_8\rangle \end{pmatrix} \quad . \tag{3.28}$$

Here the quantities on the quark level are the quark mass $m_{u,d}$ and the condensate $\langle\bar{q}q\rangle$ of two degenerate light quark flavors, the strange quark mass m_s, and the strange quark condensate $\langle\bar{s}s\rangle$. With the above mentioned physical point and the values for realistic current quark masses, $(m_u + m_d)/2 = 11.25$ MeV, $m_s = 205$ MeV [91], the parameters α and β were determined to be

$$\alpha = -0.1164\,\text{GeV}^2 \quad , \qquad \beta = -0.178\,\text{GeV}^2 \quad . \tag{3.29}$$

We assume the temperature independence of these mappings and use them to compare the sigma-model results with results from lattice simulations of staggered fermions.

In order to study the thermodynamics of the model, we define the thermodynamical potential Ω as a function of the temperature T[¶]

$$\Omega(T) = \lim_{V\to\infty}\left(-\frac{T}{V}\ln Z\right) \quad , \tag{3.30}$$

[¶]As long as we consider a pure mesonic system we have no baryon chemical potential ($\mu \equiv 0$). In the canonical ensemble Ω is called the free energy density ($\Omega_{\text{canonical}} \equiv f$), whereas here in the grand canonical ensemble we have the identity $\Omega = -p$, with p denoting the pressure.

where the partition function Z is defined as the path integral

$$Z = \int \mathcal{D}\Phi \ \exp\left\{ - \int_0^{1/T} d\tau \int d^3x \ \mathcal{L}(\Phi) \right\} \quad . \tag{3.31}$$

All thermodynamic quantities can be derived from Ω in the standard way. In practice, however we did not perform the path integral but approximated the thermodynamical potential Ω by an effective potential $\Omega_{\rm eff}$ which is given in terms of averaged σ_0 and σ_8 fields, i.e. constant fields in space-time[‖]. The order parameters are then defined to be those values of σ_0 and σ_8, that minimize the effective potential

$$\left.\frac{\partial \Omega_{\rm eff}}{\partial \sigma_0}\right|_{\sigma_0 = \langle \sigma_0 \rangle (T)} = 0 \ , \qquad \left.\frac{\partial \Omega_{\rm eff}}{\partial \sigma_8}\right|_{\sigma_8 = \langle \sigma_8 \rangle (T)} = 0 \ . \tag{3.32}$$

The first thing one usually does to derive the effective potential is to shift the $\sigma_a(x)$ and $\pi_a(x)$ by their expectation values

$$\sigma_a(x) \to \sigma_a + \sigma_a^{'}(x) \ , \qquad \pi_a(x) \to \pi_a + \pi_a^{'}(x) \quad . \tag{3.33}$$

As long as one has only non-vanishing external fields h_0 and h_8 the expectation values $\sigma_1, \ldots, \sigma_7$ and $\pi_0, \ldots, \pi_8$ should vanish. Now one expands the Lagrangian in terms of the quantum fluctuations $\sigma_a^{'}(x)$ and $\pi_a^{'}(x)$. All terms that are independent of $\sigma_a^{'}(x)$ and $\pi_a^{'}(x)$ define the classical part of the effective potential

$$\begin{aligned} \Omega_{\rm class}(\sigma_0, \sigma_8) &= -\frac{m_0^2}{2}\left(\sigma_0^2 + \sigma_8^2\right) + \frac{g}{3\sqrt{3}}\left(2\,\sigma_0^3 - \sqrt{2}\,\sigma_8^3 - 3\,\sigma_0\,\sigma_8^2\right) \\ &+ -\frac{2\sqrt{2}}{3}\,f_2\,\sigma_0\,\sigma_8^3 + \left(f_1 + \frac{f_2}{3}\right)\sigma_0^4 + \left(f_1 + \frac{f_2}{2}\right)\sigma_8^4 \\ &+ 2\,(f_1 + f_2)\,\sigma_0^2\,\sigma_8^2 - h_0\,\sigma_0 - h_8\,\sigma_8 \quad . \end{aligned} \tag{3.34}$$

All terms that are linear in $\sigma_a^{'}(x)$ and $\pi_a^{'}(x)$ vanish by definition. The quadratic terms are mass terms which define the tree-level masses of the mesons m_Q. In our parameterization the pion mass, for instance, is given by

$$\begin{aligned} m_\pi^2 &= -m_0^2 + \frac{2g}{\sqrt{3}}\sigma_0 - \frac{2\sqrt{2}g}{\sqrt{3}}\sigma_8 + \left(4f_1 + \frac{4f_2}{3}\right)\sigma_0^2 \\ &\left(4f_1 + \frac{2f_2}{3}\right)\sigma_8^2 + \frac{4\sqrt{2}f_2}{3}\sigma_0\sigma_8 \quad . \end{aligned} \tag{3.35}$$

All nonzero elements of the scalar and pseudoscalar mass matrix are given in Appendix B. The other terms are interaction terms and much harder to handle. The two quartic terms can be

[‖] Formally σ_0 and σ_8 are the Legendre conjugates of c-number sources coupled linearly to the quantum fields in the theory.

quadratized by introducing an auxiliary matrix field $\Sigma(x)$ which allows to formulate a matrix version of a Hubbard-Stratanovich transformation [92]; we apply the identity

$$\begin{aligned}
&\exp\left\{-A\left[f_1(\mathrm{Tr}\Phi^{'\dagger}\Phi^{'})^2 f_2 \mathrm{Tr}(\Phi^{'\dagger}\Phi^{'})^2\right]\right\} \\
&= \quad \text{const} \times \int_{c-i\infty}^{c+i\infty} \mathcal{D}\Sigma(x)\, \exp\left\{\mathrm{Tr}\Sigma^2 + 2B\mathrm{Tr}(\Sigma\Phi^{'\dagger}\Phi^{'}) + 2C\mathrm{Tr}(\Phi^{'\dagger}\Phi^{'})\mathrm{Tr}\Sigma\right\} \quad , \qquad (3.36)
\end{aligned}$$

where

$$B^2 = Af_2 \qquad \text{with} \qquad 2BC + 3B^2 = Af_1 \quad . \qquad (3.37)$$

In the saddle point approximation used in [93], one makes the $SU(3)$ symmetric ansatz $\Sigma(x) = \mathrm{diag}(s,s,s)$ and replaces the path integral $\int \mathcal{D}\Sigma$ by the maximum of the integrant. We are left with the approximation

$$\begin{aligned}
\mathcal{L}^{(4)} &= f_1(\mathrm{Tr}\Phi^{'\dagger}\Phi^{'})^2 + f_2\,\mathrm{Tr}(\Phi^{\dagger}\Phi)^2 \approx \\
&-\frac{3}{8(3f_1+f_2)}\left(\frac{s^2}{2} + m_0^2 s\right) + \frac{1}{2}\left(s + m_0^2\right)\mathrm{Tr}(\Phi^{'\dagger}\Phi^{'})^2 \; . \qquad (3.38)
\end{aligned}$$

The parameter s has to be chosen appropriately to maximize the effective potential. Thus we get another term that is independent of $\Phi^{'}$,

$$\Omega_{\mathrm{sadd}}(s) = -\frac{3}{8(3f_1+f_2)}\left(\frac{s^2}{2} + m_0^2 s\right) \; , \qquad (3.39)$$

and additional modifications in the tree level meson masses,

$$m_Q^2 \to \tilde{m}_Q^2 = m_Q^2 + s + m_0^2 \; . \qquad (3.40)$$

The reason for this approximation, which corresponds to the leading order in a $1/N^{**}$ expansion [94], is that problems with tachyonic masses are reduced. Unfortunately they are not completely eliminated, i.e. one finds $\tilde{m}_Q^2 < 0$ at the saddle point of the effective potential for high temperatures above the transition. The self-consistent resummation scheme as proposed by Cornwall, Jackiw and Tomboulis (CJT) [95] is believed to provide a much better approximation, which compleatly avoids tachionic masses. This method will, however, require a solution of a 12 dimensional non-linear equation, rather than the determination of a saddle point in a three dimensional parameter space. All other interaction terms were neglected. Thus all interactions are now encoded in the

**In the special case of $f_2 = 0 = g$ the model becomes an $O(16)$ model, which is invariant under $O(18)$ rotations. We have $N = 18 = 2n_f^2$, where n_f denotes the number of quark flavors, while N labels the number of mesonic modes. Terms of order $O(1/N)$ are dropped, as long as fluctuations in the auxiliary field are neglected.

meson masses, and we can use the formula of an ideal gas given in Equation (2.55). We finally have

$$\begin{aligned}\Omega_{\text{eff}}(\sigma_0,\sigma_8,s) &= \Omega_{\text{class}}(\sigma_0,\sigma_8) + \Omega_{\text{sadd}}(s) \\ &+ \frac{T^4}{2\pi^2}\sum_{Q=1}^{8} g(Q)\left\{-\left(\frac{\tilde{m}_Q}{T}\right)^2 \sum_{l=1}^{\infty}\frac{1}{l^2}K_2\left(\frac{l\tilde{m}_Q}{T}\right)\right\} \quad . \end{aligned} \tag{3.41}$$

In the second and third line of Equation (3.41) one finds the thermodynamic potential of a free Bose and Fermi gas, respectively, where g are the particle multiplicities and K_2 is a modified Bessel function. In the integration $\int \mathcal{D}\Phi$ the ultraviolet divergent zero-point energies have been neglected.

The method to compute the order parameters $\langle\sigma_0\rangle(T)$ $\langle\sigma_8\rangle(T)$ is now the following: for a given temperature T one minimizes $\Omega_{\text{eff}}(\sigma_0,\sigma_8,s^*(\sigma_0,\sigma_8))$, where $s^*(\sigma_0,\sigma_8)$ denotes the maximum of Ω_{eff} for constant (σ_0,σ_8). We determine a critical point in the (h_0,h_8)-plane via the mixed susceptibilities χ_0 and χ_8, which we define as

$$\begin{aligned}\chi_0 &\equiv \left.\frac{\partial^2\Omega_{\text{eff}}}{\partial T\partial h_0}\right|_{\text{saddle point}} = \frac{\partial}{\partial T}\langle\sigma_0\rangle(T)\ , \\ \chi_8 &\equiv \left.\frac{\partial^2\Omega_{\text{eff}}}{\partial T\partial h_8}\right|_{\text{saddle point}} = \frac{\partial}{\partial T}\langle\sigma_8\rangle(T)\ . \end{aligned} \tag{3.42}$$

These quantities should diverge as the system undergoes a phase transition of second order. For fixed values of (h_0,h_8) we compute $\langle\sigma_0\rangle$ and $\langle\sigma_8\rangle$ for different temperatures. Then we interpolate in temperature by the use of Chebycheff polynomials. The derivative of these polynomials yields the mixed susceptibilities as a function of temperature. We find that $\chi_0(T)$ and $\chi_8(T)$ peak at the same temperature T_{ps}. From the peaks we determine the pseudo critical temperature T_{ps} and the peak heights as

$$\left.\frac{\partial\chi_0(T)}{\partial T}\right|_{T\equiv T_{ps}} = 0\ , \quad \chi_0^c \equiv \chi_0(T_{ps})\ , \quad \chi_8^c \equiv \chi_8(T_{ps})\ . \tag{3.43}$$

By plotting χ_0^c along a straight line in the (h_0,h_8)-plane, starting at a point where no phase transition occurs and going towards lower external fields, one finds a power like decrease in the quantity χ_0^c. For the $n_f=3$ case this is shown in Figure 3.10(a). We parameterize several lines by

$$\begin{pmatrix} h_0 \\ h_8 \end{pmatrix} = \begin{pmatrix} h_0^{\text{offset}} \\ h_8^{\text{offset}} \end{pmatrix} + x\begin{pmatrix} \cos\vartheta \\ \sin\vartheta \end{pmatrix}\ , \tag{3.44}$$

and perform least square fits with the power law

$$\chi_0^c = a(x-x_c)^{-d} \quad . \tag{3.45}$$

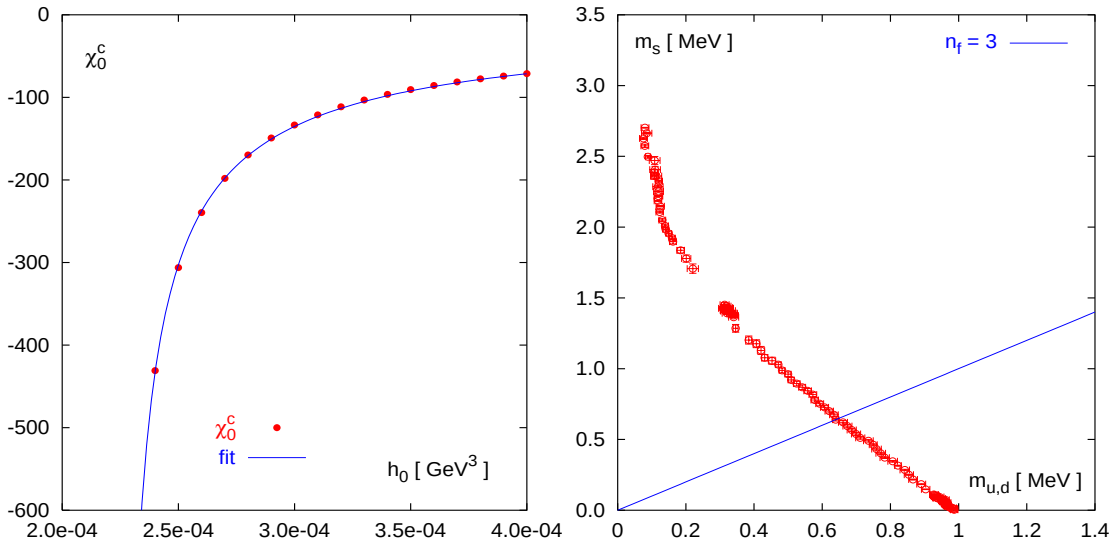

(a) (b)

Figure 3.10: (a) Mixed susceptibility χ_0^c as a function of h_0 in the $n_f = 3$ case, i.e. $h_8 = 0$. The solid line is a power law fit. (b) The critical line of second order phase transitions in the quark mass plane. The green line shows the $n_f = 3$ case, whereas the blue line indicates the line of physical quark mass ratio.

For the exponent d we find values, which are very close to the mean field exponent $d = 0.5$. From the value of x_c we get a critical point in the (h_0, h_8)-plane, which we map into the $(m_{u,s}, m_s)$-plane according to Equation (3.27). The results are shown in Figure 3.10(b). For the $n_f = 3$ case we find a critical external field of $h_0^c = 2.23(3) \times 10^{-4}\,\mathrm{GeV}^3$, which coincides with that which was found in [88] by analyzing the discontinuities of the order parameter. Our error however is an order of magnitude smaller. Qualitatively very similar lines, as shown in Figure 3.10(b), have also been found in [96] within the CJT formalism. In [96] a strong dependence on the sigma mass was found, which was not investigated here.

Figure 3.10(b) suggests, that the critical line in the $(m_{u,d}, m_s)$-quark mass plane can be approximated by a straight line over a wide range of quark mass values. A comparison with the critical line in the bar quark mass plane of staggered fermions is shown in Figure 3.5. Of course, the values for the critical external fields $h_8^c(h_0)$ also specify critical values for the meson masses at $T = 0$. The critical line in the pseudo scalar (m_π, m_K)-plane is plotted in Figure 3.8. In the $n_f = 3$ case we find critical pion mass of $m_\pi \approx 44$ MeV, which is not in contradiction with that value found from simulations with improved staggered fermions.

This model can be extended to $\mu > 0$ when using the full Hamiltonian given in 3.23. Moreover one can investigate not only the chiral phase transition but also transitions to color superconduct-

ing phases, when adding also quark-quark condensates to the Hamiltonian in a chiral invariant way. This has been done, for instance, in [97, 98]. One should, however, not for get, that those calculations are model calculations which do not involve gluons or contributions from heavier resonances. The need for the latter becomes clear form the resonance gas calculations in Section 4.4.

Chapter 4

The equation of state*

One of the central goals of studies of the QCD thermodynamics on the lattice is the calculation of the equation of state for QCD with a realistic mass spectrum. In particular the influence of the heavier strange quark mass on bulk thermodynamic observables is of fundamental importance for the analysis and interpretation of heavy ion experiments. This is so, since one of the signatures which is being discussed for the formation of a quark-gluon plasma within heavy-ion experiments is the increase of the relative abundance of strange particles (strangeness enhancement) [2]. The influence of the strange quark on the equation of state at vanishing chemical potential ($\mu_q = 0$) was discussed in [12], when calculating the pressure for two and three flavor of p4 improved quarks with mass $m_q/T = 0.4$, and for $2 + 1$ flavor with an additional strange quark of mass $m_s/T = 1$. We will study here corrections to the two flavor results from Reference [12], for non-zero chemical potential, by calculating the first two non-trivial terms in the Taylor series of the pressure $p(T, \mu)$.

The most fundamental quantity in equilibrium thermodynamics is, of course the partition function itself, or within the grand canonical ensemble the thermodynamic grand potential

$$\Omega(T, V, \mu) = -\frac{T}{V} \ln Z(T, V, \mu) \quad . \tag{4.1}$$

All basic bulk thermodynamic observables can be derived from the thermodynamic potential via Maxwell relations. In the thermodynamic limit we obtain directly the pressure, $p = -\Omega$ and subsequently also other quantities like the quark number (n_q) and energy (ϵ) densities

$$n_q = \frac{\partial p}{\partial \mu_q} \quad , \qquad \frac{\epsilon - 3p}{T^4} = T \frac{\partial}{\partial T} \left(\frac{p}{T^4} \right) \quad , \tag{4.2}$$

*Based on Reference [25]

In order to make use of the basic thermodynamic relations in numerical calculations on the lattice we have to go through an additional intermediate step. The grand canonical potential itself is not directly accessible in Monte Carlo calculations; e.g. only expectation values can be calculated easily. One thus proceeds by calculating derivatives of $\ln Z$ with respect to the parameters of the action (β, m, μ), followed by an integration [99]. This way the pressure is given up to an unknown integration constant ($C_{\text{int.}}$) by

$$\frac{p}{T^4}(\beta,m,\mu) = \frac{1}{T^3 V} \oint_{(\beta_0,m_0,\mu_0)}^{(\beta,m,\mu)} \mathrm{d}(\beta',m',\mu') \left(\left\langle \frac{\partial \ln Z}{\partial \beta'} \right\rangle, \left\langle \frac{\partial \ln Z}{\partial m'} \right\rangle, \left\langle \frac{\partial \ln Z}{\partial \mu'} \right\rangle \right) + C_{\text{int.}} \ . \quad (4.3)$$

Here the integration is to be understood as the integration along an abitrary path from point (β_0, m_0, μ_0) to point (β, m, μ), while $\mathrm{d}(\beta', m', \mu')$ is the line element of the path. The integration constant is usually set to zero at $(T = 0, \mu_q = 0)$. The integral method was used to compute the pressure at $\mu_q = 0$ [12, 14] and at $\mu_q \neq 0$ [17].

4.1 The pressure at finite density

We proceed by performing a Taylor expansion of the pressure about $\mu_q = 0$, in powers of the dimensionless quantity μ_q/T,

$$\begin{aligned} \Delta\left(\frac{p}{T^4}(\mu_q)\right) \equiv \left.\frac{p}{T^4}\right|_{T,\mu_q} - \left.\frac{p}{T^4}\right|_{T,0} &= \frac{1}{2!}\frac{\mu_q^2}{T^2}\frac{\partial^2(p/T^4)}{\partial(\mu_q/T)^2} + \frac{1}{4!}\frac{\mu_q^4}{T^4}\frac{\partial^4(p/T^4)}{\partial(\mu_q/T)^4} + \cdots \\ &\equiv \sum_{p=1}^{\infty} c_p(T)\left(\frac{\mu_q}{T}\right)^p \quad , \end{aligned} \quad (4.4)$$

where derivatives are taken at $\mu_q = 0$. Note that calculating $\Delta(p/T^4)$ is considerably easier than $p(T, \mu_q = 0)$ itself, because whereas $\ln Z$ must be estimated by integrating along a trajectory in the bare parameter plane [12, 14, 17], its derivatives can be related to observables which are directly calculabel at fixed (β, m), where β is the gauge coupling parameter and m the bare quark mass. Only even powers appear in (4.4) because as discussed in Section 2.3.3, odd derivatives of the free energy with respect to μ_q vanish at this point. Note also that we will work throughout with fixed bare mass, implying that our computation of $\Delta(p/T^4)$ is strictly valid along a line of fixed m/T. Equation (4.4) then becomes

$$\Delta\left(\frac{p}{T^4}\right) = \frac{1}{2}\frac{N_\tau^3}{N_\sigma^3}\mu^2\frac{\partial^2 \ln Z}{\partial \mu^2} + \frac{1}{24}\frac{N_\tau^3}{N_\sigma^3}\mu^4\frac{\partial^4 \ln Z}{\partial \mu^4} + \cdots \quad . \quad (4.5)$$

The derivatives may be expressed as expectation values evaluated at $\mu = 0$:

$$\frac{\partial^2 \ln Z}{\partial \mu^2} = \left\langle \frac{n_f}{4}\frac{\partial^2(\ln\det M)}{\partial \mu^2} \right\rangle + \left\langle \left(\frac{n_f}{4}\frac{\partial(\ln\det M)}{\partial \mu}\right)^2 \right\rangle \quad , \quad (4.6)$$

$$\frac{\partial^4 \ln Z}{\partial \mu^4} = \left\langle \frac{n_f}{4} \frac{\partial^4 (\ln \det M)}{\partial \mu^4} \right\rangle + 4 \left\langle \left(\frac{n_f}{4}\right)^2 \frac{\partial^3 (\ln \det M)}{\partial \mu^3} \frac{\partial (\ln \det M)}{\partial \mu} \right\rangle \tag{4.7}$$
$$+3 \left\langle \left(\frac{n_f}{4}\right)^2 \left(\frac{\partial^2 (\ln \det M)}{\partial \mu^2}\right)^2 \right\rangle + 6 \left\langle \left(\frac{n_f}{4}\right)^3 \frac{\partial^2 (\ln \det M)}{\partial \mu^2} \left(\frac{\partial (\ln \det M)}{\partial \mu}\right)^2 \right\rangle$$
$$+ \left\langle \left(\frac{n_f}{4} \frac{\partial (\ln \det M)}{\partial \mu}\right)^4 \right\rangle - 3 \left[\left\langle \frac{n_f}{4} \frac{\partial^2 (\ln \det M)}{\partial \mu^2} \right\rangle + \left\langle \left(\frac{n_f}{4} \frac{\partial (\ln \det M)}{\partial \mu}\right)^2 \right\rangle \right]^2 \quad .$$

All expectation values are calculated using the measure $Z^{-1}(\mu = 0)\mathcal{D}U(\det M[\mu = 0])^{n_f/4} e^{-S_g}$ and in deriving (4.6) and (4.7) we used the fact that $\langle \partial^n (\ln \det M)/\partial \mu^n \rangle = 0$ for n odd. To evaluate these expressions we need the following explicit forms:

$$\frac{\partial (\ln \det M)}{\partial \mu} = \mathrm{Tr} \left(M^{-1} \frac{\partial M}{\partial \mu} \right) \quad , \tag{4.8}$$

$$\frac{\partial^2 (\ln \det M)}{\partial \mu^2} = \mathrm{Tr} \left(M^{-1} \frac{\partial^2 M}{\partial \mu^2} \right) - \mathrm{Tr} \left(M^{-1} \frac{\partial M}{\partial \mu} M^{-1} \frac{\partial M}{\partial \mu} \right) \quad , \tag{4.9}$$

$$\frac{\partial^3 (\ln \det M)}{\partial \mu^3} = \mathrm{Tr} \left(M^{-1} \frac{\partial^3 M}{\partial \mu^3} \right) - 3\ \mathrm{Tr} \left(M^{-1} \frac{\partial M}{\partial \mu} M^{-1} \frac{\partial^2 M}{\partial \mu^2} \right) \tag{4.10}$$
$$+2\ \mathrm{Tr} \left(M^{-1} \frac{\partial M}{\partial \mu} M^{-1} \frac{\partial M}{\partial \mu} M^{-1} \frac{\partial M}{\partial \mu} \right) \quad ,$$

$$\frac{\partial^4 (\ln \det M)}{\partial \mu^4} = \mathrm{Tr} \left(M^{-1} \frac{\partial^4 M}{\partial \mu^4} \right) - 4\ \mathrm{Tr} \left(M^{-1} \frac{\partial M}{\partial \mu} M^{-1} \frac{\partial^3 M}{\partial \mu^3} \right) \tag{4.11}$$
$$-3\ \mathrm{Tr} \left(M^{-1} \frac{\partial^2 M}{\partial \mu^2} M^{-1} \frac{\partial^2 M}{\partial \mu^2} \right) + 12\ \mathrm{Tr} \left(M^{-1} \frac{\partial M}{\partial \mu} M^{-1} \frac{\partial M}{\partial \mu} M^{-1} \frac{\partial^2 M}{\partial \mu^2} \right)$$
$$-6\ \mathrm{Tr} \left(M^{-1} \frac{\partial M}{\partial \mu} M^{-1} \frac{\partial M}{\partial \mu} M^{-1} \frac{\partial M}{\partial \mu} M^{-1} \frac{\partial M}{\partial \mu} \right) \quad .$$

The traces can be estimated using the stochastic method reviewed in Section 2.3.3. Since $\partial^n M/\partial \mu^n$ is a local operator, expressions containing k powers of M^{-1} require k operations of matrix inversion on a vector.

We applied this formalism to numerical simulations of QCD with $n_f = 2$ quark flavors on a $16^3 \times 4$ lattice, using both Symanzik improved gauge and p4-improved staggered fermion actions. The bare quark mass was $ma = 0.1$ for which the pseudocritical point for zero chemical potential is estimated to be $\beta_c \simeq 3.649(2)$. In order to cover a range of temperatures on either side of the critical point we examined 16 values in the range $\beta \in [3.52, 4.0]$. The simulation employed a hybrid molecular dynamic 'R'-algorithm with discrete time step $\delta\tau = 0.025$, and measurements were performed on equilibrated configurations separated by $\tau = 5$. In general for each β value 500 configurations were analyzed, with 1000 used in the critical region $\beta \in [3.58, 3.66]$. On each configuration 50 stochastic noise vectors were used to estimate the required fermionic operators. For each noise vector, 7 matrix inversions are required to estimate the required operators (2.45-4.11) and (C.6-C.9).

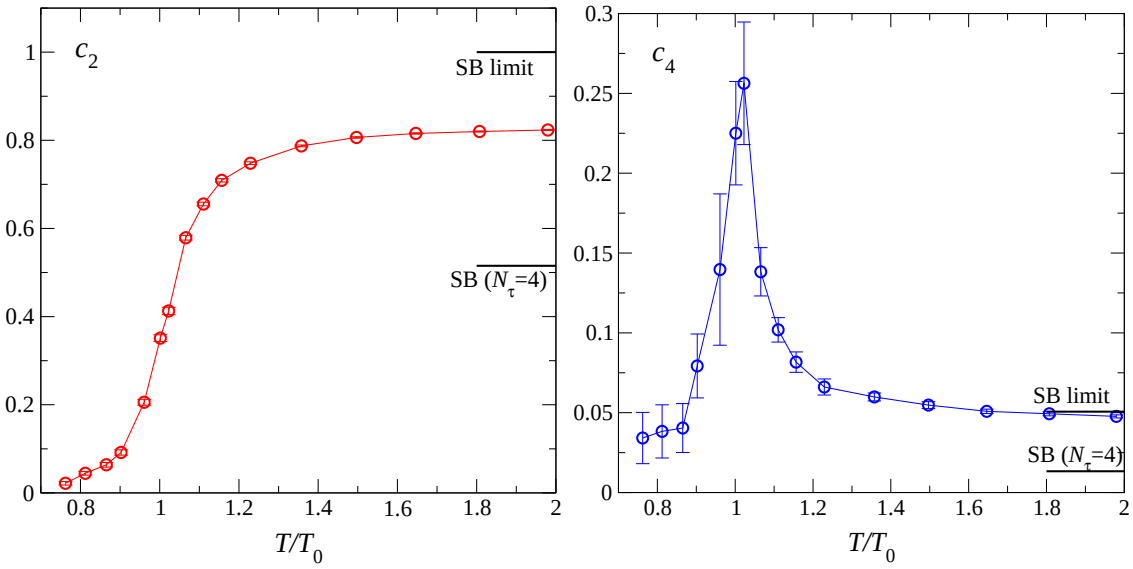

Figure 4.1: Coefficients of (a) $(\mu_q/T)^2$ and (b) $(\mu_q/T)^4$ in the Taylor expansion of $\Delta(p/T^4)$ as functions of T/T_0.

To set the temperature scale we again follow the procedure used for the equation of state at $\mu = 0$ [12], and we translate to physical units using the scaling ansatz (3.21). We find that our simulations span a temperature range $T/T_0 \in [0.76, 1.98]$, where T_0 is the critical temperature at $\mu_q = 0$.

In Figure 4.1 we show the first two coefficients, (a) c_2 and (b) c_4, of the Taylor expansion of $\Delta(p/T^4)$ introduced in (4.4) as functions of T/T_0. Also shown are the corresponding SB limits: (a) $n_f\mathcal{C}_2(N_\tau)$ and (b) $N_\mathrm{f}\mathcal{C}_4(N_\tau)$, where the coefficients $\mathcal{C}_i$ are defined in (2.62), with values relevant for both the lattice used ($N_\tau = 4$) and the continuum limit ($N_\tau = \infty$) plotted. Both c_2 and c_4 vary sharply in the critical region, but except in the immediate vicinity of the transition the quadratic term dominates the quartic. This is consistent with the results of [17] where data at varying μ obtained by reweighting was found to lie on an almost universal curve when plotted as a fraction of the SB prediction. The asymptotic value of c_4 appears to be approached from above.

A notable feature is that in the high-T limit our data lies closer to the continuum SB prediction rather than their values $\mathcal{C}_i(N_\tau = 4)$ corrected for lattice artifacts, c_2 assuming 80% of the continuum value for $T/T_0 = 2$ whereas c_4 is almost coincident with its continuum value. By contrast recent calculations with unimproved staggered fermions [17, 21] find that the high-T limit of the data lie close to the lattice-corrected SB value. This situation can be modeled by making the coefficient d of the $O(N_\tau^{-2})$ correction appearing in (2.56) temperature dependent. In thermodynamic calculations performed with pure unimproved SU(3) lattice gauge theory [100], where extrapolations to the

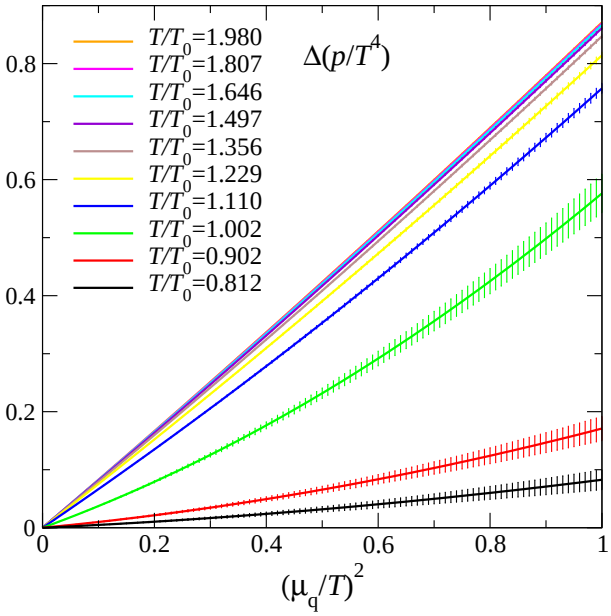

Figure 4.2: $\Delta(p/T^4)$ as a function of $(\mu_q/T)^2$ for various temperatures, increasing upwards from the lowest curve with $T/T_0 = 0.812$ to the highest with $T/T_0 = 1.980$.

continuum limit are currently practicable, it is found that $d(T) \simeq 0.5d(T = \infty)$ for $T \sim 3T_0$, becoming even smaller closer to T_0. The behavior of c_2 and c_4 we have observed using p4 fermions is broadly consistent with this behavior.

In Figure 4.2 we plot $\Delta(p/T^4)$ defined in (4.4) as a function of $(\mu_q/T)^2$ for various temperatures. In most cases $c_4 \ll c_2$ and the relation thus almost linear. The strongest departures from linearity are for $T \simeq T_0$, but even here the quadratic term is dominant for $(\mu_q/T)^2 \lesssim 0.4$, corresponding to $\mu_q \lesssim 100$MeV. Given enough terms of the Taylor expansion in μ_q/T, one could determine its radius of convergence ρ via[†]

$$\rho = \lim_{n\to\infty} \rho_n \equiv \lim_{n\to\infty} \sqrt{\left|\frac{c_n}{c_{n+2}}\right|} \quad . \tag{4.12}$$

Data from the pressure at $\mu_q = 0$ [12] and the current study enable us to plot the first two estimates ρ_0 and ρ_2 on the (μ_q, T) plane along with the estimated pseudocritical line $T_c(\mu_q)$ found in Section 3.3 in Figure 4.3. Also shown are the corresponding values from the SB limit (2.54). For $T > T_c$ one finds that ρ_n increases markedly as n increases from 0 to 2; if the SB limit is a

[†]The argument of [10] that $\rho \leq \frac{\pi}{3}$ due to the presence of a phase transition as imaginary chemical potential is increased beyond this value [101] does not hold for calculations with μ_q real; in this case the pressure p_0 corresponding to the unit element of the Z(3) sector is always the maximum and hence dominates the partition function in the thermodynamic limit – hence the issue concerns the analytic properties *within* this physical unit sector.

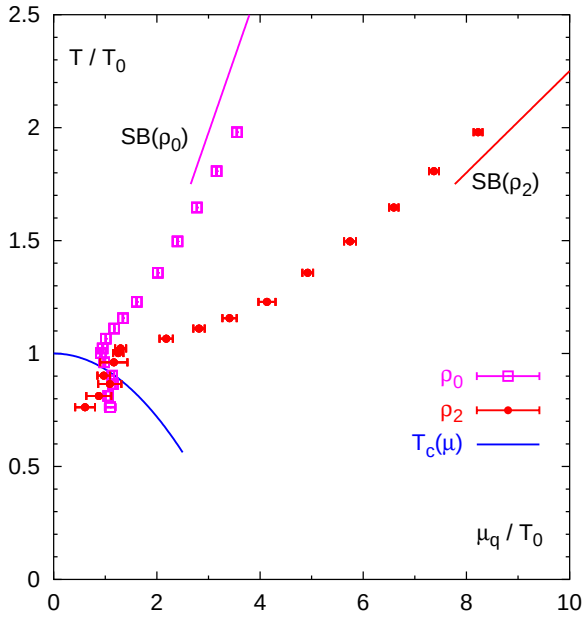

Figure 4.3: Estimates for the radius of convergence $\rho(\mu_q, T)$.

good predictor for the QGP phase we might expect c_6 to be very small, and the next estimate ρ_4 correspondingly very large in this regime. Close to the transition line, however, the thermodynamic singularities appear to restrict $\rho \sim O(1)$; this in turn gives an approximate lower bound for the position of the critical endpoint. From the figure we deduce $\mu_q^{crit} \gtrsim (1 - 1.2)T_0$, not inconsistent with the result of [9]. The new results at $O(\mu^4)$ are important because they justify in retrospect our neglect of fourth order reweighting factors in our calculation of the transition line which has been discussed in Chapter 3. Indeed, also simulations with imaginary μ suggest that neglect of these terms in the analytic continuation to physical μ_q is justified for $\mu_q \lesssim 170$MeV [10].

Figure 4.4 plots the dimensionless correction $\Delta(p/T^4)$ to the equation of state as a function of both μ_q/T and μ_q. In the latter case the correction rises steeply across the transition and peaks for $T \simeq 1.1T_0$, before rapidly approaching a form $\Delta(p/T^4) = \alpha T^{-2}$ characteristic of the SB limit, with the coefficient α having 82% of the continuum SB value. Comparison with the equation of state results at $\mu_q = 0$ from Reference [12] suggest that the correction will give a significant correction to the pressure for $0.9 \lesssim T/T_0 \lesssim 1.3$, $\mu_q/T_0 \gtrsim 0.5$, but will decrease in importance as T rises further. The curves of Figure 4.4b are in good qualitative agreement with those of References [17, 21], although we consider any quantitative agreement to be somewhat accidental as the numerical data obtained in [17, 21] with unimproved actions have large discretization errors which have been corrected for by renormalizing the raw data with the known discretization errors in the infinite temperature

limit. Experience gained in calculations of thermodynamic quantities in the pure SU(3) gauge theory suggests that in the temperature range of a few times T_0 this procedure overestimates the importance of cutoff effects by a factor two or so [100].

4.2 The quark number density

Next we discuss the quark number density n_q and its fluctuations. Starting from the definition (4.2), we can write an equation for the quark number density n_q analogous to (4.5):

$$\frac{n_q}{T^3} = \frac{N_\tau^2}{N_\sigma^3}\mu\frac{\partial^2 \ln Z}{\partial \mu^2} + \frac{1}{6}\frac{N_\tau^2}{N_\sigma^3}\mu^3\frac{\partial^4 \ln Z}{\partial \mu^4} + \cdots \quad . \tag{4.13}$$

It is also possible to interpret derivatives of p with respect to μ_q in terms of the various susceptibilities giving information on number density fluctuations [20]. We define quark number (q), isospin (I) and charge (C) susceptibilities as follows:

$$\frac{\chi_q}{T^2} = \left(\frac{\partial}{\partial(\mu_{\rm u}/T)} + \frac{\partial}{\partial(\mu_{\rm d}/T)}\right)\frac{n_{\rm u}+n_{\rm d}}{T^3} \quad , \tag{4.14}$$

$$\frac{\chi_{\rm I}}{T^2} = \frac{1}{4}\left(\frac{\partial}{\partial(\mu_{\rm u}/T)} - \frac{\partial}{\partial(\mu_{\rm d}/T)}\right)\frac{n_{\rm u}-n_{\rm d}}{T^3} \quad , \tag{4.15}$$

$$\frac{\chi_{\rm C}}{T^2} = \left(\frac{2}{3}\frac{\partial}{\partial(\mu_{\rm u}/T)} - \frac{1}{3}\frac{\partial}{\partial(\mu_{\rm d}/T)}\right)\frac{2n_{\rm u}-n_{\rm d}}{3T^3} \quad . \tag{4.16}$$

Quark and baryon number susceptibilities are related by $\chi_{\rm B} \equiv \partial n_{\rm B}/\partial\mu_{\rm B} = 3^{-2}\chi_q$. Any difference between χ_q and $4\chi_{\rm I}$ is due to correlated fluctuations in the individual densities of u and d quarks. With the choice $\mu_{\rm u} = \mu_{\rm d} = \mu_q = \mu a^{-1}$, $m_{\rm u} = m_{\rm d}$, which approximates the physical conditions at RHIC, χ_q can then be expanded in terms of quantities already used in the calculation of p and n_q:

$$\left.\frac{\chi_q}{T^2}\right|_{\mu_q=0} \equiv \frac{1}{T^2}\frac{\partial n_q}{\partial \mu_q} = \frac{N_\tau}{N_\sigma^3}\frac{\partial^2 \ln Z}{\partial \mu^2} \quad ; \qquad \left.\frac{\partial^2(\chi_q/T^2)}{\partial(\mu_q/T)^2}\right|_{\mu_q=0} = \frac{1}{N_\tau N_\sigma^3}\frac{\partial^4 \ln Z}{\partial \mu^4} \quad , \tag{4.17}$$

whereas the expansion of $\chi_{\rm I}$ is determined by the following expectation values:

$$\left.\frac{\chi_{\rm I}}{T^2}\right|_{\mu_q=0} = \frac{N_\tau}{4N_\sigma^3}\left\langle \frac{2}{4}\frac{\partial^2(\ln\det M)}{\partial\mu^2}\right\rangle \quad , \tag{4.18}$$

$$\begin{aligned}\left.\frac{\partial^2(\chi_{\rm I}/T^2)}{\partial(\mu_q/T)^2}\right|_{\mu_q=0} = \frac{1}{4N_\sigma^3 N_\tau}\Bigg[&\left\langle \frac{2}{4}\frac{\partial^4(\ln\det M)}{\partial\mu^4}\right\rangle + 2\left\langle \left(\frac{2}{4}\right)^2 \frac{\partial^3(\ln\det M)}{\partial\mu^3}\frac{\partial(\ln\det M)}{\partial\mu}\right\rangle \\ &+ \left\langle \left(\frac{2}{4}\right)^2 \left(\frac{\partial^2(\ln\det M)}{\partial\mu^2}\right)^2\right\rangle + \left\langle \left(\frac{2}{4}\right)^3 \frac{\partial^2(\ln\det M)}{\partial\mu^2}\left(\frac{\partial(\ln\det M)}{\partial\mu}\right)^2\right\rangle \\ &- \left[\left\langle \frac{2}{4}\frac{\partial^2(\ln\det M)}{\partial\mu^2}\right\rangle + \left\langle \left(\frac{2}{4}\frac{\partial(\ln\det M)}{\partial\mu}\right)^2\right\rangle\right]\left\langle \frac{2}{4}\frac{\partial^2(\ln\det M)}{\partial\mu^2}\right\rangle\Bigg] \quad ,\end{aligned} \tag{4.19}$$

where we have explicitly set $n_f = 2$. Charge fluctuations are then given by the relation

$$\frac{\chi_{\rm C}}{T^2} = \frac{1}{36}\frac{\chi_q}{T^2} + \frac{\chi_{\rm I}}{T^2} + \frac{1}{6}\left(\frac{\partial(n_{\rm u}/T^3)}{\partial(\mu_{\rm u}/T)} - \frac{\partial(n_{\rm d}/T^3)}{\partial(\mu_{\rm d}/T)}\right) \quad , \tag{4.20}$$

where the third term vanishes for $\mu_{\rm u} = \mu_{\rm d}$, $m_{\rm u} = m_{\rm d}$.

Figure 4.5a shows the quark number density n_q evaluated using Equation (4.13). As μ_q increases, n_q rises steeply as the QGP phase is entered; for reference, if the quark number density in nuclear matter is denoted $\bar{n}_q$, then the ratio $\bar{n}_q/T_0^3 \approx 0.75$. Our results are numerically very similar to those obtained using exact reweighting in [17], where a mass $ma \approx 0.1$ for the light quark flavors was used. Note that a significant quark mass dependence for n_q was observed in [19], and indeed is present even in the SB limit as described in Section 2.4; however analysis of the SB limit suggests that the difference between the chiral limit and $m/T = 0.4$ is about 4%. In Figure 4.5(b) we show the result of eliminating μ_q in favour of n_q via

$$\Delta\left(\frac{p}{T^4}\right) = \frac{1}{4c_2}\left(\frac{n_q}{T^3}\right)^2 - \frac{3c_4}{16c_2^4}\left(\frac{n_q}{T^3}\right)^4 + O\left(\frac{n_q}{T^3}\right)^6 \quad . \tag{4.21}$$

The relation (4.21) approximates the "true" equation of state in terms of physically measurable quantities; we have plotted the resulting $\Delta(p/T^4)$ against $(n_q/T^3)^2$ up to the point where the ratio of the magnitude of the second term of (4.21) to that of the first is 40%: the point $n_q/T^3 = \sqrt{2c_2^3/3c_4}$ where the ratio is 50% marks a mechanical instability $\partial p/\partial n_q = 0$, which is an artifact due to the truncation of the series. Stability of the equilibrium state under local fluctuations δn_q requires $\partial p/\partial n_q > 0$, an example of Le Châtelier's principle. As T/T_0 increases through unity, the equation of state changes from a form resembling the low-T SB limit $p \propto n_q^{4/3}$ to the stiffer $p \propto n_q^2$ characteristic of the high-T SB limit. Interestingly enough, to the order we have calculated the instability artifact sets in at $\mu_q/T \simeq 1.4$ for T large, but at $\mu_q/T \simeq 0.4$ for $T \approx T_0$, thus providing an independent, and more stringent, limit to the physical validity of our approach, and reflecting the importance of contributions from higher orders in the Taylor expansion close to $T_c(\mu_q)$.

Next, in Figure 4.6 we plot the expansion coefficients corresponding to the various susceptibilities defined in (4.14-4.16). For $T \lesssim T_0$ there is a significant difference between $\chi_q(\mu_q = 0)$ and $4\chi_{\rm I}(\mu_q = 0)$, implying anti-correlated fluctuations of $n_{\rm u}$ and $n_{\rm d}$ which rapidly decrease in magnitude above T_0 and vanish as T approaches the infinite temperature SB limit[‡]. In the same limit the

[‡]There has recently been a discussion whether the difference $(4\chi_I - \chi_q)/T^2$ is exactly zero in the high temperature phase, as suggested by some lattice calculations [102], or just small but non-zero, as found in perturbative calculations [103]. We find that the difference stays non-zero but decreases by one order of magnitude between $T \simeq T_0$ and $T \simeq 1.5T_0$. At $T \simeq 1.36T_0$ we find a value of 0.0066(28) for this difference calculated in 2-flavor QCD which clearly disagrees with the quenched result $(2 \pm 4) \cdot 10^{-6}$ presented in [102] as well as the recent 2-flavor results of this group [21]. Our results are, however, in agreement with the findings of Reference [104]. At $T \simeq 2T_0$ the numerical value

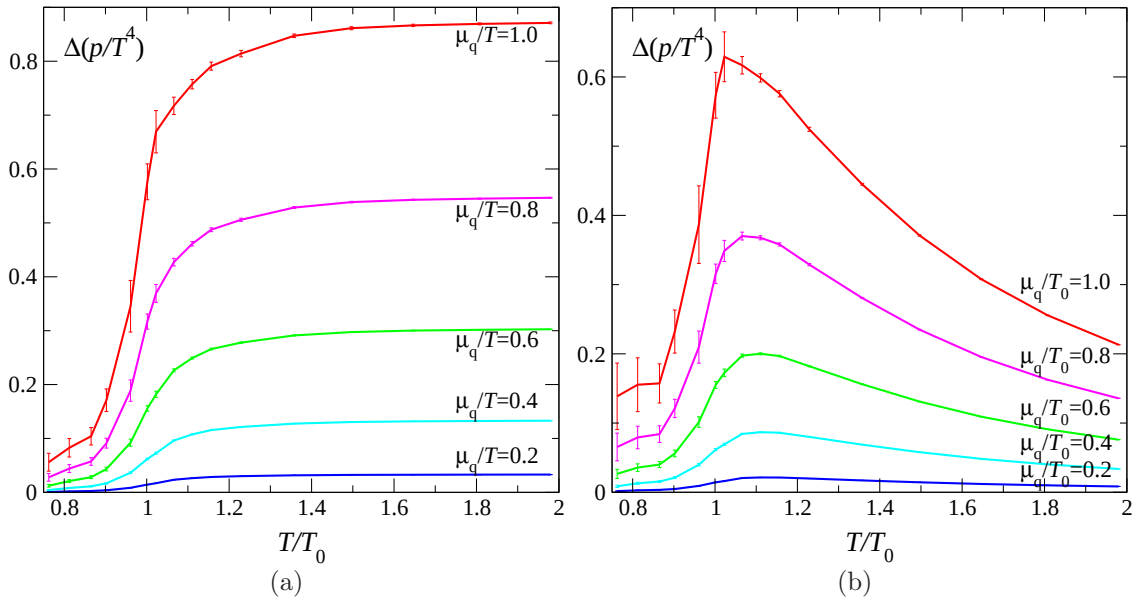

Figure 4.4: The equation of state correction $\Delta(p/T^4)$ vs. T/T_0 for (a) various μ_q/T, and (b) various μ_q/T_0.

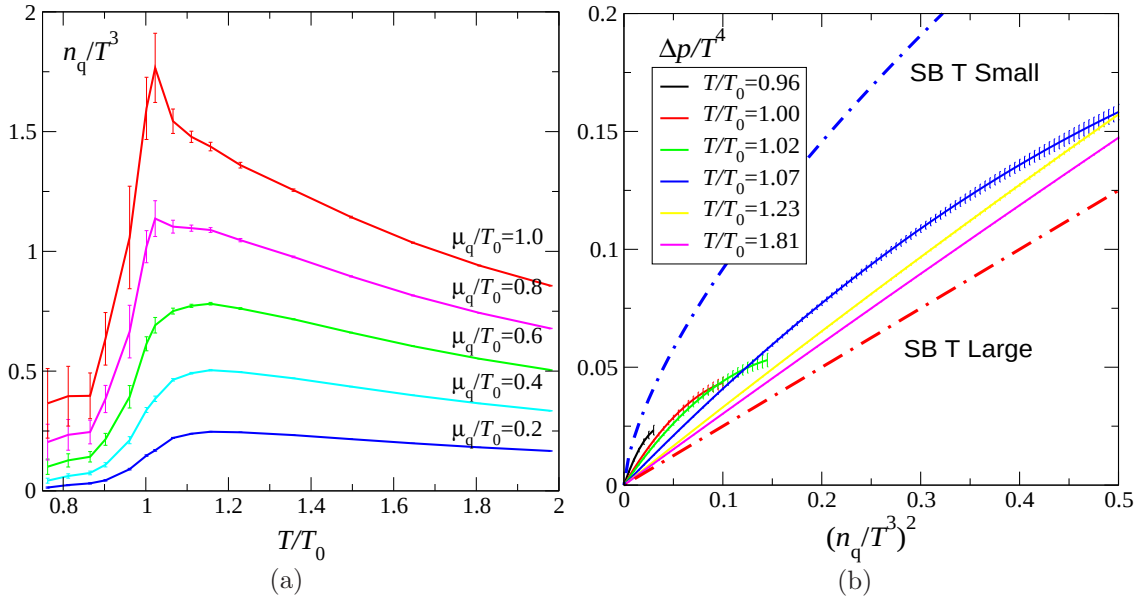

Figure 4.5: (a) n_q/T^3 as a function of T/T_0 for various μ_q/T_0, and (b) the "true" equation of state $\Delta(p/T^4)$ vs. $(n_q/T^3)^2$ for various temperatures. The continuum SB forms $\frac{1}{4}(\pi^2/N_{\rm f})^{1/3}(n_q/T^3)^{4/3}$ (low T) and $(2n_f)^{-1}(n_q/T^3)^2$ (high T) are also shown as functions of T/T_0.

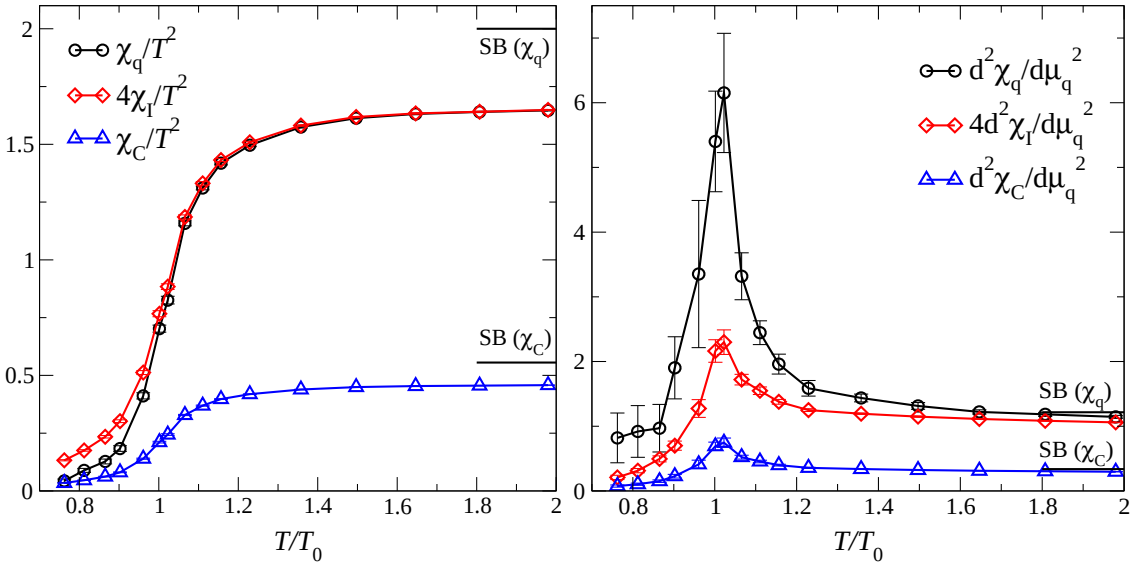

Figure 4.6: Susceptibilities (a) $\chi_i/T^2|_{\mu_q=0}$, and (b) $\partial^2\chi_i/\partial\mu_q^2|_{\mu_q=0}$ as functions of T/T_0.

charge susceptibility $\chi_{\rm C}$ approaches the value $\frac{5}{18}\chi_q$. The critical singularity in $4\chi_{\rm I}$ and $\chi_{\rm C}$ is weaker than that of χ_q, which can be traced back to the differing coefficients of $\langle(\partial^2 \ln \det M/\partial\mu^2)^2\rangle$, the dominant term in the vicinity of T_c, in the definitions (4.7) and (4.19). The dimensionless quantity $T\chi_{\rm C}/s$, where $s = (\epsilon + p - \mu_q n_q)/T$ is the entropy density, can be related to event-by-event fluctuations in charged particle multiplicities in RHIC collisions, and has been proposed as a signal for QGP formation [106]. Event-by-event fluctuations in baryon number have also recently been discussed in [107].

In Figure 4.7 the relation (4.17) and data of Figure 4.1 have been used to plot the dimensionless quark number susceptibility χ_q/T^2 as a function of T/T_0 for various μ_q/T. The peak which develops in χ_q as μ_q increases is a sign that fluctuations in the baryon density are growing as the critical endpoint in the (μ, T) plane is approached. Physically, this shows that at the critical point, as well as strong fluctuations in the $(\bar\psi\psi)$ bilinear expected at a chiral phase transition there are also fluctuations in $(\bar\psi\gamma_0\psi)$ since Lorentz symmetry is explicitly broken by the background baryon charge density. For quantities such as n_q and χ_q defined as higher derivatives of the free energy with respect to μ_q, the relative importance of the higher order terms in the Taylor series expansion is increased; for example, at $T \simeq T_0$ and $\mu_q/T = 1$ the quadratic contribution to $\chi_q(\mu_q)$ is about 3 times that of the leading order term. For this reason we do not expect the data of Figure 4.7

of this difference drops below our current error level of about $2 \cdot 10^{-3}$. In the high temperature limit this error is thus not yet small enough to discuss numerical effects at the level of 10^{-4} as suggested in the discussion presented in [105].

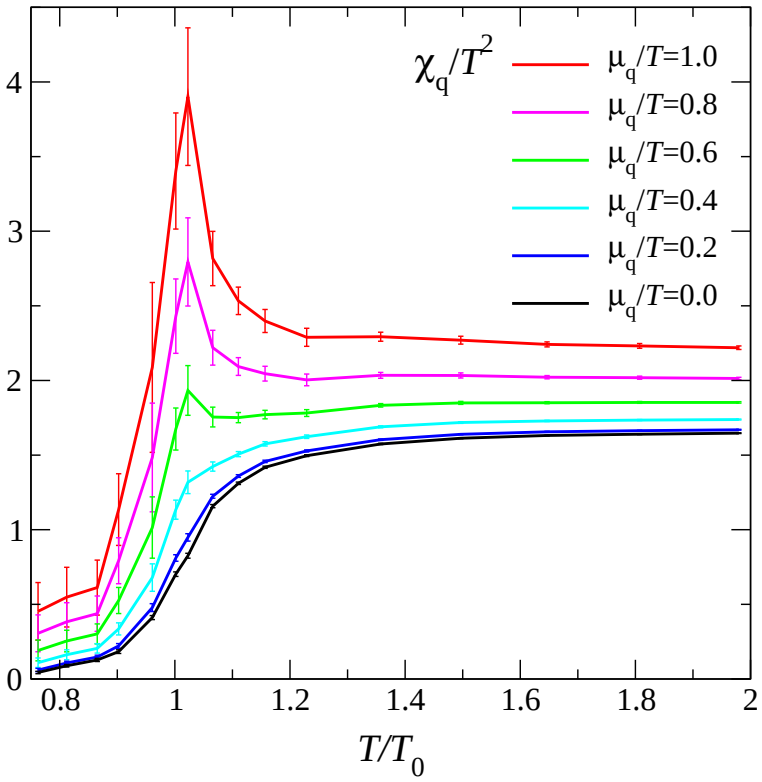

Figure 4.7: χ_q/T^2 as a function of T/T_0 for various μ_q/T.

to be quantitatively accurate in the critical region. Note, however, that at each temperature the expansions for p, n_q and χ_q all have the *same* radius of convergence.

4.3 The energy density

Finally we discuss the energy density ϵ, most conveniently extracted using the conformal anomaly relation

$$\frac{\epsilon - 3p}{T^4} = -\frac{1}{VT^3}\left[a\frac{\partial\beta}{\partial a}\frac{\partial \ln Z}{\partial \beta} + a\frac{\partial m}{\partial a}\frac{\partial \ln Z}{\partial m}\right] \quad , \tag{4.22}$$

where β and m are the bare coupling and quark mass respectively. In fact, for $\mu \neq 0$ the derivation of this expression needs careful discussion. Start from the defining relation

$$\Omega = E - T\mathcal{S} - \mu_q N_q = -pV = -T \ln Z \quad , \tag{4.23}$$

where $\mathcal{S}$ is entropy. For a Euclidean action $S = S(\beta, m, \mu)$ defined on an isotropic lattice of spacing a we have the identity

$$a\frac{dS}{da} = 3V\frac{\partial S}{\partial V} - T\frac{\partial S}{\partial T} \quad . \tag{4.24}$$

It follows that

$$V\frac{\partial\Omega}{\partial V} = VT\left\langle\frac{\partial S}{\partial V}\right\rangle = -pV \tag{4.25}$$

$$T\frac{\partial\Omega}{\partial T} = \Omega + T^2\left\langle\frac{\partial S}{\partial T}\right\rangle = -T\mathcal{S} = \Omega - E + \mu_q N_q \tag{4.26}$$

implying

$$\epsilon - 3p - \mu_q n_q = \frac{T}{V}\left\langle a\frac{\partial S}{\partial a}\right\rangle = -\frac{T}{V}\left[a\frac{\partial\beta}{\partial a}\frac{\partial\ln Z}{\partial\beta} + a\frac{\partial m}{\partial a}\frac{\partial\ln Z}{\partial m} + a\frac{\partial\mu}{\partial a}\frac{\partial\ln Z}{\partial\mu}\right] \tag{4.27}$$

where we have allowed for the dependence of the lattice action on all bare parameters. Since however $\mu \equiv \mu_q a$, and a parameter multiplying a conserved charge experiences no renormalization, the third terms on each side cancel leaving the relation (4.22).

Taylor expansion of (4.22) about $\mu = 0$ leads to the expression

$$\begin{aligned}\Delta\left(\frac{\epsilon-3p}{T^4}\right) = &- a\frac{\partial\beta}{\partial a}\frac{N_\tau^3}{N_\sigma^3}\left[\frac{1}{2}\mu^2\frac{\partial^3\ln Z}{\partial\beta\partial\mu^2} + \frac{1}{24}\mu^4\frac{\partial^5\ln\mathcal{Z}}{\partial\beta\partial\mu^4} + \cdots\right] \\ &- a\frac{\partial m}{\partial a}\frac{N_\tau^3}{N_\sigma^3}\left[\frac{1}{2}\mu^2\frac{\partial^3\ln Z}{\partial m\partial\mu^2} + \frac{1}{24}\mu^4\frac{\partial^5\ln\mathcal{Z}}{\partial m\partial\mu^4} + \cdots\right] \quad .\end{aligned} \tag{4.28}$$

The beta function $a(\partial\beta/\partial a)$ may be estimated by measurements of observables at $(T,\mu_q) = (0,0)$; the factor $a(\partial m/\partial a)$ is poorly constrained by current lattice data but vanishes in the chiral limit, so is frequently neglected. In order to assess the magnitude of the resulting error, it is nonetheless useful to calculate all the derivative terms. They may be estimated using the formulæ

$$\frac{\partial\langle\mathcal{O}\rangle}{\partial\beta} = \left\langle\mathcal{O}\left(-\frac{\partial S_g}{\partial\beta}\right)\right\rangle - \langle\mathcal{O}\rangle\left\langle-\frac{\partial S_g}{\partial\beta}\right\rangle \quad ; \tag{4.29}$$

$$\frac{\partial\langle\mathcal{O}\rangle}{\partial m} = \left\langle\frac{\partial\mathcal{O}}{\partial m}\right\rangle + \left\langle\mathcal{O}\frac{n_f}{4}\frac{\partial(\ln\det M)}{\partial m}\right\rangle - \langle\mathcal{O}\rangle\left\langle\frac{n_f}{4}\frac{\partial(\ln\det M)}{\partial m}\right\rangle \quad . \tag{4.30}$$

The derivative $\partial S_g/\partial\beta$ is, of course, simply the combination of plaquettes comprising the gauge action itself, and derivatives with respect to m can be evaluated using

$$\frac{\partial^{n+1}(\ln\det M)}{\partial m\partial\mu^n} = \frac{\partial^n(\ \mathrm{Tr}\ M^{-1})}{\partial\mu^n} \quad . \tag{4.31}$$

The implementation of the second square bracket in (4.28) in terms of lattice operators is straightforward but unwieldy; for reference the non-vanishing terms are listed in Appendix C.3.

The Taylor expansion of the energy density involves derivatives of the expansion coefficients $c_p(T)$ used to calculate the pressure,

$$\Delta\left(\frac{\epsilon-3p}{T^4}\right) = \sum_{p=1}^{\infty} c_p'(T)\left(\frac{\mu_q}{T}\right)^p \quad , \tag{4.32}$$

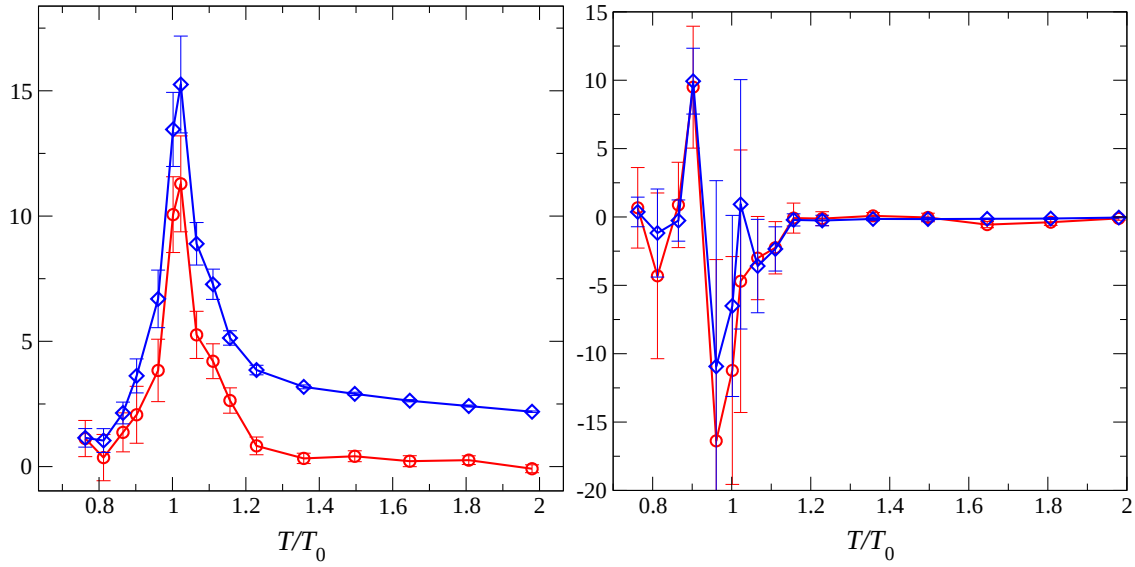

Figure 4.8: Derivatives necessary for calculating the response of the energy density ϵ to increasing chemical potential (μ_q): (a) $(2VT^3)^{-1} \cdot \partial^3 \ln \mathcal{Z}/\partial\beta\partial(\mu_q/T)^2$ (circles) and $-(2VT^3)^{-1} \cdot \partial^3 \ln Z/\partial m\partial(\mu_q/T)^2$ (diamonds), and (b) $(24VT^3)^{-1} \cdot \partial^5 \ln \mathcal{Z}/\partial\beta\partial(\mu_q/T)^4$ (circles) and $-(24VT^3)^{-1} \cdot \partial^5 \ln Z/\partial m\partial(\mu_q/T)^4$ (diamonds).

with $c_p'(T) = T(\mathrm{d}c_p(T)/\mathrm{d}T)|_{\mu_q=0}$. It is apparent from the temperature dependence of the expansion coefficients $c_2(T)$ and $c_4(T)$ shown in Figure 4.1 that the coefficients $c_p'(T)$ can become large in the vicinity of T_0. On the other hand that figure also shows that $c_p'(T)$ will be small, i.e. close to zero, at high temperature as expected in the ideal gas limit. A comparison with Equation (4.28) shows that the numerical evaluation of $c_p'(T)$ requires the knowledge of lattice beta-functions and a calculation of mixed derivatives of $\ln Z$ with respect to μ as well as β and m. In Figure 4.8 we plot these derivative terms; the signals in this case are much noisier than for $\partial^n \ln \mathcal{Z}/\partial\mu^n$, although we have been able to check that the numerical values for $\partial^3 \ln Z/\partial\beta\partial\mu^2$ are consistent with the slope of the curve in Figure 4.1(a). It is clear firstly that with the exception of $\partial^3 \ln Z/\partial m\partial\mu^2$ the signal only differs significantly from zero in the immediate neighborhood of the transition, and secondly that derivatives with respect to m are strongly anti-correlated with those with respect to β. The latter suggests it might be possible to learn something from Equation (4.28) about the shape of the $\Delta((\epsilon - 3p)/T^4)$ curve as a function of T/T_0 away from the chiral limit even in the absence of quantitative information about $a\partial m/\partial a$.

Consider however ignoring mass derivatives and focusing on those performed with respect to coupling. In this case all derivatives are consistent with zero for $T \gtrsim 1.2\ T_0$; i.e. the difference $\Delta\left((\epsilon - 3p)/T^4\right)$ is to a good approximation independent of μ_q for these high temperatures. This

observation is consistent with the results obtained by using exact reweighting in [17]. Consider now temperatures close to T_0. The beta function at the critical β_c has the value $a^{-1}da/d\beta = -2.08(43)$ [12]; substituting the derivatives from Figure 4.8 in Equation (4.28) we find at T_0

$$\Delta\left(\frac{\epsilon - 3p}{T^4}\right) \approx (4.8 \pm 1.2) \times \left(\frac{\mu_q}{T}\right)^2 - (5 \pm 4) \times \left(\frac{\mu_q}{T}\right)^4 + \cdots \tag{4.33}$$

Taking the central values of the coefficients in this expansion one may conclude that the ratio c_2'/c_4' is comparable with c_2/c_4. At present the large error on the coefficient of the $(\mu_q/T)^4$ term, however, does not allow a firm conclusion on the convergence radius of the expansion of $\epsilon - 3p$. We also note that the coefficient c_4' will change sign for $T \sim T_0$. This suggests that large cancellations can occur for $\mu_q/T \sim \mathcal{O}(1)$ and indicates that higher order terms are needed to determine this difference reliably. In any event, it would appear that extending our current analysis to determine energy and entropy densities (ϵ, s) in the critical region will be far more demanding.

4.4 The resonance gas

A realistic description of the hadronic phase ($T < T_0$) is achieved by a hadronic resonance gas. The resonance gas was shown to provide a quite satisfactory description of particle production in heavy ion collisions [11, 86, 108, 109, 110], and recently also of the equation of state at $\mu_q = 0$ [111] and $\mu_q \neq 0$ [112]. It contains the relevant degrees of freedom of the confined, strongly interacting matter and implicitly includes interactions that result in resonance formation [113].

Since the resonance gas is non interacting, the partition function can be expressed as a sum over one-particle partition functions Z_i^1 of all massive states,

$$\ln Z(T,V,\mu) = \sum_i \ln Z_i^1(T,V,\mu) \quad . \tag{4.34}$$

Due to this factorization of the partition function the energy density and the pressure of the hadron resonance gas are also expressed as a sum over single particle contributions ϵ_i^1 and P_i^1 respectively:

$$\epsilon = \sum_i \epsilon_i^1 \quad , \qquad P = \sum_i P_i^1 \quad . \tag{4.35}$$

To complete the discussion of the single particle contributions, we give here the energy density ϵ_i^1, the interaction measure Δ_i^1 and the particle density n_i^1 of particle i,

$$\begin{aligned}
\frac{\epsilon_i^1}{T^4} &= \frac{g_i}{2\pi^2}\left(\frac{m_i}{T}\right)^3 \sum_{l=1}^{\infty} (-\eta)^{l+1} l^{-1} \left[\frac{3K_2(lm_i/T)}{lm_i/T} + K_1(lm_i/T)\right] (z^l + z^{-l}) \quad , \\
\Delta_i^1 &\equiv \frac{\epsilon_i^1 - 3P_i^1}{T^4} = \frac{g_i}{2\pi^2}\left(\frac{m_i}{T}\right)^3 \sum_{l=1}^{\infty} (-\eta)^{l+1} l^{-1} K_1(lm_i/T)\,(z^l + z^{-l}) \quad , \\
\frac{n_i^1}{T^3} &= \frac{g_i}{2\pi^2}\left(\frac{m_i}{T}\right)^2 \sum_{l=1}^{\infty} (-\eta)^{l+1} l^{-1} K_2(lm_i/T)(z^l - z^{-l}) \quad ,
\end{aligned} \tag{4.36}$$

the pressure was given in Equation (2.55). Here, m_i is the particle mass, g_i the isospin degeneracy factor, and K_1, K_2 are modified Bessel functions. Note that the formulation (4.36) is for both, bosons and fermions. Thus we have $\eta = -1$ for all mesonic states and $\eta = 1$ for all baryonic states; consequently the fugacity z is given by $z = \exp\{B_i\mu/T\}$ with baryon number B_i. By taking only the first term of the series (4.36) one obtains the Boltzmann approximation, respectively. Although the interaction is implicitly encoded in the resonance formation, the implementation of a hard core repulsion, i.e., a van der Waals-type interaction, is rather easy to achieve, by taking corrections from the excluded volume into account. The thermodynamically consistent approach proposed in [114, 115] is

$$P^{\text{excl.}}(T,\mu) = P^{\text{id.gas}}(T,\hat{\mu}) \quad , \qquad \text{with} \qquad \hat{\mu} = \mu - v_{\text{eigen}}\, p^{\text{excl.}}(T,\mu) \quad , \tag{4.37}$$

where $v_{\text{eigen}} = 4\frac{4}{3}\pi R^3$ is the eigenvolume of a particle with radius R.

Already in 1965 it was noticed by Hagedorn [113] that an exponentially increasing density of states would lead to a divergent partition function, which is known as the Hagedorn limiting temperature. By using all mesonic and baryonic resonances up to 1.8 GeV and 2.0 GeV respectively, which amounts to 1026 resonances, one has no divergence but finds a rapid rise of the energy density at a temperature of about 160 MeV. The temperature dependence of the energy density and interaction measure from Equations (4.35)-(4.36) at $\mu_q = 0$ are plotted in Figure 4.9(a),(b). Moreover it was recently shown in [111] that the lattice data from [74] agree quite well with the resonance gas, although the lattice calculations are not yet performed with the correct quark mass spectrum realized in nature. To compare the resonance gas with the lattice data a parameterization of the hadron spectrum was introduced in [111], based on the MIT-bag model [116, 117]. Using this parameterization the unphysical hadron spectrum on the lattice can be modeled in the resonance gas.

In Figure 4.9(c) we show the resonance gas results for χ_q/T^2 in comparison with the Taylor expanded lattice data for various values of μ_q/T. Here also the resonance gas was calculated in next-to-leading order in μ_q/T. An interesting feature is, that the Boltzmann approximation is applicable in the regime $\mu_q \lesssim T \lesssim 200$ MeV. The heavy baryonic bound states are thus the relevant degrees of freedom for the finite μ_q corrections to the equation of state. This becomes clear from the fact that for $m \gtrsim m_N$ and $T \lesssim 200$ MeV the Bessel functions appearing in Equations (4.36) can always be approximated by the expansion valid for large arguments, e.g., $K_2(x) \simeq \sqrt{\pi/2x}\exp\{-x\}$. This shows, that higher order terms in the fugacity expansion are suppressed by factors $\exp\{-l(m - \mu_B)/T\}$. As long as $(m_N - \mu_B) \gtrsim T$ the contribution of baryons to the resonance gas partition function is well approximated by the leading term in the fugacity expansion.

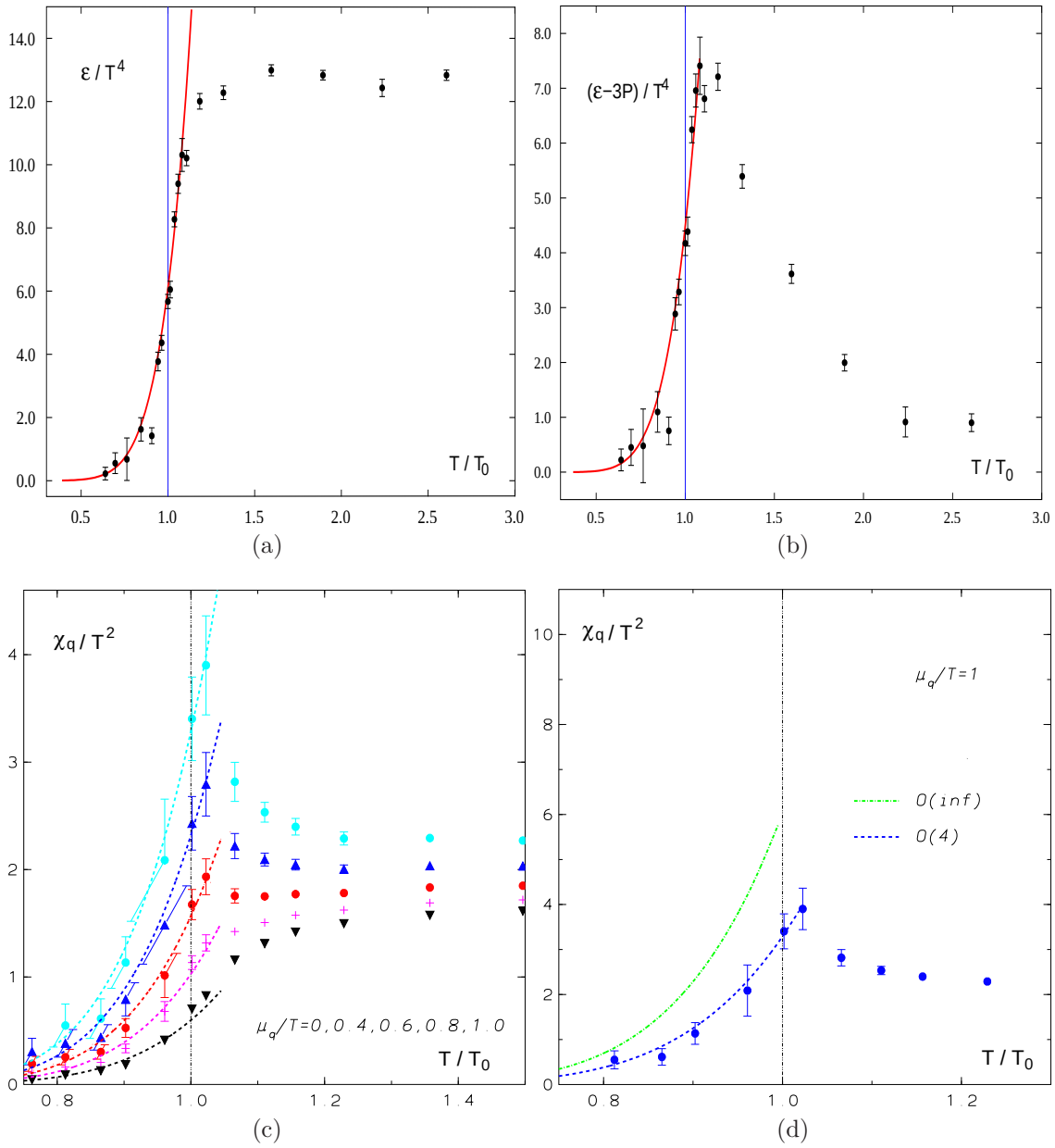

Figure 4.9: Comparison of the QCD equation of state from the lattice (points) and from the resonance gas (lines): (a) The energy density ϵ at $\mu_q = 0$ in units of T^4 calculated on the lattice with (2+1) quark flavors [13] as a function of the T/T_c ratio and (b) the corresponding results for the interaction measure $(\epsilon - 3P)/T^4$. The baryon number susceptibility χ_q/T^2 for various values of quark chemical potential ($\mu_q/T = 0, 0.4, 0.6, 0.8, 1.0$) and in next-to-leading order approximation in μ_q/T (c), and the comparison between the full expression and the next-to-leading approximation for $\mu_q/T = 1$, as a function of T/T_0.

Further on, the resonance gas results suggests that the truncation error is about 15% for $\Delta(p/T^4)$. The truncation of the Taylor expansion is, however, more severe in the calculations of the quark number susceptibility as the expansion stops here already at $\mathcal{O}((\mu_q/T)^2)$. Here errors of about 80% occur at $\mu_q/T = 1$, as can be seen in Figure 4.9(d). The major part of this truncation error could be removed by calculating the $\mathcal{O}((\mu_q/T)^6)$ contribution to $\Delta p/T^4$. More important seem to be systematic errors resulting from the distortion of the hadron mass spectrum due to the use of too heavy quarks in the present lattice calculation of the equation of state.

The resonance gas and resulting statistical models have been able to describe much more characteristics of particle production in heavy ion collisions, for a recent review see for instance [118]. Finally note, that the resonance gas is only a description of the hadronic phase and does not incorporate a phase transition in any way. A simple phenomenological model that includes a parameterization of the confinement effect, and thus contains a phase transition, was proposed in Reference [119]. In the high temperature plasma phase ($T > T_c$), the lattice data for the equation of state from Reference [17] was recently successfully described in the framework of quasi-particle models [120, 121, 122].

Chapter 5

Summary and Conclusions

In this thesis we studied QCD thermodynamics and investigated the QCD phase diagram. In this context, existing results for vanishing quark chemical potential (μ_q) have been verified and extended to small but non-zero μ_q via Taylor expansion or reweighting.

Through an analysis of Binder cumulants we have verified that the chiral critical point in three flavor QCD belongs to the universality class of the three dimensional Ising model. Although the chiral condensate itself is not the order parameter at this critical point one has reasons to believe [8] that Binder cumulants constructed from it are little influenced by finite volume effects and are good observables to locate the critical point as well as the universality class. This study has been done with unimproved staggered fermions, however, the universal properties of the QCD critical point are not expected to change with the reduction of cutoff effects.

Having determined the universality class of the chiral critical point for three degenerate quark masses we could use this information to determine the critical parameters also for non-degenerate quarks from calculations of Binder cumulants on finite lattices. As the chiral critical line corresponds to those sets of quark masses where the Binder cumulant attains the 3-d Ising value one has to determine the line on which $B_4(0)$ stays constant in the $(m_{u,d}, m_s)$-plane. A first order Taylor expansion of $B_4(0)$ in terms of degenerate up/down quark masses $m_{u,d}$ and a strange quark mass m_s around the three flavor critical point $\bar{m} = 0.033$ made it possible to confirm that to leading order the critical line is indeed given by

$$m_s = \bar{m} - 2\,(m_{u,d} - \bar{m}) \quad , \tag{5.1}$$

or in terms of the pseudoscalar meson masses m_π and m_K,

$$m_K^2 = \bar{m}_\pi^2 - \frac{1}{2}\,(m_\pi^2 - \bar{m}_\pi^2) \quad . \tag{5.2}$$

This is consistent with the results of [68] where no sign for a first order transition has been found for $(m_{u,d}, m_s) = (0.025, 0.1)$ and is also not in contradiction with [123] where a "weak first order like behavior" at $(m_{u,d}, m_s) = (0.025, 0.05)$ was reported as opposed to two state signals at lower m_s values. Higher order terms in the Taylor expansion of the critical line are easily accessible by measuring higher order derivatives of $\mathrm{Tr}\, M^{-1}$ with respect to the quark masses. With those terms it will be possible in future to study the validity range of the leading order approximation of the critical line. Furthermore, it might be possible to investigate how the critical line approaches the strange quark axis, in the chiral limit of up and down quark mass. This could provide a first estimate for the location of the QCD tri-critical point.

The 3-flavor chiral critical point has been determined in calculations with unimproved as well as improved gauge and staggered fermion actions on lattices with temporal extent $N_\tau = 4$. The physical scale extracted from calculations of the pseudoscalar meson mass at these endpoints is quite different in both cases. We obtain with the p4 improved action a critical pion mass of $m_\pi = 67(17)$ MeV, which is only about 24% of the value found in calculations with unimproved actions. This indicates that cutoff effects are still significant and calculations closer to the continuum limit are definitely needed to fix a physical scale for the location of the chiral critical point. A critical pion mass of $m_\pi = 67(17)$ is, however, compatible with the result we obtained from a mean-field calculation within the $SU(3)_L \times SU(3)_R$ linear sigma model. Our findings thus strongly suggest that the transition in the physically realized case of two light and a heavier strange quark is neither first nor second order, but a smooth crossover between the high temperature and the low temperature phase.

Moreover, we have proposed a new method to investigate the thermodynamic properties of QCD at non-vanishing chemical potential μ. This method, which is based on a Taylor expansion in μ, enabled us to extend our discussion of the critical line to non vanishing chemical potential. The critical line then becomes a critical surface of constant $B_4(0)$, in the parameter space of quark masses and chemical potential. From an analysis of the Binder cumulant $B_4(0)$ as a function of chemical potential, for 3-flavor calculations at $m_\pi \approx 172$ MeV, we obtained a critical up and down quark chemical potential of $\bar{\mu}_{u,d} = 52(10)$ MeV. Assuming the slope of $-1/2$ for the critical line in the (m_π^2, m_K^2)-plane at $\mu = 0$, we could approximate the critical surface by the parameterization

$$\bar{\mu}_{u,d}^2 = 0.109(36) \cdot \frac{1}{3}\left(m_\pi^2 + 2m_K^2 - 3\bar{m}_\pi^2(0)\right) \quad . \tag{5.3}$$

From this estimate we obtained at the physical point a critical chemical potential of $\mu_{u,d} = 135(21)$ MeV, corresponding to a baryon chemical potential of $\mu_B = 404(62)$ MeV. For the mass point $(m_\pi, m_K) = (300, 500)$ MeV, we obtain $\mu_q = 144(22)$ MeV, while in Reference [9] $\mu_q = 240$ MeV

was found from calculations with unimproved actions. This again indicates the importance of cutoff effects.

By computing the chiral susceptibility and the Polyakov loop susceptibility for two and three flavors of p4 improved staggered fermions, we have been able to estimate the dependence of β_c, and hence the critical temperature T_c, on μ on moderately large volumes, thus reinforcing the recent advances of lattice QCD calculations in the interior of the (μ_q, T) plane [61]. We find that T_c decreases as μ increases, i.e., it can be described by

$$\frac{T_c}{T_0} = 1 - 0.070(35) \left(\frac{\mu_{u,d}}{T}\right)^2 \quad , \tag{5.4}$$

for 2-flavor of p4 improved fermions on a $16^3 \times 4$ lattice and $m = 0.1$. This is in broad agreement with estimates based on exact reweighting [9] and analytical continuation of results obtained by simulation with imaginary μ [10]. Between 2 and 3-flavor QCD no significant difference was found for $T_c(\mu)$, however, we have hints that the slope of the transition line indeed becomes steeper with decreasing quark masses. The results suggest that the deviation of T_c from its value at $\mu = 0$ is small in the interesting region for heavy-ion collisions at RHIC. Moreover, there exists a large region in the (T, μ)-parameter space for $\mu_B \gtrsim 0.4$ GeV where the phenomenological freeze-out temperature $T_f(\mu)$ [86] is significantly lower than the critical temperature $T_c(\mu)$. This gives the chance to experimentally observe a strongly interacting hadron gas and is a strong motivation for future GSI experiments.

An unresolved issue is the validity range of our Taylor expanded reweighting method. We have been able to estimate the complex phase of the fermion determinant for a $16^3 \times 4$ lattice and found that the sign problem is not serious in the range $\mu_{u,d}/T < 0.1$-0.4 for $m = 0.005$-0.1, covered by this study. This region rapidly shrinks with increasing volume, and it is not yet clear if a reliable extrapolation to the thermodynamic limit can be performed on the basis of reweighted data.

Furthermore, we have presented the first Monte Carlo calculation of the QCD equation of state at non-zero quark chemical potential within the analytic framework, here no reweighting has been performed. As in our investigations of the phase diagram, we have exploited the relative simplicity of a Taylor expansion in μ to explore larger physical volumes than those used in comparable studies [17, 21]. In addition, the compatibility of our method with the use of an improved lattice fermion action has meant that our results suffer from relatively mild discretization artifacts, our data for the pressure correction $\Delta p(\mu_q)$ reach 80% of the Stefan-Boltzmann value by $T \simeq 2T_0$.

Our results for Δp and its μ-derivatives, n_q and the various susceptibilities χ_i, are in good qualitative agreement with those of [17, 21]. Higher derivatives suffer from larger truncation errors, and are inherently noisier when estimated by Monte Carlo simulation. Since we have calculated

the Taylor series for Δp up to $\mathcal{O}((\mu_q/T)^4)$, the series for, say, χ_q already terminates at $\mathcal{O}((\mu_q)^2)$. Resonance gas calculations suggest truncation errors for Δp of about 15% while they can reach about 80% for χ_q. Thus the results for χ_q are thus less quantitatively reliable than those for Δp; nonetheless the singularity developing in χ_q as μ_q is increased, seen in Figure 4.7, is evidence for the presence of a critical endpoint in the (μ_q, T) plane, and for the importance of quark number fluctuations in its vicinity.

The calculation of fourth order derivatives has enabled us to estimate the limitations of our method, both analytically through the radius of convergence of the Taylor expansion in μ_q/T, and physically via the requirement of mechanical stability (Le Châtelier's principle). For both criteria the most stringent bounds are reached unsurprisingly in the vicinity of the critical line, where the convergence of the series limits us to $\mu_q/T \lesssim 1$, and mechanical stability of the equilibrium state to $\mu_q/T \lesssim 0.5$. Of course, the picture should change with the inclusion of still higher derivatives since on physical grounds we expect stability of the equilibrium state everywhere within the domain of convergence. We are currently investigating the feasibility of including the relevant $O(\mu^6)$ terms in our calculation.

Other quantities of phenomenological importance such as the energy ϵ and entropy s densities, which require mixed derivatives with respect to the other bare parameters β and m, appear more difficult to calculate with quantitative accuracy with this approach. It remains an open question whether the radius of convergence for these quantities is the same as that for quantities defined by series in $\partial^n\Omega/\partial\mu^n$.

Finally, it is necessary to stress the importance of refining the current calculation, firstly by simulating systems with $N_\tau \geq 6$ so that a reliable extrapolation to the continuum can be performed, and secondly by repeating it with a realistic spectrum of 2+1 fermion flavors.

Appendix A

The pressure of free staggered fermions

Expanding the quantity p/T^4 as discussed in section 2.4 one finds

$$\frac{p}{T^4}\Big|_{N_\tau} = n_f \sum_{i=0}^{\infty} \mathcal{C}_i\Big|_{N_\tau} \left(\frac{\mu}{T}\right)^i = \frac{3}{8} n_f \left[\sum_{i=0}^{\infty} \left(\frac{N_\tau^{3-i}}{(2\pi)^3} \int_0^{2\pi} d^3\vec{p} \sum_{p_4} c_i(p) \right) \left(\frac{\mu}{T}\right)^i - \frac{N_\tau^4}{(2\pi)^4} \int_0^{2\pi} d^4p \; c_0(p) \right] \quad . \tag{A.1}$$

Here only the even expansion coefficients give non-vanishing contributions. Introducing the abbreviation,

$$D = 4 \sum_\mu f_\mu^2(p) \quad , \tag{A.2}$$

with $f_\mu(p)$ as given in (2.60), the even expansion coefficients for the standard action are given by:

$$c_0 = \ln(D) \quad , \tag{A.3}$$

$$c_2 = \frac{1}{4D^2}\big(1 - 4D\cos(2p_4) - \cos(4p_4)\big) \quad , \tag{A.4}$$

$$c_4 = \frac{1}{96D^4}\big(-9 + 8D^2 - 8D(-3+4D^2)\cos(2p_4) + (12 - 56D^2)\cos(4p_4) - 24D\cos(6p_4) - 3\cos(8p_4)\big) \quad , \tag{A.5}$$

$$c_6 = \frac{1}{2880D^6}\big(150 - 180D^2 + 32D^4 - 8D(45 - 60D^2 + 16D^4)\cos(2p_4) + (-225 + 960D^2 - 992D^4)\cos(4p_4) + 540D\cos(6p_4) - 1440D^3\cos(6p_4) + 90\cos(8p_4) - 780D^2\cos(8p_4) - 180D\cos(10p_4) - 15\cos(12p_4)\big) \quad . \tag{A.6}$$

For the Naik action we introduce an additional function,

$$g_4(p) \equiv -i\frac{df_4(\vec{p}, p_4 - i\mu)}{d\mu}\bigg|_{\mu=0} = -\frac{9}{16}\cos(p_4) + \frac{3}{48}\cos(3p_4) \quad . \tag{A.7}$$

The even expansion coefficients can then be written as:

$$\begin{aligned}
c_0 &= \ln(D) \quad , && \text{(A.8)}\\
c_2 &= \frac{-2}{3D^2}\big(-6Df_4^2(p) + 6Dg_4^2(p) - 48f_4^2(p)g_4^2(p) \\
&\quad +Df_4(p)\sin(3p_4)\big) \quad , && \text{(A.9)}\\
c_4 &= \frac{1}{36D^4}\Big(48\big(-768f_4^4(p)g_4^4(p) + D^3\big(f_4^2(p) - g_4^2(p)\big) \\
&\quad -192Df_4^2(p)g_4^2(p)\big(f_4^2(p) - g_4^2(p)\big) + D^2\big(-6f_4^4(p) \\
&\quad +44f_4^2(p)g_4^2(p) - 6g_4^4(p)\big)\big) - 24D^2\big(D - 8f_4^2(p)\big)g_4(p)\cos(3p_4) \\
&\quad -32Df_4(p)\big(D^2 - 3Df_4^2(p) + 9Dg_4^2(p) - 48f_4^2(p)g_4^2(p)\big)\sin(3p_4) \\
&\quad +D^2\big(D - 8f_4^2(p)\big)\sin^2(3p_4)\Big) \quad , && \text{(A.10)}\\
c_6 &= \frac{1}{1620D^6}\Big(-720D^2g_4(p)\big(D^3 + 768f_4^4(p)g_4^2(p) + D^2\big(-26f_4^2(p) \\
&\quad +6g_4^2(p)\big) + 96D\big(f_4^4(p) - 2f_4^2(p)g_4^2(p)\big)\big)\cos(3p_4) \\
&\quad -45D^4\big(D - 8f_4^2(p)\big)\cos^2(3p_4) - 96Df_4(p)\big(8D^4 + 46080f_4^4(p)g_4^4(p) \\
&\quad -75D^3\big(f_4^2(p) - 3g_4^2(p)\big) + 60D^2\big(3f_4^4(p) - 50f_4^2(p)g_4^2(p) + 15g_4^4(p)\big) \\
&\quad +2880D\big(3f_4^4(p)g_4^2(p) - 5f_4^2(p)g_4^4(p)\big)\big)\sin(3p_4) + 15D^2\big(5D^3 \\
&\quad +4608f_4^4(p)g_4^2(p) + D^2\big(-76f_4^2(p) + 36g_4^2(p)\big) + 192D\big(f_4^4(p) \\
&\quad -6f_4^2(p)g_4^2(p)\big)\big)\sin^2(3p_4) + 10D^3f_4(p)\big(3D - 16f_4^2(p)\big)\sin^3(3p_4) \\
&\quad +72\big(4\big(245760f_4(p)^6g_4^6(p) + D^5\big(f_4^2(p) - g_4^2(p)\big)\big) \\
&\quad +92160Df_4^4(p)g_4^4(p)\big(f_4^2(p) - g_4^2(p)\big) - 2D^4\big(15f_4^4(p) - 94f_4^2(p)g_4^2(p) \\
&\quad +15g_4^4(p)\big) + 120D^3\big(f_4^6(p) - 23f_4^4(p)g_4^2(p) + 23f_4^2(p)g_4^4(p) - g_4^6(p)\big) \\
&\quad +960D^2\big(9f_4^6(p)g_4^2(p) - 34f_4^4(p)g_4^4(p) + 9f_4^2(p)g_4^6(p)\big)\big) \\
&\quad -5D^3f_4(p)\big(3D - 16f_4^2(p)\big)g_4(p)\sin(6p_4)\big)\Big) \quad . && \text{(A.11)}
\end{aligned}$$

To simplify the expressions for the p4 action we define the expansion coefficients recursively and thus also list the odd expansion coefficients. However, after integration over the momenta also in this case only even powers of μ/T contribute to the expansion of the pressure. Introducing further abbreviations,

$$S_\mu = \sum_{\nu\neq\mu}\sin^2(p_\nu) \qquad \text{and} \qquad \bar{c}_k = -ic_k \quad , \tag{A.12}$$

the expansion coefficients for the p4 action can be written as

$$
\begin{aligned}
c_0 &= \ln(D) \quad , && \text{(A.13)}\\
c_1 &= -\frac{i}{6D}\big(-S_1 - S_2 - S_3 + 6S_4^2 + S_1\cos(2p_1) + S_2\cos(2p_2) \\
&\quad +S_3\cos(2p_3)\big)\sin(2p_4) \quad , && \text{(A.14)}\\
c_2 &= \frac{1}{18D}\big(9D\bar{c}_1^2 + 6\big(3S_4^2 - S_1\sin^2(p_1) - S_2\sin^2(p_2) \\
&\quad -S_3\sin^2(p_3)\big)\sin^2(p_4) - 2\cos^2(p_4)\big(9S_4^2 \\
&\quad +\sin^2(p_1)\big(-3S_1 + \sin^2(p_4)\big) + \sin^2(p_2)\big(-3S_2 + \sin^2(p_4)\big) \\
&\quad +\sin^2(p_3)\big(-3S_3 + \sin^2(p_4)\big)\big)\big) \quad , && \text{(A.15)}\\
c_3 &= \frac{i}{18D}\big(3D\bar{c}_1\big(\bar{c}_1^2 - 6c_2\big) - \big(-3 + \cos(2p_1) + \cos(2p_2) \\
&\quad +\cos(2p_3)\big)\cos^3(p_4)\sin(p_4) - 2\cos(p_4)\sin(p_4)\big(12S_4^2 \\
&\quad +\sin^2(p_1)\big(-4S_1 + \sin^2(p_4)\big) + \sin^2(p_2)\big(-4S_2 + \sin^2(p_4)\big) \\
&\quad +\sin^2(p_3)\big(-4S_3 + \sin^2(p_4)\big)\big)\big) \quad , && \text{(A.16)}\\
c_4 &= \frac{1}{216D}\big(6\cos^4(p_4)\big(\sin^2(p_1) + \sin^2(p_2) + \sin^2(p_3)\big) \\
&\quad -3\big(3D\big(\bar{c}_1^4 - 12\bar{c}_1^2c_2 + 12c_2^2 - 24\bar{c}_1\bar{c}_3\big) + 8\big(-3S_4^2 + S_1\sin^2(p_1) \\
&\quad +S_2\sin^2(p_2) + S_3\sin^2(p_3)\big)\sin^2(p_4) + \big(-3 + \cos(2p_1) \\
&\quad +\cos(2p_2) + \cos(2p_3)\big)\sin^4(p_4)) - 4\cos^2(p_4)\big(18S_4^2 \\
&\quad +\sin^2(p_1)\big(-6S_1 + 11\sin^2(p_1)\big) + \sin^2(p_2)\big(-6S_2 + 11\sin^2(p_2)\big) \\
&\quad +\sin^2(p_3)\big(-6S_3 + 11\sin^2(p_3)\big)\big)\big) \quad , && \text{(A.17)}\\
c_5 &= -\frac{i}{360D}\big(3D\big(\bar{c}_1^5 - 20c_1^3c_2 - 60\bar{c}_1^2\bar{c}_3 + 120c_2\bar{c}_3 + 60\bar{c}_1\big(c_2^2 + 2c_4\big)\big) \\
&\quad +20\big(-3 + \cos(2p_1) + \cos(2p_2) + \cos(2p_3)\big)\cos^3(p_4)\sin(p_4) \\
&\quad +8\cos(p_4)\sin(p_4)\big(12S_4^2 + \sin^2(p_1)\big(-4S_1 + 5\sin^2(p_4)\big) \\
&\quad +\sin^2(p_2)\big(-4S_2 + 5\sin^2(p_4)\big) + \sin^2(p_3)\big(-4S_3 + 5\sin^2(p_4)\big)\big)\big) \quad , && \text{(A.18)}\\
c_6 &= -\frac{1}{6480D}\big(6 - 9D\bar{c}_1^6 + 270D\bar{c}_1^4c_2 - 1620D\bar{c}_1^2c_2^2 + 1080Dc_2^3 \\
&\quad +1080D\bar{c}_1^3\bar{c}_3 - 6480D\bar{c}_1c_2\bar{c}_3 - 3240D\bar{c}_3^2 - 3240D\bar{c}_1^2c_4 \\
&\quad +6480Dc_2c_4 - 6480D\bar{c}_1\bar{c}_5 - 2\cos(2p_1) - 2\cos(2p_2) - 2\cos(2p_3) \\
&\quad +31\cos(2(p_1 - 2p_4)) + 31\cos(2(p_2 - 2p_4)) + 31\cos(2(p_3 - 2p_4)) \\
&\quad +24S_1\cos(2(p_1 - p_4)) + 24S_2\cos(2(p_2 - p_4)) + 24S_3\cos(2(p_3 - p_4)) \\
&\quad -48S_1\cos(2p_4) - 48S_2\cos(2p_4) - 48S_3\cos(2p_4) + 288S_4^2\cos(2p_4) \\
&\quad -186\cos(4p_4) + 24S_1\cos(2(p_1 + p_4)) + 24S_2\cos(2(p_2 + p_4)) \\
&\quad +24S_3\cos(2(p_3 + p_4)) + 31\cos(2(p_1 + 2p_4))
\end{aligned}
$$

$$+31\cos(2(p_2+2p_4))+31\cos(2(p_3+2p_4))\big) \quad . \tag{A.19}$$

Note that we have defined here the coefficients c_i without N_τ factors, which can be found in front of the integrals in (A.1).

Appendix B

Tree-level masses in the $SU(3)_L \times SU_R(3)$ linear sigma model

In Section 3.4 we investigate the chiral Lagrangian given in Equation (3.23). We parametize the matrix fields $\Phi(x)$ according to

$$\Phi(x) = \frac{1}{\sqrt{2}} \sum_{a=0}^{8} \left[\sigma_a(x) + i\pi_a(x)\right] \lambda_a \quad , \tag{B.1}$$

where λ_a are the Gell-Mann matrices with $\lambda_0 = \sqrt{2/3}\mathrm{diag}(1,1,1)$. The σ_a fields are members of the scalar ($J^P = 0^+$)-nonet and the π_a fields are members of the pseudoscalar ($J^P = 0^-$)-nonet. The matrix of scalar fields $(\Phi + \Phi^\dagger)/2$ is given by

$$\frac{\Phi + \Phi^\dagger}{2} = \begin{pmatrix} \frac{1}{\sqrt{2}}a_0^0 + \frac{1}{\sqrt{3}}\sigma_0 + \frac{1}{\sqrt{6}}\sigma_8 & a_0^- & K^{*-} \\ a_0^+ & -\frac{1}{\sqrt{2}}a_0^0 + \frac{1}{\sqrt{3}}\sigma_0 + \frac{1}{\sqrt{6}}\sigma_8 & \overline{K^*}^0 \\ K^{*+} & K^{*0} & \frac{1}{\sqrt{3}}\sigma_0 - \frac{2}{\sqrt{3}}\sigma_8 \end{pmatrix} \quad , \tag{B.2}$$

while the matrix of pseudoscalar fields $(\Phi - \Phi^\dagger)/2$ is

$$\frac{\Phi - \Phi^\dagger}{2} = \begin{pmatrix} \frac{1}{\sqrt{2}}\pi^0 + \frac{1}{\sqrt{3}}\pi_0 + \frac{1}{\sqrt{6}}\pi_8 & \pi^- & K^- \\ \pi^+ & -\frac{1}{\sqrt{2}}\pi^0 + \frac{1}{\sqrt{3}}\pi_0 + \frac{1}{\sqrt{6}}\pi_8 & \overline{K}^0 \\ K^+ & K^0 & \frac{1}{\sqrt{3}}\pi_0 - \frac{2}{\sqrt{3}}\pi_8 \end{pmatrix} \quad . \tag{B.3}$$

Here, $\pi^\pm \equiv (\pi_1 \pm i\pi)/\sqrt{2}$ and $\pi^0 \equiv \pi_3$ are the charged and neutral pions, respectively. $K^\pm \equiv (\pi_4 \pm i\pi_5)/\sqrt{2}$, $K^0 \equiv (\pi_6 + i\pi_7)/\sqrt{2}$ and $\overline{K}^0 \equiv (\pi_6 - i\pi_7)/\sqrt{2}$ are the kaons. In general, because

the strange quark is much heavier than the up or down quark, the π_0 and π_8 are admixtures of the η and the $\eta^{'}$ meson.

The situation with the scalar nonet is not as clear. The parity partner of the pion is the $a_0(980)$ meson, i.e., $a_0^{\pm} \equiv (\sigma_1 \pm i\sigma_2)/\sqrt{2}$ and $a_0^0 \equiv \sigma_3$. We identify the parity partner of the kaon with the $K_0^*(1430)$ meson. Finally, in general the σ_0 and σ_8 are admixtures of the σ [now also referred to as the $f_0(400-1200)$] and $f_0(980)$ mesons. Instead of the $f_0(980)$ meson, one could have choosen the $f_0(1370)$ meson also.

After shifting the Φ field by its vacuum expectation value ($\Phi(x) \to \Phi + \Phi^{'}(x)$), the Lagrangian can be written as

$$\mathcal{L} = \Omega_{\rm class}(\sigma_a, \pi_a) + \frac{1}{2}\left[\partial_\mu \sigma_a^{'} \partial_\mu \sigma_a + \partial_\mu \pi_a^{'} \partial_\mu \pi_a + \sigma_a (m_S^2)_{ab} \sigma_b + \sigma_a (m_P^2)_{ab} \sigma_b\right] + \mathcal{L}^{(3)} + \mathcal{L}^{(4)} \ , \quad \text{(B.4)}$$

where $\Omega_{\rm class}$ is the classical tree-level potential and $\mathcal{L}^{(3)}$ and $\mathcal{L}^{(4)}$ are additional interaction terms, which are cubic and quartic in the vacuum expectation values. The nonzero elements of the scalar mass matrix $(m_S^2)_{ab}$ are:

$$(m_S^2)_{00} = -m_0^2 + \frac{4\,g}{\sqrt{3}}\,\sigma_0 + (12\,f_1 + 4\,f_2)\ {\sigma_0}^2 + (4\,f_1 + 4\,f_2)\ {\sigma_8}^2 \quad , \quad \text{(B.5)}$$

$$(m_S^2)_{11} = (m_S^2)_{22} = (m_S^2)_{33} = -m_0^2 - \frac{2\,g}{\sqrt{3}}\,\sigma_0 + (4\,f_1 + 4\,f_2)\ {\sigma_0}^2 + 2\sqrt{\frac{2}{3}}\,g\,\sigma_8 + 4\sqrt{2}\,f_2\,\sigma_0\,\sigma_8 + (4\,f_1 + 2\,f_2)\ {\sigma_8}^2 \quad , \quad \text{(B.6)}$$

$$(m_S^2)_{44} = (m_S^2)_{55} = (m_S^2)_{66} = (m_S^2)_{77} = -m_0^2 - \frac{2\,g}{\sqrt{3}}\,\sigma_0 + (4\,f_1 + 4\,f_2)\ {\sigma_0}^2 - \sqrt{\frac{2}{3}}\,g\,\sigma_8 - 2\sqrt{2}\,f_2\,\sigma_0\,\sigma_8 + (4\,f_1 + 2\,f_2)\ {\sigma_8}^2 \quad , \quad \text{(B.7)}$$

$$(m_S^2)_{88} = -m_0^2 - \frac{2\,g}{\sqrt{3}}\,\sigma_0 + (4\,f_1 + 4\,f_2)\ {\sigma_0}^2 - 2\sqrt{\frac{2}{3}}\,g\,\sigma_8 - 4\sqrt{2}\,f_2\,\sigma_0\,\sigma_8 + (12\,f_1 + 6\,f_2)\ {\sigma_8}^2 \quad , \quad \text{(B.8)}$$

$$(m_S^2)_{08} = (m_S^2)_{80} = \frac{-2\,g}{\sqrt{3}}\,\sigma_8 + (8\,f_1 + 8\,f_2)\ \sigma_0\,\sigma_8 - 2\sqrt{2}\,f_2\,{\sigma_8}^2 \quad . \quad \text{(B.9)}$$

While the masses of the a_0 and the K^* meson are given by the (11) and the (44) elements of the mass matrix, $m_{a_0}^2 = (m_S^2)_{11}$, $m_{K^*}^2 = (m_S^2)_{44}$ the σ and f_0 meson masses are obtained by diagonalising the (08) sector of the mass matrix. We have

$$m_\sigma^2 = (m_S^2)_{00}\cos^2(\theta_S) + (m_S^2)_{88}\sin^2(\theta_S) + 2(m_S^2)_{08}\cos(\theta_S)\sin(\theta_S) \quad , \quad \text{(B.10)}$$

$$m_{f_0}^2 = (m_S^2)_{00}\sin^2(\theta_S) + (m_S^2)_{88}\cos^2(\theta_S) - 2(m_S^2)_{08}\cos(\theta_S)\sin(\theta_S) \quad , \quad \text{(B.11)}$$

where the scalar mixing angle θ_S is given by

$$\tan(2\theta_S) = \frac{2(m_S^2)_{08}}{(m_S^2)_{00} - (m_S^2)_{88}} \quad . \quad \text{(B.12)}$$

The nonzero elements of the pseudoscalar mass matrix $(m_P^2)_{ab}$ are:

$$(m_P^2)_{00} = -m_0^2 - \frac{4\,g}{\sqrt{3}}\,\sigma_0 + \left(4\,f_1 + \frac{4\,f_2}{3}\right)\,{\sigma_0}^2 + \left(4\,f_1 + \frac{4\,f_2}{3}\right)\,{\sigma_8}^2 \quad , \tag{B.13}$$

$$\begin{aligned}(m_P^2)_{11} &= (m_P^2)_{22} = (m_P^2)_{33} = -m_0^2 + \frac{2\,g}{\sqrt{3}}\,\sigma_0 + \left(4\,f_1 + \frac{4\,f_2}{3}\right)\,{\sigma_0}^2 \\ &\quad -2\,\sqrt{\frac{2}{3}}\,g\,\sigma_8 + \frac{4\,\sqrt{2}\,f_2}{3}\,\sigma_0\,\sigma_8 + \left(4\,f_1 + \frac{2\,f_2}{3}\right)\,{\sigma_8}^2 \quad ,\end{aligned} \tag{B.14}$$

$$\begin{aligned}(m_P^2)_{44} &= (m_P^2)_{55} = (m_P^2)_{66} = (m_P^2)_{77} = -m^2 + \frac{2\,g}{\sqrt{3}}\,\sigma_0 + \left(4\,f_1 + \frac{4\,f_2}{3}\right)\,\sigma_0^2 \\ &\quad +\sqrt{\frac{2}{3}}\,g\,\sigma_8 - \frac{2\,\sqrt{2}\,f_2}{3}\,\sigma_0\,\sigma_8 + \left(4\,f_1 + \frac{14\,f_2}{3}\right)\,\sigma_8^2 \quad ,\end{aligned} \tag{B.15}$$

$$\begin{aligned}(m_P^2)_{88} &= -m_0^2 + \frac{2\,g}{\sqrt{3}}\,\sigma_0 + \left(4\,f_1 + \frac{4\,f_2}{3}\right)\,{\sigma_0}^2 + 2\,\sqrt{\frac{2}{3}}\,g\,\sigma_8 - \frac{4\,\sqrt{2}\,f_2}{3}\,\sigma_0\,\sigma_8 \\ &\quad + (4\,f_1 + 2\,f_2)\,{\sigma_8}^2 \quad ,\end{aligned} \tag{B.16}$$

$$(m_P^2)_{08} = (m_P^2)_{80} = \frac{2\,g}{\sqrt{3}}\,\sigma_8 + \frac{8\,f_2}{3}\,\sigma_0\,\sigma_8 - \frac{2\,\sqrt{2}\,f_2}{3}\,\sigma_8^2 \quad . \tag{B.17}$$

While the masses of the pion and the kaon are given by the (11) and the (44) elements of the mass matrix, $m_\pi^2 = (m_P^2)_{11}$, $m_K^2 = (m_S^2)_{44}$ the $\eta^{'}$ and η meson masses are obtained by diagonalising the (08) sector of the mass matrix. We have

$$m_{\eta'}^2 = (m_P^2)_{00}\cos^2(\theta_P) + (m_P^2)_{88}\sin^2(\theta_P) + 2(m_P^2)_{08}\cos(\theta_P)\sin(\theta_P) \quad , \tag{B.18}$$

$$m_\eta^2 = (m_P^2)_{00}\sin^2(\theta_P) + (m_P^2)_{88}\cos^2(\theta_P) - 2(m_P^2)_{08}\cos(\theta_P)\sin(\theta_P) \quad , \tag{B.19}$$

where the scalar mixing angle θ_P is given by

$$\tan(2\theta_P) = \frac{2(m_P^2)_{08}}{(m_P^2)_{00} - (m_P^2)_{88}} \quad . \tag{B.20}$$

Appendix C

Simulation details

C.1 Simulation parameters

We used for our simulations the hybrid-R-algorithm [78]. The step size was set to $\Delta\tau = 0.015$ for our unimproved calculations and to $\Delta\tau = 0.0025, 0.025$ for our p4 improved calculations with quark mass $m = 0.005, 0.1$, respectively. In calculations concerning the structure of the QCD phase diagram, discussed in Chapter 3, the molecular dynamical trajectory length was chosen to $\tau = 0.675$ for the standard action and $\tau = 0.4, 0.5$ for the p4 action at quark mass $m = 0.005, 0.1$. Within the calculations of the equation of state (Chapter 4) the analyzed configurations were separated by $\tau = 5$. The simulation points (m, β), lattice sizes $(N_\sigma^3 \times 4)$ and number of configurations $(N_{\rm conf})$ are given in Table C.1-C.2. The number of Z_2 noise vectors per configuration which have been used to calculate derivatives of $\ln Z$ with respect to quark mass (m) and quark chemical potential (μ) was set to $N_{\rm noise} = 25$ for calculations with unimproved actions and $N_{\rm noise} = 15, 50$ for calculations with improved actions. Here the larger number of noise vectors has been used to calculate operators needed at 4th order in the Taylor expansion ($\mathcal{O}(\mu^4)$, Chapter 4) while the smaller number was used to calculate the 2nd order expansion coefficients discussed in Chapter 3.

C.2 Remark on the noise method

The calculation of an operator such as $(\ {\rm Tr}\ A)^2$, where A is a matrix, using the noise method has to be treated carefully. Because the random noise vectors should be independent for each calculation of ${\rm Tr}\ A$,

$$(\ {\rm Tr}\ A)^2 = \lim_{N\to\infty} \frac{1}{N}\sum_{a=1}^{N} \eta_a^\dagger A \eta_a \frac{1}{N}\sum_{b=1}^{N} \eta_b^\dagger A \eta_b = \lim_{N\to\infty} \frac{1}{N(N-1)} \sum_{a\neq b} \eta_a^\dagger A \eta_a \eta_b^\dagger A \eta_b \quad . \tag{C.1}$$

$n_f = 3$			
m	N_σ	β	N_{conf}
0.0300	8	5.138	30000
		5.141	34000
		5.145	26000
	12	5.128	21200
		5.140	21200
		5.142	21200
		5.144	21200
	16	5.135	5000
		5.140	30000
		5.141	10000
		5.145	13000
		5.150	30000
0.0325	8	5.145	40000
		5.147	30000
	16	5.145	45000
		5.146	43000
0.0350	8	5.148	8000
		5.150	30000
		5.152	8000
	12	5.147	19700
		5.149	19700
		5.150	19700
		5.152	19700
	16	5.147	9000
		5.1485	25000
		5.1495	28000
		5.150	30000

$n_f = 3$			
m	N_σ	β	N_{conf}
0.0400	12	5.158	20000
		5.160	20000
		5.162	20000
		5.164	20000
	16	5.157	10000
		5.159	15000
		5.161	10000

$n_f = 2 + 1$				
$m_{u,d}$	m_s	N_σ	β	N_{conf}
0.03	0.045	12	5.140	2000
			5.150	21850
			5.152	25000
			5.155	10000
0.03	0.060	12	5.150	2650
			5.155	5000
			5.160	4700

Table C.1: Simulation points (m, β), lattice sizes $(N_\sigma^3 \times 4)$ and number of configurations (N_{conf}) that have been used for unimproved calculations.

$n_f = 3, \quad \mathcal{O}(\mu^2)$			
m	N_σ	β	$N_{\rm conf}$
0.005	12	3.250	3290
		3.260	3520
		3.270	3610
		3.280	3580
	16	3.250	4100
		3.255	4200
		3.260	4500
		3.265	5250
		3.270	5050
		3.275	4000
		3.285	2075
0.1	16	3.460	20200
		3.470	42300
		3.480	40200
		3.490	30200

$n_f = 2, \quad \mathcal{O}(\mu^2)$			
m	N_σ	β	$N_{\rm conf}$
0.1	16	3.640	20000
		3.650	38000
		3.660	40000
		3.670	30000

$n_f = 2, \quad \mathcal{O}(\mu^4)$			
m	N_σ	β	$N_{\rm conf}$
0.1	16	3.520	1000
		3.550	1000
		3.580	1000
		3.600	1000
		3.630	1000
		3.650	1000
		3.660	1000
		3.680	800
		3.700	800
		3.720	500
		3.750	500
		3.800	500
		3.850	500
		3.900	500
		3.950	500
		4.000	500

Table C.2: Simulation points (m, β), lattice sizes $(N_\sigma^3 \times 4)$ and number of configurations $(N_{\rm conf})$ that have been used for p4 improved calculations.

This equation can be rewritten as

$$(\text{ Tr } A)^2 = \lim_{N\to\infty} \left[\left(\frac{1}{N} \sum_{a=1}^{N} \eta_a^\dagger A \eta_a \right)^2 - \varepsilon^2(A) \right] \quad , \tag{C.2}$$

where $\varepsilon(A)$ is the error due to finite N:

$$\varepsilon^2(A) = \frac{1}{N-1} \left\{ \frac{1}{N} \sum_{a=1}^{N} \left(\eta_a^\dagger A \eta_a \right)^2 - \left(\frac{1}{N} \sum_{a=1}^{N} \eta_a^\dagger A \eta_a \right)^2 \right\} \quad . \tag{C.3}$$

The error decreases as $(N-1)^{-1}$ as N increases, but can be significant for small N. Moreover, $\varepsilon^2(A)$ is found to be negligible for an operator which always has the same sign such as $\mathrm{Tr}\, M^{-1}$; in this case its contribution is about 0.001% for $\langle(\ \mathrm{Tr}\ M^{-1})^2\rangle$ with $N = 10$. However, for an operator which changes sign frequently such as $\mathrm{Tr}\,[M^{-1}(\partial M/\partial\mu)]$, the effect of the additional term is important. We calculate the quark number susceptibility and the value of "STD(Imp.)" given in Table 2.1 by taking this additional term into account. The difference between "STD" and "STD(Imp.)" shown in Table 2.1 is the contribution from the additional term.

C.3 Derivatives needed to calculate the energy density

Here we present the non-vanishing terms in the expressions for $\partial^{n+1}\ln\mathcal{Z}/\partial m\partial\mu^n$:

$$
\begin{aligned}
\frac{\partial^3 \ln\mathcal{Z}}{\partial\mu^2\partial m} &= \left\langle \frac{n_f}{4}\frac{\partial^2\ \mathrm{Tr}\ M^{-1}}{\partial\mu^2}\right\rangle + 2\left\langle\left(\frac{n_f}{4}\right)^2\frac{\partial(\ln\det M)}{\partial\mu}\frac{\partial\ \mathrm{Tr}\ M^{-1}}{\partial\mu}\right\rangle \\
&+\left\langle\left(\frac{n_f}{4}\right)^2\frac{\partial^2(\ln\det M)}{\partial\mu^2}\ \mathrm{Tr}\ M^{-1}\right\rangle + \left\langle\left(\frac{n_f}{4}\right)^3\left(\frac{\partial(\ln\det M)}{\partial\mu}\right)^2\ \mathrm{Tr}\ M^{-1}\right\rangle \\
&-\left[\left\langle\frac{n_f}{4}\frac{\partial^2(\ln\det M)}{\partial\mu^2}\right\rangle + \left\langle\left(\frac{n_f}{4}\frac{\partial(\ln\det M)}{\partial\mu}\right)^2\right\rangle\right]\left\langle\frac{n_f}{4}\ \mathrm{Tr}\ M^{-1}\right\rangle \quad ,
\end{aligned}
\tag{C.4}
$$

$$
\begin{aligned}
\frac{\partial^5 \ln\mathcal{Z}}{\partial\mu^4\partial m} &= \left\langle \frac{n_f}{4}\frac{\partial^4(\ \mathrm{Tr}\ M^{-1})}{\partial\mu^4}\right\rangle + 4\left\langle\left(\frac{n_f}{4}\right)^2\frac{\partial^3(\ \mathrm{Tr}\ M^{-1})}{\partial\mu^3}\frac{\partial(\ln\det M)}{\partial\mu}\right\rangle \\
&+4\left\langle\left(\frac{n_f}{4}\right)^2\frac{\partial^3(\ln\det M)}{\partial\mu^3}\frac{\partial(\ \mathrm{Tr}\ M^{-1})}{\partial\mu}\right\rangle + 6\left\langle\left(\frac{n_f}{4}\right)^2\frac{\partial^2(\ln\det M)}{\partial\mu^2}\frac{\partial^2(\ \mathrm{Tr}\ M^{-1})}{\partial\mu^2}\right\rangle \\
&+6\left\langle\left(\frac{n_f}{4}\right)^3\frac{\partial^2(\ \mathrm{Tr}\ M^{-1})}{\partial\mu^2}\left(\frac{\partial(\ln\det M)}{\partial\mu}\right)^2\right\rangle \\
&+12\left\langle\left(\frac{n_f}{4}\right)^3\frac{\partial^2(\ln\det M)}{\partial\mu^2}\frac{\partial(\ln\det M)}{\partial\mu}\frac{\partial(\ \mathrm{Tr}\ M^{-1})}{\partial\mu}\right\rangle \\
&+4\left\langle\left(\frac{n_f}{4}\right)^4\left(\frac{\partial(\ln\det M)}{\partial\mu}\right)^3\frac{\partial(\ \mathrm{Tr}\ M^{-1})}{\partial\mu}\right\rangle + \left\langle\left(\frac{n_f}{4}\right)^2\frac{\partial^4(\ln\det M)}{\partial\mu^4}\ \mathrm{Tr}\ M^{-1}\right\rangle \\
&+4\left\langle\left(\frac{n_f}{4}\right)^3\frac{\partial^3(\ln\det M)}{\partial\mu^3}\frac{\partial(\ln\det M)}{\partial\mu}\ \mathrm{Tr}\ M^{-1}\right\rangle \\
&+3\left\langle\left(\frac{n_f}{4}\right)^3\left(\frac{\partial^2(\ln\det M)}{\partial\mu^2}\right)^2\ \mathrm{Tr}\ M^{-1}\right\rangle \\
&+6\left\langle\left(\frac{n_f}{4}\right)^4\frac{\partial^2(\ln\det M)}{\partial\mu^2}\left(\frac{\partial(\ln\det M)}{\partial\mu}\right)^2\ \mathrm{Tr}\ M^{-1}\right\rangle \\
&+\left\langle\left(\frac{n_f}{4}\right)^5\left(\frac{\partial(\ln\det M)}{\partial\mu}\right)^4\ \mathrm{Tr}\ M^{-1}\right\rangle \\
&-\left[\left\langle\frac{n_f}{4}\frac{\partial^4(\ln\det M)}{\partial\mu^4}\right\rangle + 4\left\langle\left(\frac{n_f}{4}\right)^2\frac{\partial^3(\ln\det M)}{\partial\mu^3}\frac{\partial(\ln\det M)}{\partial\mu}\right\rangle\right.
\end{aligned}
\tag{C.5}
$$

$$
\begin{aligned}
&+3\left\langle\left(\frac{n_f}{4}\right)^2\left(\frac{\partial^2(\ln\det M)}{\partial\mu^2}\right)^2\right\rangle+\left\langle\left(\frac{n_f}{4}\frac{\partial(\ln\det M)}{\partial\mu}\right)^4\right\rangle\\
&+6\left\langle\left(\frac{n_f}{4}\right)^3\frac{\partial^2(\ln\det M)}{\partial\mu^2}\left(\frac{\partial(\ln\det M)}{\partial\mu}\right)^2\right\rangle\left]\left\langle\frac{n_f}{4}\ \mathrm{Tr}\ M^{-1}\right\rangle\right.\\
&-6\left[\left\langle\frac{n_f}{4}\frac{\partial^2(\ \mathrm{Tr}\ M^{-1})}{\partial\mu^2}\right\rangle+2\left\langle\left(\frac{n_f}{4}\right)^2\frac{\partial(\ln\det M)}{\partial\mu}\frac{\partial(\ \mathrm{Tr}\ M^{-1})}{\partial\mu}\right\rangle\right.\\
&+\left\langle\left(\frac{n_f}{4}\right)^2\frac{\partial^2(\ln\det M)}{\partial\mu^2}\ \mathrm{Tr}\ M^{-1}\right\rangle+\left\langle\left(\frac{n_f}{4}\right)^3\left(\frac{\partial(\ln\det M)}{\partial\mu}\right)^2\ \mathrm{Tr}\ M^{-1}\right\rangle\\
&-\left(\left\langle\frac{n_f}{4}\frac{\partial^2(\ln\det M)}{\partial\mu^2}\right\rangle+\left\langle\left(\frac{n_f}{4}\frac{\partial(\ln\det M)}{\partial\mu}\right)^2\right\rangle\right)\left\langle\frac{n_f}{4}\ \mathrm{Tr}\ M^{-1}\right\rangle\left.\right]\\
&\times\left[\left\langle\frac{n_f}{4}\frac{\partial^2(\ln\det M)}{\partial\mu^2}\right\rangle+\left\langle\left(\frac{n_f}{4}\frac{\partial(\ln\det M)}{\partial\mu}\right)^2\right\rangle\right]\quad .
\end{aligned}
$$

As explained above, all terms involving the expectation value of an odd number of derivations with respect to μ have been set to zero. The evaluation of Equations (C.4) and (C.5) requires the following expressions for the derivatives of $\mathrm{tr}M^{-1}$:

$$
\frac{\partial\ \mathrm{Tr}\ M^{-1}}{\partial\mu}=-\ \mathrm{Tr}\ \left(M^{-1}\frac{\partial M}{\partial\mu}M^{-1}\right)\quad , \tag{C.6}
$$

$$
\frac{\partial^2\ \mathrm{Tr}\ M^{-1}}{\partial\mu^2}=-\ \mathrm{Tr}\ \left(M^{-1}\frac{\partial^2 M}{\partial\mu^2}M^{-1}\right)+2\ \mathrm{Tr}\ \left(M^{-1}\frac{\partial M}{\partial\mu}M^{-1}\frac{\partial M}{\partial\mu}M^{-1}\right)\quad , \tag{C.7}
$$

$$
\begin{aligned}
\frac{\partial^3\ \mathrm{Tr}\ M^{-1}}{\partial\mu^3}=&-\ \mathrm{Tr}\ \left(M^{-1}\frac{\partial^3 M}{\partial\mu^3}M^{-1}\right)+3\ \mathrm{Tr}\ \left(M^{-1}\frac{\partial^2 M}{\partial\mu^2}M^{-1}\frac{\partial M}{\partial\mu}M^{-1}\right)\\
&+3\ \mathrm{Tr}\ \left(M^{-1}\frac{\partial M}{\partial\mu}M^{-1}\frac{\partial^2 M}{\partial\mu^2}M^{-1}\right)-6\ \mathrm{Tr}\ \left(M^{-1}\frac{\partial M}{\partial\mu}M^{-1}\frac{\partial M}{\partial\mu}M^{-1}\frac{\partial M}{\partial\mu}M^{-1}\right)\quad ,
\end{aligned} \tag{C.8}
$$

$$
\begin{aligned}
\frac{\partial^4\ \mathrm{Tr}\ M^{-1}}{\partial\mu^4}=&-\ \mathrm{Tr}\ \left(M^{-1}\frac{\partial^4 M}{\partial\mu^4}M^{-1}\right)+4\ \mathrm{Tr}\ \left(M^{-1}\frac{\partial^3 M}{\partial\mu^3}M^{-1}\frac{\partial M}{\partial\mu}M^{-1}\right)\\
&+6\ \mathrm{Tr}\ \left(M^{-1}\frac{\partial^2 M}{\partial\mu^2}M^{-1}\frac{\partial^2 M}{\partial\mu^2}M^{-1}\right)+4\ \mathrm{Tr}\ \left(M^{-1}\frac{\partial M}{\partial\mu}M^{-1}\frac{\partial^3 M}{\partial\mu^3}M^{-1}\right)\\
&-12\ \mathrm{Tr}\ \left(M^{-1}\frac{\partial^2 M}{\partial\mu^2}M^{-1}\frac{\partial M}{\partial\mu}M^{-1}\frac{\partial M}{\partial\mu}M^{-1}\right)\\
&-12\ \mathrm{Tr}\ \left(M^{-1}\frac{\partial M}{\partial\mu}M^{-1}\frac{\partial^2 M}{\partial\mu^2}M^{-1}\frac{\partial M}{\partial\mu}M^{-1}\right)\\
&-12\ \mathrm{Tr}\ \left(M^{-1}\frac{\partial M}{\partial\mu}M^{-1}\frac{\partial M}{\partial\mu}M^{-1}\frac{\partial^2 M}{\partial\mu^2}M^{-1}\right)\\
&+24\ \mathrm{Tr}\ \left(M^{-1}\frac{\partial M}{\partial\mu}M^{-1}\frac{\partial M}{\partial\mu}M^{-1}\frac{\partial M}{\partial\mu}M^{-1}\frac{\partial M}{\partial\mu}M^{-1}\right)\quad .
\end{aligned} \tag{C.9}
$$

Appendix D

Tables of results

	from $\langle L \rangle$			from $\langle \bar{\psi}\psi \rangle$		
m	$\beta_{\rm pc}$	$\chi(\beta_{\rm pc})$	$B_4(0)$	$\beta_{\rm pc}$	$\chi(\beta_{\rm pc})$	$B_4(0)$
0.0000	3.2404(38)	0.344(93)	2.66(54)	3.2443(5)	25.1(4.0)	2.30(24)
0.0005	3.2456(51)	0.349(82)	2.69(45)	3.2472(25)	23.8(3.8)	2.35(22)
0.0010	3.2528(57)	0.351(77)	2.75(42)	3.2496(29)	22.6(3.7)	2.34(24)
0.0015	3.2572(59)	0.354(72)	2.78(37)	3.2525(29)	21.4(3.5)	2.33(25)
0.0020	3.2599(52)	0.358(70)	2.78(33)	3.2549(28)	20.3(3.3)	2.34(26)
0.0025	3.2595(30)	0.360(68)	2.78(31)	3.2574(25)	19.3(3.2)	2.36(27)
0.0030	3.2600(20)	0.362(67)	2.78(31)	3.2590(23)	18.3(3.1)	2.39(27)
0.0035	3.2611(20)	0.363(66)	2.78(30)	3.2610(20)	17.3(3.0)	2.42(28)
0.0040	3.2630(20)	0.362(65)	2.79(30)	3.2630(18)	16.4(2.9)	2.46(28)
0.0045	3.2644(21)	0.361(64)	2.80(30)	3.2647(18)	15.5(2.8)	2.50(28)
0.0050	3.2663(23)	0.359(63)	2.82(29)	3.2660(18)	14.6(2.6)	2.55(29)
0.0055	3.2675(27)	0.355(62)	2.84(29)	3.2676(19)	13.8(2.5)	2.60(29)
0.0060	3.2690(33)	0.352(61)	2.87(29)	3.2694(21)	13.0(2.4)	2.65(30)
0.0065	3.2689(42)	0.347(61)	2.90(29)	3.2704(25)	12.2(2.2)	2.71(30)
0.0070	3.2691(55)	0.342(60)	2.93(29)	3.2712(32)	11.4(2.1)	2.77(30)

Table D.1: Mass reweighted data for pseudo critical couplings ($\beta_{\rm pc}$), peak heights of the susceptibilities ($\chi(\beta_{\rm pc})$) and Binder cumulants ($B_4(0)$), calculated from the Polyakov loop (L) and chiral condensate ($\bar{\psi}\psi$). Simulations have been performed with p4 improved fermions on the $12^3 \times 4$ lattice and quark mass $m = 0.005$.

	from $\langle L \rangle$			from $\langle \bar{\psi}\psi \rangle$		
m	$\beta_{\rm pc}$	$\chi(\beta_{\rm pc})$	$B_4(0)$	$\beta_{\rm pc}$	$\chi(\beta_{\rm pc})$	$B_4(0)$
0.0000	3.2442(16)	0.510(105)	0.79(68)	3.2444(14)	49.1(16.0)	1.14(39)
0.0005	3.2463(14)	0.474(90)	1.28(43)	3.2468(12)	48.3(15.0)	1.39(31)
0.0010	3.2486(12)	0.448(75)	1.64(30)	3.2493(10)	45.1(13.5)	1.64(26)
0.0015	3.2509(10)	0.428(61)	1.92(22)	3.2516(9)	39.3(11.1)	1.93(22)
0.0020	3.2535(9)	0.412(50)	2.15(16)	3.2540(8)	32.6(8.1)	2.21(21)
0.0025	3.2558(9)	0.398(43)	2.33(13)	3.2560(8)	26.7(5.5)	2.40(25)
0.0030	3.2579(10)	0.385(39)	2.46(13)	3.2580(9)	22.6(3.8)	2.46(27)
0.0035	3.2603(11)	0.374(36)	2.55(14)	3.2599(9)	19.8(2.9)	2.46(25)
0.0040	3.2622(12)	0.365(34)	2.62(15)	3.2619(11)	17.8(2.4)	2.47(23)
0.0045	3.2641(13)	0.357(33)	2.67(16)	3.2639(12)	16.2(2.1)	2.48(21)
0.0050	3.2658(14)	0.351(32)	2.73(17)	3.2657(13)	14.9(1.9)	2.51(20)
0.0055	3.2679(14)	0.346(31)	2.79(18)	3.2674(14)	13.8(1.7)	2.54(19)
0.0060	3.2696(15)	0.343(30)	2.85(20)	3.2696(14)	12.9(1.5)	2.56(18)
0.0065	3.2711(15)	0.341(29)	2.94(23)	3.2712(14)	12.1(1.4)	2.59(18)
0.0070	3.2725(15)	0.341(29)	3.03(26)	3.2726(14)	11.5(1.3)	2.61(16)
0.0075	3.2736(15)	0.344(29)	3.11(29)	3.2744(14)	10.9(1.2)	2.63(15)

Table D.2: Mass reweighted data for pseudo critical couplings ($\beta_{\rm pc}$), peak heights of the susceptibilities ($\chi(\beta_{\rm pc})$) and Binder cumulants ($B_4(0)$), calculated from the Polyakov loop (L) and chiral condensate ($\bar{\psi}\psi$). Simulations have been performed with p4 improved fermions on the $16^3 \times 4$ lattice and quark mass $m = 0.005$.

		from $\langle L \rangle$			from $\langle \bar{\psi}\psi \rangle$		
N_σ	$\mu_{u,d}$	$\beta_{\rm pc}$	$\chi(\beta_{\rm pc})$	$B_4(0)$	$\beta_{\rm pc}$	$\chi(\beta_{\rm pc})$	$B_4(0)$
12	0.000	3.2654(11)	0.372(58)	2.84(27)	3.2650(8)	15.4(2.7)	2.51(28)
	0.005	3.2648(10)	0.372(58)	2.85(27)	3.2652(8)	15.4(2.7)	2.51(28)
	0.010	3.2648(10)	0.372(58)	2.84(27)	3.2646(8)	15.5(2.7)	2.52(28)
	0.015	3.2655(10)	0.373(59)	2.84(27)	3.2643(8)	15.5(2.7)	2.53(28)
	0.020	3.2648(9)	0.374(59)	2.84(28)	3.2650(8)	15.5(2.8)	2.53(28)
	0.025	3.2646(9)	0.375(60)	2.84(28)	3.2642(7)	15.6(2.8)	2.54(28)
	0.030	3.2646(8)	0.376(61)	2.83(29)	3.2633(7)	15.8(2.9)	2.56(29)
	0.035	3.2644(7)	0.377(62)	2.81(29)	3.2635(9)	16.0(2.9)	2.57(29)
	0.040	3.2635(8)	0.378(63)	2.79(30)	3.2626(11)	16.3(3.0)	2.58(30)
	0.045	3.2633(8)	0.380(64)	2.76(32)	3.2617(14)	16.9(3.0)	2.58(30)
	0.050	3.2630(11)	0.381(65)	2.72(34)	3.2610(16)	17.8(3.0)	2.55(30)
	0.055	3.2618(15)	0.384(69)	2.66(38)	3.2606(18)	19.1(3.2)	2.46(31)
	0.060	3.2616(18)	0.391(79)	2.59(44)	3.2596(19)	20.9(3.6)	2.29(33)
16	0.000	3.2661(11)	0.345(34)	2.73(18)	3.2658(11)	14.6(1.9)	2.49(22)
	0.010	3.2659(11)	0.345(34)	2.71(18)	3.2657(11)	14.6(1.8)	2.49(22)
	0.020	3.2656(12)	0.345(34)	2.68(18)	3.2654(12)	14.6(1.8)	2.49(22)

Table D.3: In up and down quark chemical potential ($\mu_{u,d}$) reweighted data, for pseudo critical couplings ($\beta_{\rm pc}$), peak heights of the susceptibilities ($\chi(\beta_{\rm pc})$) and Binder cumulants ($B_4(0)$), calculated from the Polyakov loop (L) and chiral condensate ($\bar{\psi}\psi$). Simulations have been performed with p4 improved fermions on the $12^3 \times 4$ and $16^3 \times 4$ lattice and quark mass $m = 0.005$.

β	T/T_0	c_2	c_4
3.52	0.7623	0.0218(40)	0.0342(160)
3.55	0.8122	0.0444(43)	0.0383(167)
3.58	0.8652	0.0638(52)	0.0404(153)
3.60	0.9024	0.0917(61)	0.0793(200)
3.63	0.9608	0.2057(67)	0.1397(474)
3.65	1.0017	0.3512(77)	0.2251(324)
3.66	1.0226	0.4129(83)	0.2563(384)
3.68	1.0658	0.5790(54)	0.1382(151)
3.70	1.1104	0.6554(40)	0.1019(76)
3.72	1.1566	0.7092(38)	0.0817(64)
3.75	1.2289	0.7481(31)	0.0661(50)
3.80	1.3576	0.7873(21)	0.0599(25)
3.85	1.4966	0.8065(17)	0.0548(22)
3.90	1.6464	0.8156(16)	0.0509(14)
3.95	1.8073	0.8200(13)	0.0493(13)
4.00	1.9796	0.8234(13)	0.0477(10)

Table D.4: Coefficients of $(\mu_q/T)^2$ and $(\mu_q/T)^4$ in the Taylor expansion of $\Delta(p/T^4)$. For the pressure (p), quark number density (n_q) and quark number susceptibility (χ_q) the following approximative relations hold: $\Delta p/T^4 \simeq c_2(T)(\mu_q/T)^2 + c_4(\mu_q/T)^4$, $n_q/T^3 \simeq 2c_2(T)(\mu_q/T) + 4c_4(\mu_q/T)^3$ and $\chi_q/T^2 \simeq 2c_2(T) + 12c_4(T)(\mu_q/T)^2$.

β	T/T_0	ρ_0	ρ_2	$(\mu_q/T)_{\text{instability}}$
3.52	0.762	1.436(133)	0.799(252)	
3.55	0.812	1.300(62)	1.078(299)	0.585
3.58	0.865	1.328(55)	1.257(260)	0.395
3.60	0.902	1.257(42)	1.076(134)	0.347
3.63	0.961	1.021(17)	1.214(274)	0.401
3.65	1.002	0.914(10)	1.249(99)	0.414
3.66	1.023	0.927(9)	1.269(105)	0.412
3.68	1.066	0.949(4)	2.047(121)	0.683
3.70	1.110	1.056(3)	2.536(100)	0.822
3.72	1.157	1.161(3)	2.947(120)	0.984
3.75	1.229	1.310(3)	3.364(135)	1.123
3.80	1.358	1.487(2)	3.626(77)	1.211
3.85	1.497	1.604(2)	3.838(78)	1.281
3.90	1.646	1.686(2)	4.004(55)	1.337
3.95	1.807	1.747(1)	4.078(53)	1.361
4.00	1.980	1.794(1)	4.155(43)	1.387

Table D.5: Estimates for the radius of convergence in the μ_q/T expansion of $\Delta p/T^4$ from $\rho_n(T) \equiv \sqrt{|c_n(T)/c_{n+2}(T)|}$ and from the requirement of mechanical instability $(\mu_q/T)_{instability}$.

β	T/T_0	$\frac{1}{2VT^3}\frac{\partial^3 \ln Z}{\partial\beta\partial(\mu_q/T)^2}$	$-\frac{1}{2VT^3}\frac{\partial^3 \ln Z}{\partial m\partial(\mu_q/T)^2}$	$\frac{1}{24VT^3}\frac{\partial^5 \ln Z}{\partial\beta\partial(\mu_q/T)^4}$	$-\frac{1}{24VT^3}\frac{\partial^5 \ln Z}{\partial m\partial(\mu_q/T)^4}$
3.52	0.762	1.12(72)	1.15(37)	0.67(2.95)	0.37(1.08)
3.55	0.812	0.36(92)	1.04(48)	-4.31(6.06)	-1.17(3.22)
3.58	0.865	1.37(78)	2.14(43)	0.88(3.12)	-0.26(1.51)
3.60	0.902	2.07(1.14)	3.62(68)	9.49(4.46)	9.93(2.41)
3.63	0.961	3.84(1.25)	6.69(1.15)	-16.38(13.26)	-10.93(13.59)
3.65	1.002	10.06(1.51)	13.46(1.48)	-11.23(8.33)	-6.51(6.62)
3.66	1.023	11.29(1.91)	15.25(1.93)	-4.70(9.60)	0.92(9.12)
3.68	1.066	5.26(94)	8.89(85)	-3.01(3.04)	-3.59(3.42)
3.70	1.110	4.21(69)	7.28(60)	-2.25(1.91)	-2.34(1.62)
3.72	1.157	2.64(51)	5.13(29)	-0.08(1.10)	-0.21(0.45)
3.75	1.229	0.83(35)	3.85(19)	-0.12(51)	-0.26(0.39)
3.80	1.358	0.33(20)	3.18(8)	0.08(25)	-0.15(0.12)
3.85	1.497	0.41(22)	2.90(7)	-0.04(31)	-0.16(0.13)
3.90	1.646	0.22(22)	2.63(4)	-0.56(26)	-0.13(0.04)
3.95	1.807	0.26(17)	2.42(4)	-0.39(23)	-0.11(0.07)
4.00	1.980	-0.08(16)	2.19(3)	-0.11(13)	-0.05(0.03)

Table D.6: Derivatives necessary for calculating the response of the energy density (ϵ) to increasing quark chemical potential (μ_q).

List of Figures

List of Tables

Bibliography

[1] CERN, *A new state of matter*. http://cern.web.cern.ch/CERN/Announcements/2000/NewStateMatter/, 2000.

[2] U. W. Heinz, *The little bang: Searching for quark-gluon matter in relativistic heavy-ion collisions*, *Nucl. Phys.* **A685** (2001) 414 [hep-ph/0009170].

[3] K. Rajagopal and F. Wilczek, *The condensed matter physics of QCD*, hep-ph/0011333.

[4] S. Hands, *The phase diagram of QCD*, *Contemp. Phys.* **42** (2001) 209–225 [physics/0105022].

[5] M. A. Stephanov, K. Rajagopal and E. V. Shuryak, *Event-by-event fluctuations in heavy ion collisions and the QCD critical point*, *Phys. Rev.* **D60** (1999) 114028 [hep-ph/9903292].

[6] J. Pochodzalla *et. al.*, *Probing the nuclear liquid - gas phase transition*, *Phys. Rev. Lett.* **75** (1995) 1040.

[7] W. Trautmann, *Multifragmentation in relativistic heavy-ion reactions*, nucl-ex/9611002.

[8] F. Karsch, E. Laermann and C. Schmidt, *The chiral critical point in 3-flavor QCD*, *Phys. Lett.* **B520** (2001) 41 [hep-lat/0107020].

[9] Z. Fodor and S. D. Katz, *Lattice determination of the critical point of QCD at finite T and μ*, *JHEP* **03** (2002) 014 [hep-lat/0106002].

[10] P. de Forcrand and O. Philipsen, *The QCD phase diagram for small densities from imaginary chemical potential*, *Nucl. Phys.* **B642** (2002) 290 [hep-lat/0205016].

[11] P. Braun-Munzinger, D. Magestro, K. Redlich and J. Stachel, *Hadron production in Au Au collisions at RHIC*, *Phys. Lett.* **B518** (2001) 41 [hep-ph/0105229].

[12] F. Karsch, E. Laermann and A. Peikert, *The pressure in 2, 2+1 and 3 flavour QCD*, *Phys. Lett.* **B478** (2000) 447 [hep-lat/0002003].

[13] F. Karsch, E. Laermann and A. Peikert, *Quark mass and flavor dependence of the QCD phase transition*, *Nucl. Phys.* **B605** (2001) 579 [hep-lat/0012023].

[14] A. Ali Khan *et. al.* [**CP-PACS** Collaboration], *Equation of state in finite-temperature QCD with two flavors of improved wilson quarks*, *Phys. Rev.* **D64** (2001) 074510 [hep-lat/0103028].

[15] J. Engels, O. Kaczmarek, F. Karsch and E. Laermann, *The quenched limit of lattice QCD at non-zero baryon number*, *Nucl. Phys.* **B558** (1999) 307 [hep-lat/9903030].

[16] Z. Fodor and S. D. Katz, *A new method to study lattice QCD at finite temperature and chemical potential*, *Phys. Lett.* **B534** (2002) 87 [hep-lat/0104001].

[17] Z. Fodor, S. D. Katz and K. K. Szabo, *The QCD equation of state at nonzero densities: Lattice result*, hep-lat/0208078.

[18] S. Choe *et. al.*, *Responses of hadrons to the chemical potential at finite temperature*, *Phys. Rev.* **D65** (2002) 054501.

[19] C. R. Allton *et. al.*, *The QCD thermal phase transition in the presence of a small chemical potential*, *Phys. Rev.* **D66** (2002) 074507 [hep-lat/0204010].

[20] S. Gottlieb, W. Liu, D. Toussaint, R. L. Renken and R. L. Sugar, *Fermion number susceptibility in lattice gauge theory*, *Phys. Rev.* **D38** (1988) 2888.

[21] R. V. Gavai and S. Gupta, *Pressure and non-linear susceptibilities in QCD at finite chemical potentials*, hep-lat/0303013.

[22] M. D'Elia and M.-P. Lombardo, *Finite density QCD via imaginary chemical potential*, *Phys. Rev.* **D67** (2003) 014505 [hep-lat/0209146].

[23] A. Hart, M. Laine and O. Philipsen, *Testing imaginary vs. real chemical potential in finite-temperature QCD*, *Phys. Lett.* **B505** (2001) 141 [hep-lat/0010008].

[24] U. M. Heller, F. Karsch and B. Sturm, *Improved staggered fermion actions for QCD thermodynamics*, *Phys. Rev.* **D60** (1999) 114502 [hep-lat/9901010].

[25] C. R. Allton *et. al.*, *The equation of state for two flavor QCD at non-zero chemical potential*, hep-lat/0305007. To appear in Phys. Rev. D.

[26] C. Schmidt, F. Karsch and E. Laermann, *The chiral critical point in 3-flavour QCD*, *Nucl. Phys. Proc. Suppl.* **106** (2002) 423–425 [hep-lat/0110039].

[27] C. Schmidt *et. al.*, *The quark mass and μ dependence of the QCD chiral critical point*, *Nucl. Phys. Proc. Suppl.* **119** (2003) 517 [hep-lat/0209009].

[28] C. Schmidt, *The QCD phase diagram for small chemical potentials*, hep-lat/0210037.

[29] M. Creutz, *Quarks, gluons and lattices*, . Cambridge, Uk: Univ. Pr. (1983) 169 p. (Cambridge Monographs On Mathematical Physics).

[30] I. Montvay and G. Münster, *Quantum fields on a lattice*, . Cambridge, UK: Univ. Pr. (1994) 491 p. (Cambridge monographs on mathematical physics).

[31] H. J. Rothe, *Lattice gauge theories: An introduction*, *World Sci. Lect. Notes Phys.* **59** (1997) 512 p.

[32] K. Wilson, *Confinement of quarks*, *Phys. Rev.* **D10** (1974) 2445.

[33] K. G. Wilson, *Quarks and strings on a lattice*, . New Phenomena In Subnuclear Physics. Part A. Proceedings of the First Half of the 1975 International School of Subnuclear Physics, Erice, Sicily, July 11 - August 1, 1975, ed. A. Zichichi, Plenum Press, New York, 1977, p. 69, CLNS-321.

[34] J. Kogut and L. Susskind, *Hamiltonian formulation of Wilson's lattice gauge theories*, *Phys. Rev.* **D11** (1975) 395.

[35] H. B. Nielsen and M. Ninomiya, *No go theorem for regularizing chiral fermions*, *Phys. Lett.* **B105** (1981) 219.

[36] D. B. Kaplan, *A method for simulating chiral fermions on the lattice*, *Phys. Lett.* **B288** (1992) 342 [hep-lat/9206013].

[37] P. Hasenfratz, V. Laliena and F. Niedermayer, *The index theorem in QCD with a finite cut-off*, *Phys. Lett.* **B427** (1998) 125 [hep-lat/9801021].

[38] P. Chen *et. al.*, *The finite temperature QCD phase transition with domain wall fermions*, *Phys. Rev.* **D64** (2001) 014503 [hep-lat/0006010].

[39] R. V. Gavai, S. Gupta and R. Lacaze, *Quenched QCD at finite temperature with overlap fermions*, *Nucl. Phys. Proc. Suppl.* **106** (2002) 435 [hep-lat/0109023].

[40] G. T. Fleming, *Thermodynamics of free domain wall and overlap fermions*, *Nucl. Phys. Proc. Suppl.* **94** (2001) 393 [hep-lat/0011069].

[41] Y.-b. Luo, *Improvement of the staggered fermion operators*, *Phys. Rev.* **D55** (1997) 353 [hep-lat/9604025].

[42] K. Symanzik, *Continuum limit and improved action in lattice theories. 1. principles and ϕ^4 theory*, *Nucl. Phys.* **B226** (1983) 187.

[43] K. Symanzik, *Continuum limit and improved action in lattice theories. 2. O(N) nonlinear sigma model in perturbation theory*, *Nucl. Phys.* **B226** (1983) 205.

[44] Y. Iwasaki and T. Yoshie, *Instantons and topological charge in lattice gauge theory*, *Phys. Lett.* **B131** (1983) 159.

[45] S. Itoh, Y. Iwasaki and T. Yoshie, *Stability of instantons on the lattice and the renormalized trajectory*, *Phys. Lett.* **B147** (1984) 141.

[46] P. Hasenfratz and F. Niedermayer, *Perfect lattice action for asymptotically free theories*, *Nucl. Phys.* **B414** (1994) 785–814 [hep-lat/9308004].

[47] T. DeGrand, A. Hasenfratz, P. Hasenfratz and F. Niedermayer, *The classically perfect fixed point action for SU(3) gauge theory*, *Nucl. Phys.* **B454** (1995) 587 [hep-lat/9506030].

[48] T. DeGrand, A. Hasenfratz, P. Hasenfratz and F. Niedermayer, *Nonperturbative tests of the fixed point action for SU(3) gauge theory*, *Nucl. Phys.* **B454** (1995) 615 [hep-lat/9506031].

[49] B. Beinlich, F. Karsch and E. Laermann, *Improved actions for QCD thermodynamics on the lattice*, *Nucl. Phys.* **B462** (1996) 415 [hep-lat/9510031].

[50] P. Weisz, *Continuum limit improved lattice action for pure yang-mills theory. 1*, *Nucl. Phys.* **B212** (1983) 1.

[51] P. Weisz and R. Wohlert, *Continuum limit improved lattice action for pure yang-mills theory. 2*, *Nucl. Phys.* **B236** (1984) 397.

[52] T. Blum, L. Karkkainen, D. Toussaint and S. Gottlieb, *The beta function and equation of state for QCD with two flavors of quarks*, *Phys. Rev.* **D51** (1995) 5153 [hep-lat/9410014].

[53] C. W. Bernard *et. al.* [**MILC** Collaboration], *The equation of state for two flavor QCD at n(t) = 6*, *Phys. Rev.* **D55** (1997) 6861 [hep-lat/9612025].

[54] T. Blum *et. al.*, *Improving flavor symmetry in the kogut-susskind hadron spectrum*, *Phys. Rev.* **D55** (1997) 1133 [hep-lat/9609036].

[55] J. F. Lagae and D. K. Sinclair, *Improved staggered quark actions with reduced flavour symmetry violations for lattice QCD*, *Phys. Rev.* **D59** (1999) 014511 [hep-lat/9806014].

[56] S. Naik, *On-shell improved lattice action for QCD with susskind fermions and asymptotic freedom scale*, *Nucl. Phys.* **B316** (1989) 238.

[57] P. Hasenfratz and F. Karsch, *Chemical potential on the lattice*, *Phys. Lett.* **B125** (1983) 308.

[58] J. B. Kogut *et. al.*, *Chiral symmetry restoration in baryon rich environments*, *Nucl. Phys.* **B225** (1983) 93.

[59] R. V. Gavai, *Chemical potential on the lattice revisited*, *Phys. Rev.* **D32** (1985) 519.

[60] F. Fucito, E. Marinari, G. Parisi and C. Rebbi, *A proposal for monte carlo simulations of fermionic systems*, *Nucl. Phys.* **B180** (1981) 369.

[61] S. Hands, *Lattice matter*, *Nucl. Phys. Proc. Suppl.* **106** (2002) 142 [hep-lat/0109034].

[62] A. M. Ferrenberg and R. H. Swendsen, *New Monte Carlo technique for studying phase transitions*, *Phys. Rev. Lett.* **61** (1988) 2635.

[63] A. M. Ferrenberg and R. H. Swendsen, *Optimized Monte Carlo analysis*, *Phys. Rev. Lett.* **63** (1989) 1195.

[64] I. M. Barbour and A. J. Bell, *Complex zeros of the partition function for lattice QCD*, *Nucl. Phys.* **B372** (1992) 385.

[65] B. Svetitsky and L. G. Yaffe, *Critical behavior at finite temperature confinement transitions*, *Nucl. Phys.* **B210** (1982) 423.

[66] R. D. Pisarski and F. Wilczek, *Remarks on the chiral phase transition in chromodynamics*, *Phys. Rev.* **D29** (1984) 338.

[67] S. Gavin, A. Gocksch and R. D. Pisarski, *QCD and the chiral critical point*, *Phys. Rev.* **D49** (1994) 3079 [hep-ph/9311350].

[68] F. R. Brown *et. al.*, *On the existence of a phase transition for QCD with three light quarks*, *Phys. Rev. Lett.* **65** (1990) 2491.

[69] S. Aoki *et. al.* [**JLQCD** Collaboration], *Phase structure of lattice QCD at finite temperature for 2+1 flavors of Kogut-Susskind quarks*, *Nucl. Phys. Proc. Suppl.* **73** (1999) 459 [hep-lat/9809102].

[70] J. J. Rehr and N. D. Mermin, *Revised scaling equation of state at the liquid-vapor critical point*, *Phys. Rev.* **A8** (1973) 472.

[71] N. B. Wilding, *Simulation studies of fluid critical behavior*, *J. Phys.: Condens. Matter* **9** (1997) 585.

[72] J. L. Alonso *et. al.*, *The U(1) Higgs model: Critical behavior in the confining Higgs region*, *Nucl. Phys.* **B405** (1993) 574 [hep-lat/9210014].

[73] K. Rummukainen, M. Tsypin, K. Kajantie, M. Laine and M. E. Shaposhnikov, *The universality class of the electroweak theory*, *Nucl. Phys.* **B532** (1998) 283 [hep-lat/9805013].

[74] F. Karsch and S. Stickan, *The three-dimensional, three-state Potts model in an external field*, *Phys. Lett.* **B488** (2000) 319 [hep-lat/0007019].

[75] H. W. J. Blöte, J. R. Heringa and M. M. Tsypin, *Three-dimensional Ising model in the fixed-magnetization ensemble: a Monte Carlo study*, *Phys. Rev.* **E62** (2000) 77 [cond-mat/9910145].

[76] A. Cucchieri, J. Engels, S. Holtmann, T. Mendes and T. Schulze, *Universal amplitude ratios from numerical studies of the three-dimensional O(2) model*, *J. Phys.* **A35** (2002) 6517 [cond-mat/0202017].

[77] K. Kanaya and S. Kaya, *Critical exponents of a three dimensional O(4) spin model*, *Phys. Rev.* **D51** (1995) 2404 [hep-lat/9409001].

[78] S. Gottlieb, W. Liu, D. Toussaint, R. L. Renken and R. L. Sugar, *Hybrid molecular dynamics algorithms for the numerical simulation of quantum chromodynamics*, *Phys. Rev.* **D35** (1987) 2531.

[79] B. Beinlich, F. Karsch and A. Peikert, *SU(3) latent heat and surface tension from tree level and tadpole improved actions*, *Phys. Lett.* **B390** (1997) 268 [hep-lat/9608141].

[80] J. Gasser and H. Leutwyler, *Chiral perturbation theory: Expansions in the mass of the strange quark*, *Nucl. Phys.* **B250** (1985) 465.

[81] J. B. Kogut and D. K. Sinclair, *Lattice QCD at finite isospin density at zero and finite temperature*, *Phys. Rev.* **D66** (2002) 034505 [hep-lat/0202028].

[82] J. B. Kogut and D. K. Sinclair, *Quenched lattice QCD at finite isospin density and related theories*, *Phys. Rev.* **D66** (2002) 014508 [hep-lat/0201017].

[83] S. Gupta, *Critical behaviour in QCD at finite isovector chemical potential*, hep-lat/0202005.

[84] D. T. Son and M. A. Stephanov, *QCD at finite isospin density*, *Phys. Rev. Lett.* **86** (2001) 592 [hep-ph/0005225].

[85] C. R. Allton, *Lattice Monte Carlo data versus perturbation theory*, hep-lat/9610016.

[86] J. Cleymans and K. Redlich, *Unified description of freeze-out parameters in relativistic heavy ion collisions*, *Phys. Rev. Lett.* **81** (1998) 5284 [nucl-th/9808030].

[87] J. T. Lenaghan, D. H. Rischke and J. Schaffner-Bielich, *Chiral symmetry restoration at nonzero temperature in the* $\mathrm{SU_R}(3)$ *x* $\mathrm{SU_L}(3)$ *linear sigma model*, *Phys. Rev.* **D62** (2000) 085008 [nucl-th/0004006].

[88] H. Meyer-Ortmanns and B.-J. Schaefer, *How sharp is the chiral crossover phenomenon for realistic meson masses?*, *Phys. Rev.* **D53** (1996) 6586 [hep-ph/9409430].

[89] N. Bilic and H. Nikolic, *Chiral-symmetry restoration in the linear sigma model at nonzero temperature and baryon density*, *Eur. Phys. J.* **C6** (1999) 513 [hep-ph/9711513].

[90] M. Gell-Mann and M. Levy, *The axial vector current in beta decay*, *Nuovo Cim.* **16** (1960) 705.

[91] S. Narison, *Qcd spectral sum rules*, *World Sci. Lect. Notes Phys.* **26** (1989) 1–527.

[92] J. Hubbard, *Calculation of partition functions*, *Phys. Rev. Lett.* **3** (1959) 77.

[93] Z. Frei and A. Patkos, *Chiral interface at the finite temperature transition point of QCD*, *Phys. Lett.* **B247** (1990) 381.

[94] S. R. Coleman, R. Jackiw and H. D. Politzer, *Spontaneous symmetry breaking in the O(N) model for large N*, *Phys. Rev.* **D10** (1974) 2491.

[95] J. M. Cornwall, R. Jackiw and E. Tomboulis, *Effective action for composite operators*, *Phys. Rev.* **D10** (1974) 2428.

[96] J. T. Lenaghan, *Influence of the* $\mathrm{U_A}(1)$ *anomaly on the QCD phase transition*, *Phys. Rev.* **D63** (2001) 037901 [hep-ph/0005330].

[97] M. Oertel and M. Buballa, *Color-flavor (un-)locking*, hep-ph/0202098.

[98] M. Buballa and M. Oertel, *Color-flavor unlocking and phase diagram with self- consistently determined strange quark masses*, *Nucl. Phys.* **A703** (2002) 770 [hep-ph/0109095].

[99] J. Engels, J. Fingberg, F. Karsch, D. Miller and M. Weber, *Nonperturbative thermodynamics of SU(N) gauge theories*, *Phys. Lett.* **B252** (1990) 625.

[100] G. Boyd *et. al.*, *Thermodynamics of SU(3) lattice gauge theory*, *Nucl. Phys.* **B469** (1996) 419 [hep-lat/9602007].

[101] A. Roberge and N. Weiss, *Gauge theories with imaginary chemical potential and the phases of QCD*, *Nucl. Phys.* **B275** (1986) 734.

[102] R. V. Gavai and S. Gupta, *The continuum limit of quark number susceptibilities*, *Phys. Rev.* **D65** (2002) 094515 [hep-lat/0202006].

[103] J. P. Blaizot, E. Iancu and A. Rebhan, *Quark number susceptibilities from HTL-resummed thermodynamics*, *Phys. Lett.* **B523** (2001) 143 [hep-ph/0110369].

[104] C. Bernard *et. al.* [**MILC** Collaboration], *High temperature QCD with three flavors of improved staggered quarks*, hep-lat/0209079.

[105] J. P. Blaizot, E. Iancu and A. Rebhan, *Comparing different hard-thermal-loop approaches to quark number susceptibilities*, *Eur. Phys. J.* **C27** (2003) 433 [hep-ph/0206280].

[106] M. Asakawa, U. W. Heinz and B. Müller, *Fluctuation probes of quark deconfinement*, *Phys. Rev. Lett.* **85** (2000) 2072 [hep-ph/0003169].

[107] Y. Hatta and M. A. Stephanov, *Proton number fluctuation as a signal of the QCD critical end-point*, hep-ph/0302002.

[108] D. Magestro, *Evidence for chemical equilibration at RHIC*, *J. Phys.* **G28** (2002) 1745 [hep-ph/0112178].

[109] J. Cleymans and K. Redlich, *Chemical and thermal freeze-out parameters from 1-A-GeV to 200-A-GeV*, *Phys. Rev.* **C60** (1999) 054908 [nucl-th/9903063].

[110] F. Becattini, J. Cleymans, A. Keranen, E. Suhonen and K. Redlich, *Features of particle multiplicities and strangeness production in central heavy ion collisions between 1.7-A-GeV/c and 158-A-GeV/c*, *Phys. Rev.* **C64** (2001) 024901 [hep-ph/0002267].

[111] F. Karsch, K. Redlich and A. Tawfik, *Hadron resonance mass spectrum and lattice QCD thermodynamics*, hep-ph/0303108.

[112] F. Karsch, K. Redlich and A. Tawfik, *Thermodynamics at non-zero baryon number density: A comparison of lattice and hadron resonance gas model calculations*, hep-ph/0306208.

[113] R. Hagedorn *Nuovo Cimento* **35** (1965) 395.

[114] D. H. Rischke, M. I. Gorenstein, H. Stöcker and W. Greiner, *Excluded volume effect for the nuclear matter equation of state*, *Z. Phys.* **C51** (1991) 485.

[115] G. D. Yen, M. I. Gorenstein, W. Greiner and S.-N. Yang, *Excluded volume hadron gas model for particle number ratios in A + A collisions*, *Phys. Rev.* **C56** (1997) 2210 [nucl-th/9711062].

[116] A. Chodos, R. L. Jaffe, K. Johnson, C. B. Thorn and V. F. Weisskopf, *A new extended model of hadrons*, *Phys. Rev.* **D9** (1974) 3471.

[117] T. DeGrand, R. L. Jaffe, K. Johnson and J. E. Kiskis, *Masses and other parameters of the light hadrons*, *Phys. Rev.* **D12** (1975) 2060.

[118] P. Braun-Munzinger, K. Redlich and J. Stachel, *Particle production in heavy ion collisions*, nucl-th/0304013.

[119] V. V. Dixit and E. Suhonen, *Bare bones model for phase transition in hadronic matter*, *Z. Phys.* **C18** (1983) 355.

[120] J. Letessier and J. Rafelski, *QCD equations of state and the QGP liquid model*, *Phys. Rev.* **C67** (2003) 031902 [hep-ph/0301099].

[121] K. K. Szabo and A. I. Toth, *Quasiparticle description of the QCD plasma, comparison with lattice results at finite T and μ*, *JHEP* **06** (2003) 008 [hep-ph/0302255].

[122] A. Rebhan and P. Romatschke, *HTL quasiparticle models of deconfined QCD at finite chemical potential*, hep-ph/0304294.

[123] S. Aoki *et. al.* [**JLQCD** Collaboration], *Scaling study of the two-flavor chiral phase transition with the Kogut-Susskind quark action in lattice QCD*, *Phys. Rev.* **D57** (1998) 3910 [hep-lat/9710048].